

SORPTION AND DESTRUCTION OF VETERINARY ANTIBIOTICS
ON NATURAL MINERALS

by

Aslin Erdiç

BS. in Environmental Eng., Trakya University, 2005

Submitted to the Institute of Environmental Sciences in partial fulfillment of
the requirements for the degree of
Master of Science
in
Environmental Sciences

Boğaziçi University

2009

SORPTION AND DESTRUCTION OF VETERINARY ANTIBIOTICS
ON NATURAL MINERALS

APPROVED BY:

Prof. Dr. Işıl Balcıoğlu
(Thesis Supervisor)



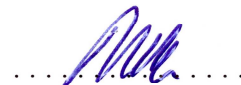
.....

Prof. Dr. Ferhan Çeçen



.....

Prof. Dr. Mehmet Sabri Çelik



.....

DATE OF APPROVAL: 15.06.2009

ACKNOWLEDGEMENT

I would like to express my sincere gratitude to my thesis supervisor Prof. Dr. Işıl Balcıođlu for her valuable suggestions, encouragement, support and endless patience.

This thesis is based upon work supported by The Scientific and Technological Research Council of Turkey (TÜBİTAK) under Project No. 106YO73. I am very grateful to TÜBİTAK for their financial support during my study.

I would like to thank my jury members Prof. Dr. Ferhan Çeçen and Prof. Dr. Mehmet Sabri Çelik for their constructive criticism and suggestions.

I am also very grateful to Mrs. Gülhan Özkösem and Mehmet Ali Küçüker for their kindness, support and suggestions during my laboratory study.

I am indebted to my laboratory friends Merih Ötker Uslu and Derya Aydın for their endless support and kindness.

I owe my deepest gratitude to my special friends Asu Ziylan, Serpil Sarıođlu and, Moris Abolafya for their valuable friendship, patience and support.

I would like to give my special thanks to Murat Karanfil, for his endless love, patience and support.

Last but not least, I would like to thank my dear parents Taşhan and Silva Erdinç, my brother and his wife Arda and Serli Erdinç for supporting me with their endless love, patience, and for being my side whenever I needed.

ABSTRACT

Excessive use of antibiotics induces accumulation of them in the environment and due to their adverse effects antibiotics are classified as an emergent pollutant. Considering the importance of antibiotic pollution control, the adsorption of a widely used tetracycline group antibiotic, oxytetracycline (OTC) onto perlite, sepiolite, and bentonite as natural adsorbents was investigated. The effects of initial antibiotic concentration, contact time, and pH on the adsorption of OTC were studied. Batch adsorption experiments indicate that the extent of sorption is strongly dependent on the pH of solution. The adsorption capacity of perlite, sepiolite, and bentonite for OTC at pH 6.5 was found 5.87, 5.57, and 10.93 mg g⁻¹, respectively. Pseudo-first order, pseudo-second order, Elovich, and intraparticle diffusion kinetic models were applied to the experimental data to describe the adsorption process. It was found that OTC adsorption on each adsorbent could be described more favorably by the pseudo-second order kinetic model. Standard adsorption isotherms were used to fit the equilibrium data and isotherms of each adsorbent were adequately described by Freundlich and Temkin models. Among the investigated adsorbents bentonite exhibited the highest adsorption performance. The treatment of spent bentonite was also performed by Fenton and ozonation processes which efficiently degraded OTC. While the extraction pretreatment enhanced the OTC degradation efficiency of ozonation process, it didn't affect the performance of Fenton process.

ÖZET

Antibiyotiklerin aşırı kullanılması doğada birikmelerine sebep olur ve zararlı etkileri nedeniyle kirletici olarak sınıflandırılırlar. Bu çalışmada antibiyotik kirliliği kontrolünün önemi dikkate alınarak, yaygın bir şekilde kullanılan tetrasiklin grubu antibiyotiği oksitetrasiklinin (OTC) doğal mineraller olan perlit, sepiyolit ve bentonite adsorpsiyonu incelenmiştir. Antibiyotik adsorpsiyonunda başlangıç antibiyotik konsantrasyonu, temas süresi ve pH etkileri kesikli adsorpsiyon deneyleri ile incelenmiştir ve adsorpsiyon veriminin büyük ölçüde ortam pH'ına bağlı olduğu saptanmıştır. Perlit, sepiyolit ve bentonitin pH 6.5'da OTC için adsorpsiyon kapasiteleri, sırasıyla 5.87, 5.57 ve 10.93 mg g⁻¹ olarak bulunmuştur. Adsorpsiyon prosesini tanımlamak için yalancı-birinci derece, yalancı-ikinci derece, Elovich ve partiküllerarası difüzyon kinetik modelleri uygulanmıştır ve herbir adsorbent için OTC adsorpsiyonu yalancı-ikinci derece kinetik model ile tanımlanmıştır. Adsorpsiyon mekanizmasının açıklanması için standart adsorpsiyon izotermi kullanılmış ve herbir adsorbent için Freundlich ve Temkin modelleri uygunluk göstermiştir. Adsorbentler arasında en yüksek verimi bentonit vermiş ve kullanılan bentonitin rejenerasyonu da adsorplanan OTC'nin ozon ve hidrojen peroksit ile giderimi sağlanarak gerçekleştirilmiştir. OTC'nin bentonitten ekstraksiyonu ozon prosesi için bir avantaj sağlasa da Fenton prosesinin performansını etkilememiştir.

TABLE OF CONTENTS

ACKNOWLEDGEMENT	iii
ABSTRACT.....	iv
ÖZET	v
LIST OF FIGURES	ix
LIST OF TABLES	xi
1. INTRODUCTION	1
2. THEORETICAL BACKGROUND.....	3
2.1. Occurrence of Antibiotics in the Environment.....	3
2.1.1. Pathways of Antibiotics in the Environment	3
2.1.2. Accumulation of Antibiotics in the Environment.....	6
2.1.2.1. Surface Water.....	6
2.1.2.2. Ground Water and Marine Sediment.	7
2.1.2.3. Soil.	8
2.1.2.4. Plants.	8
2.1.3. Environmental Fate of Antibiotics.....	10
2.1.3.1. Sorption of Antibiotics by Soil and Clay Minerals.....	10
2.1.3.2. Transport of Antibiotics in Soil.....	10
2.1.3.3. Biodegradation and Photodegradation of Antibiotics.	11
2.1.4. Possible Effects on the Environment	13
2.2. Classification of Antibiotics.....	14
2.2.1. Physical and Chemical Properties of Tetracycline Antibiotics.....	15
2.3. Sorption of Tetracyclines by Soils and Clay Minerals.....	17
2.4. Removal of Antibiotics	19
2.5. Regeneration of Adsorbents	21

3. MATERIALS AND METHODS.....	24
3.1. Materials.....	24
3.1.1. Adsorbents.....	24
3.1.2. Oxytetracycline Hydrochloride Antibacterial Compound.....	24
3.1.3. Other Chemicals.....	24
3.2. Methods.....	27
3.2.1. Preparation of Adsorbents.....	27
3.2.2. Characterization of Adsorbents.....	27
3.2.2.1. Surface Area Analysis.....	27
3.2.2.2. Determination of Cation Exchange Capacity (CEC).	27
3.2.2.3. X-ray Diffraction Analysis (XRD).....	28
3.2.2.4. Fourier Transform Infrared (FTIR) Analysis.....	28
3.2.2.5. Elemental Analysis.....	28
3.2.2.6. Scanning Electron Microscopy (SEM) Analysis.	28
3.2.3. Batch Adsorption Tests.....	29
3.2.4. Extraction of OTC from Adsorbent.....	30
3.2.5. Oxidation of OTC on Adsorbents.....	30
3.2.5.1. Degradation of OTC by Ozonation Process.....	30
3.2.5.2. Degradation of OTC by Fenton Process.	31
3.2.6. Analytical Methods.....	32
3.2.6.1. Determination of Released Ions from the Adsorbents.	32
3.2.6.2. Spectrophotometric Analysis of OTC.....	32
3.2.6.3. HPLC Analysis of OTC.	32
3.2.7. Error Analysis Method.....	33
4. RESULTS AND DISCUSSION.....	34
4.1. Characterization of Virgin Adsorbents.....	34
4.1.1. Cation Exchange Capacity (CEC) of Virgin Adsorbents.....	34

4.1.2. Surface Area and Porosity of Virgin Adsorbents	35
4.1.3. Fourier Transformed Infrared (FTIR) Surface Analysis of Virgin Adsorbents	35
4.1.4. X-ray Diffraction (XRD) Analysis of Virgin Adsorbents	37
4.1.5. Scanning Electron Microscopy (SEM) of Adsorbents.....	38
4.2. Sorption Kinetics of OTC on Adsorbents	42
4.3. Equilibrium Modeling	55
4.4. Effect of pH on Sorption	60
4.5. Released Ions from Adsorbents.....	62
4.6. Properties of Spent Adsorbents	65
4.6.1. XRD Analysis of Spent Adsorbents	65
4.6.2. FTIR Analysis of Spent Adsorbents	67
4.6.3. Elemental Analysis of Adsorbents Before and After Adsorption.....	69
4.7. Regeneration of Spent Bentonite.....	69
4.7.1. Extraction of OTC from Spent Bentonite	70
4.7.2. Ozonation of OTC on Spent Bentonite	72
4.7.3. Fenton Oxidation of OTC on Spent Bentonite	75
5. CONCLUSION.....	79
REFERENCES	81
APPENDIX A Calibration Curves and HPLC Chromatogram of OTC.....	99
APPENDIX B Interlayer Spacings and Peak Intensities of Adsorbents	103
APPENDIX C Surface Area Data of Adsorbents.....	118

LIST OF FIGURES

Figure 2.1. Principal routes of environmental exposure to drugs consumed in human and veterinary medicine.....	4
Figure 2.2. Molecular structure and pK _a values of tetracycline antibiotics.....	16
Figure 2.3. Speciation of OTC as a function of pH.....	16
Figure 3.1. Schematic presentation of ozonation process.....	31
Figure 4.1. FTIR spectra of virgin adsorbents.....	36
Figure. 4.2. XRD patterns of perlite.	37
Figure. 4.3. XRD patterns of sepiolite.	37
Figure 4.4. XRD pattern of bentonite.	38
Figure 4.5. SEM images of perlite.....	39
Figure 4.6. SEM images of sepiolite.....	40
Figure 4.7. SEM images of bentonite.	41
Figure 4.8. Kinetics of OTC sorption.....	43
Figure 4.9. Pseudo-first-order order plots of OTC adsorption.....	46
Figure 4.10. Pseudo-second-order order plots of OTC adsorption.....	49
Figure 4.11. Sorption of OTC described by Elovich model.....	51
Figure 4.12. Intraparticle diffusion model plot of OTC adsorption.....	53
Figure 4.13. Comparison of experimental and estimated sorption kinetics of OTC.	54
Figure 4.14. Comparison of experimental and estimated sorption isotherms of OTC..	58
Figure 4.15. Effect of pH on the sorption of OTC.....	61
Figure 4.16. Release of cations from adsorbents (mg L ⁻¹) initial pH=7.	64
Figure 4.17. XRD patterns of virgin and spent adsorbents.....	66
Figure 4.18. FTIR spectra of OTC and adsorbents before and after adsorption.....	68
Figure 4.19. OTC extraction efficiency of different solutions.	71

Figure 4.20. Effect of $\text{Mg}(\text{NO}_3)_2$ on extraction efficiency of OTC from bentonite.	72
Figure 4.21. Comparison of OTC removal efficiency of ozone before and after extraction.	73
Figure 4.22. Effect of hydrogen peroxide concentration and Fe catalyst on the OTC removal efficiency	75
Figure 4.24. Effect of pH on Fenton process.	78
Figure A.1. Calibration curves of OTC at different pH values.....	100
Figure A.2. HPLC calibration curve of OTC.....	101
Figure A.3. Representative chromatogram of OTC.....	102

LIST OF TABLES

Table 2.1. Representative pharmaceutical antibiotics and typical ranges of physicochemical properties from selected classes of antibiotics.....	15
Table 3.1. Properties and chemical structure of oxytetracycline hydrochloride.	25
Table 3.2. Chemicals used in the experiments.....	26
Table 4.1. Cation exchange capacity of virgin adsorbents.	34
Table 4.2. Textural parameters of virgin adsorbents.	35
Table 4.3. EDAX analysis of adsorbents.	42
Table 4.4. Kinetic model equations.	44
Table 4.5. Experimental and predicted adsorption kinetics of OTC by different adsorbents.	47
Table 4.6. Adsorption isotherms equations.	57
Table 4.7. Adsorption isotherm parameters.....	59
Table 4.8. Interlayer spacings (d_{001}) of virgin and spent adsorbents.	66
Table 4.9. Elemental content of adsorbents before and after the adsorption of OTC.....	69
Table 4.10. Desorption of OTC by various extraction solutions.....	70
Table A.1. Maximum absorption peak and extinction coefficient of OTC at different pH values.	100
Table B.1. Interlayer spacings and peak intensities of virgin perlite.....	104
Table B.2. Interlayer spacings and peak intensities of spent perlite.....	106
Table B.3. Interlayer spacings and peak intensities of virgin sepiolite.	108
Table B.4. Interlayer spacings and peak intensities of spent sepiolite.	110
Table B.5. Interlayer spacings and peak intensities of virgin bentonite.....	112
Table B.6. Interlayer spacings and peak intensities of spent bentonite.	114
Table B.7. Interlayer spacings and peak intensities of ozonated bentonite.	116
Table C.1. Surface area data of virgin perlite.....	119

Table C.2. Surface area data of virgin sepiolite.....	120
Table C.3. Surface area data of virgin bentonite.	121

1. INTRODUCTION

Large quantities of antibiotics are administered to humans and animals to treat infectious diseases every year. Veterinary antibiotics are also commonly used at subtherapeutic levels for prophylactic purposes and to promote growth. Subsequently, the presence of antibiotics in different environmental compartments such as soil, groundwater, surface water, and plants have been reported in recent studies (Hamscher et al., 2002; Boxall et al., 2006; Kim and Carlson, 2007; Dolliver et al., 2007; Barnes et al., 2008). Antibiotics are classified as an emergent pollutant since they could perturb microbial ecology, increase the reproduction of antibiotic-resistant pathogens, and could pose threats to human health (Frick et al., 2001). The contamination of waters with antibiotics presents challenges for the water industry on the issues of water reuse and water resource planning (Huang et al., 2001).

Generally, conventional wastewater treatment plants (WWTPs) including biological treatment processes have been shown to be ineffective in the removal of antibiotics (Glassmeyer et al., 2005; Kolpin et al., 2002; Stumpf et al., 1999). Oxidative treatments such as ozonation, Fenton and photocatalytic processes have been shown to be an option for the treatment of antibiotics (Hofl et al. 1997; Rey et al. 1999; Akmehmet Balcioglu and Ötker, 2003; Iketha et al., 2006). However, these treatment methods may cause the production of oxidation by products in the treated water. On the other hand, an efficient removal of some antibiotics was achieved by granular activated carbon, membrane bioreactors, membrane filtration processes using reverse osmosis and nanofiltration (Snyder et al., 2007).

Recent studies related with the fate of the antibiotics in the environment indicated that some of the antibiotics (e.g. tetracyclines) exhibited strong sorption tendency to the soil and the clay content of soil was found to be mainly responsible for the sorption of these antibiotics (Boxall et al., 2002; Figueroa et al., 2004). It is known that natural microporous materials including clay minerals as low cost adsorbents and barriers are utilized in the field of water pollution control and decontamination (Babel and Kurniawan, 2003; Crini, 2006; Ahmaruzzaman, 2008). Considering these facts, in the present study,

the sorption of a tetracycline group antibiotic, oxytetracycline (OTC) on perlite, sepiolite, and bentonite was investigated and the removal of OTC from the water was evaluated at different pH values. The sorption kinetics and the sorption isotherms were studied on three different adsorbents by using different models. The degradation of OTC, loaded on one of the adsorbents, which exhibited a higher removal performance, was also examined by the application of Fenton and ozone treatments.

2. THEORETICAL BACKGROUND

2.1. Occurrence of Antibiotics in the Environment

In recent years, the occurrence and the fate of pharmaceutically active compounds in the environment has been recognized as one of the emerging issues in environmental chemistry (Stan and Heberer, 1997; Halling- Sørensen et al., 1998; Daughton and Ternes, 1999; Daughton and Jones-Lepp, 2001; Kümmerer, 2001a, b).

Today, a wide range of naturally occurring and of synthetic antibiotics is frequently used for the therapy of infectious diseases in human and veterinary medicine (Grafe, 1992). For this purpose, antibiotics are designed to act very effectively even at low doses and, in case of intra-corporal administration, to be completely excreted from the body after a short time of residence. Consequently, these substances are released into the environment via the waste of organisms. Therefore, the residual concentrations of pharmaceutical antibiotics are found in the environment. The contaminations of surface, ground and drinking water, of aquatic sediments and soils with pharmaceuticals have been reported by several researchers (Richardson and Bowron, 1985; Heberer and Stan, 1996; Hirsch et al., 1999; Kümmerer, 2001a, b; Hamscher et al., 2002). The residues of antibiotics in soil result mostly from the use of contaminated excrements as fertilizer on agricultural land. It has been estimated that loads of up to kilograms per hectare may enter agricultural soils and that a concentration level of antibiotics similar to pesticides is easily reached (van Gool, 1993). Due to surface runoff and leaching, soils can even act as a source of antibiotic contaminants for the aqueous environment (Alder et al., 2001).

2.1.1. Pathways of Antibiotics in the Environment

The introduction of drugs into the environment is a function of the combination of several factors: the quantity manufactured; the dosage (amount, frequency and duration); the excretion efficiency of parent compound and metabolites; the adsorption/desorption on soil; and, the metabolic decomposition in sewage treatment (Diaz-Cruz et al., 2003).

The amount of pharmaceuticals and their bioactive metabolites being introduced into the environment is probably low. However, their continual input into the environment and their persistence may lead to a high, long-term concentration and promote unnoticed adverse effects on aquatic and terrestrial organisms. Effects can accumulate so slowly that changes remain undetected until they become irreversible (Diaz-Cruz et al., 2003).

Figure 2.1 shows the principal routes of environmental exposure to drugs used in human and veterinary medicine.

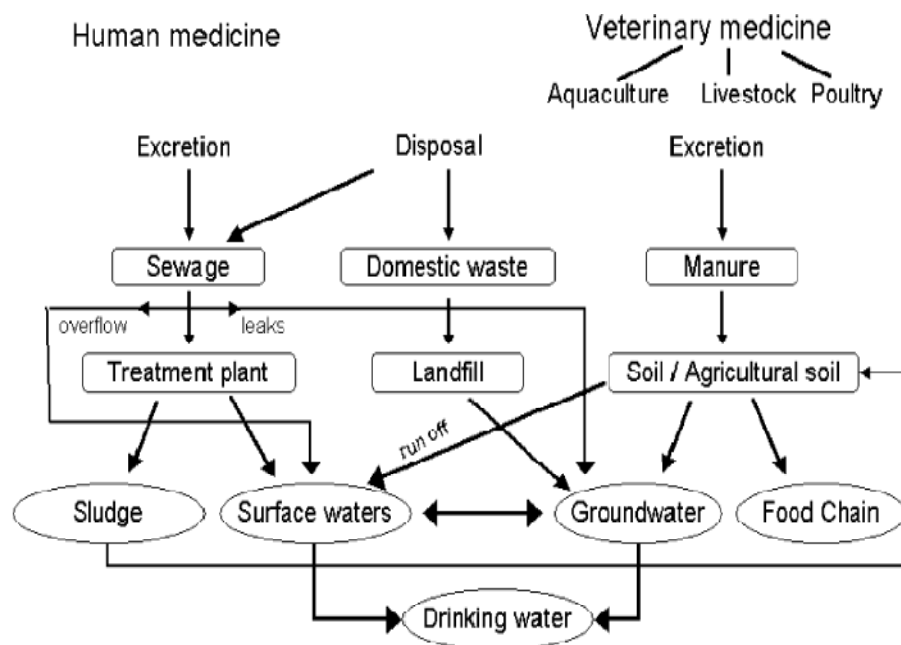


Figure 2.1. Principal routes of environmental exposure to drugs consumed in human and veterinary medicine (Diaz-Cruz et al., 2003).

The most important ways that drugs are introduced into the environment are through waste effluents of manufacturing processes, excreta, disposal of unused or expired drug products, and accidental spills during manufacturing or distribution. Among these, animal excreta can be the major source of environmental contamination by drugs (Diaz-Cruz et al., 2003) due to their higher consumption rate. Antibiotics are not completely metabolized in animal organisms, and excreted after a short time of residence. Antibiotics are optimised with regard to their pharmacokinetics in the organisms: organic accumulation is, as in other

pharmaceutics, objectionable and thus, they are excreted as parent compounds or metabolites (Kümmerer et al., 2000; Thiele-Bruhn, 2003). Excretion rates are dependent on the substance, the mode of application, the excreting species and time after administration, but it has been shown that rates vary between 40 and 90 % for tetracyclines and sulphonamides which are commonly used antibiotics (Berger et al., 1986; Haller et al., 2001; Halling-Sørensen, 2001). Thus, most of the drugs used in veterinary medicine end up in manure. The manure and slurry (urine and faeces) are either stored or immediately applied to agricultural fields as fertilizers. When this manure is dispersed on the field, the unmetabolized drugs present in the manure or their biologically active metabolites, may threaten the groundwater by depending on their mobility in the soil system and surface water by surface runoff and affect terrestrial and aquatic organisms as a result of leaching from these fields (Diaz-Cruz et al., 2003).

The same situation is found when sludge from sewage treatment plants is used to fertilize soils. Antibiotics used by humans are discharged into sewers together with urine and faeces and then enter sewage treatment plants. During sewage treatment, it is likely that many organic compounds, particularly hydrophobic compounds are sorbed onto sludge where they are concentrated by several orders of magnitude (Diaz-Cruz et al., 2003) compared with the sewage from which the sludge was derived. Hydrophilic compounds may be unaffected by sewage treatment and remain in the water effluent. Further possibilities are that compounds can be completely degraded, mineralized or partially degraded to produce breakdown products. The controlled application of sludge to soils presents clear benefits, since it results in the recycling of organic matter and nutrients. However, if the sludge contains pollutants, the application of sludge directly adds undesirable substances to the soil and leads to corresponding negative effects (Diaz-Cruz et al., 2003). Ingerslev and Halling Sorensen (2000) were assessed the biodegradability of 12 sulfonamides (SAs) in activated sludge solutions and concluded biodegradation of them is so slow compared to other known recalcitrant compounds (e.g., pentachlorophenol) and sulfonamides may pass the sewage treatment systems because of nonsorbing properties.

Another increasingly important source of drugs in the environment is, as mentioned in Figure 2.1, fish farming. In aquaculture, drugs used as feed additives are discharged directly into the water. Through overfeeding, loss of appetite by diseased fish and poor

adsorption of the drugs, it has been estimated that around 70 % of the drugs administered is released into the environment (Jacobsen and Berglind, 1988) . Therefore, large amounts of veterinary drugs and active metabolites end up in sediments in the vicinity of aquacultural areas. The presence of these substances in sediments, where many of them are known to be stable, favors the development of bacterial resistance, which gives rise to infections that are difficult to treat; also, the sediments act as a reservoir for both the antimicrobial compounds and the resistant bacteria (Diaz-Cruz et al., 2003).

2.1.2. Accumulation of Antibiotics in the Environment

Once released into the environment, antibiotics can be transported either in a dissolved phase or (ad)sorbed to colloids or soil particles into surface- and groundwater (Campagnolo et al., 2002; Kolpin et al., 2002; Yang and Carlson, 2003; Krapac et al., 2004). Monitoring studies for human and veterinary antibiotics in different environmental compartments are discussed below.

2.1.2.1. Surface Water. The first reported case of surface water contamination by antibiotics was in England almost three decades ago, when Watts et al. (1982) detected at least one compound from the macrolide (ML), sulfonamide (SA), and tetracycline (TC) group of antibiotics in river water at concentrations of $1 \mu\text{g L}^{-1}$. Following this, a variety of other antibiotics were also detected in surface water in concentrations up to $1 \mu\text{g L}^{-1}$ (Richardson and Bowron, 1985; Pearson and Inglis, 1993; Ternes, 1998; Hirsch et al., 1999). Tetracyclines were not detected in any water samples collected by Hamscher et al. (2002). Further findings by Lindsey et al. (2001) and Zhu et al. (2001) supported this. However, chlortetracycline has been detected in low levels in U.S. surface water samples (-690 ng L^{-1}) (Kolpin et al., 2002). On the other hand, oxytetracycline and tetracycline have been detected in higher levels in overland flow water ($32,000 \text{ ng L}^{-1}$) (Kay et al., 2005) and groundwater (400 ng L^{-1}) (Krapac et al., 2005).

Hydrologists within the United States Geological Survey (USGS) tested water samples in 30 states for 95 common compounds, an emerging class of contaminants known as pharmaceutical and personal care pollutants (Kolpin et al., 2002). USGS reported the

occurrence of 21 antibiotic compounds in samples collected from 139 streams across a number of US sites. Of these, large proportions were antibiotics used in animals as growth promoters, such as tylosin, tetracyclines, sulfonamides and carbadox. The frequency of detection was the highest for sulfonamides and lincomycin, followed by tylosin. The concentrations of the individual compounds detected in this study were generally less than $1.0 \mu\text{g L}^{-1}$ (Sarmah et al., 2006).

More recently, Focazio et al. (2008) sampled untreated drinking water sources in the United States and tested pharmaceuticals and other organic wastewater contaminants. In their study, antibiotics were not detected in any water sample. They concluded that many of these compounds likely transform or degrade as they are transported into and through the environment as a result of metabolic, photolytic, and other natural attenuation processes and therefore, it is possible that the parent compounds, though not detected, could have degraded into other compounds that were not targeted.

2.1.2.2. Ground Water and Marine Sediment. In a study performed by Capone et al. (1996) residual oxytetracycline at concentrations ranging from 500 to 4000 $\mu\text{g kg}^{-1}$ was observed in marine sediment following chemotherapy treatment in fish farms in the US.

Another study carried out elsewhere by Hamscher et al. (2000) reported the presence of chlortetracycline, oxytetracycline, tetracycline, and tylosin at the limit of detection of $0.1\text{--}0.3 \mu\text{g L}^{-1}$ in soil water samples collected from agricultural land. Multiple classes of antimicrobial compounds (tetracycline, macrolide, β -lactam, sulfonamide) were also detected in groundwater samples collected in nearby swine farms in the US (Campagnolo et al., 2002).

Kim and Carlson (2007) studied the presence of antibiotics in both water and sediment samples collected along a river in Northern Colorado. The limit of quantification was determined by two different methods and calculated to be in the range of $0.01\text{--}0.04 \mu\text{g L}^{-1}$ and $0.3\text{--}2.5 \mu\text{g kg}^{-1}$ for TCs, SAs, and MLs in water and sediment, respectively.

Recently, the occurrence of 65 organic wastewater contaminants including antibiotics were investigated in groundwater samples collected from 47 wells by Barnes et

al. (2008). Results showed that sulfamethoxazole was the most frequently detected antibiotic (23 %) and maximum concentration detected was $1.11 \mu\text{g L}^{-1}$ in groundwater samples.

2.1.2.3. Soil. Antibiotics used for veterinary purposes are excreted by the animals and end up in soils via grazing livestock or manure used as agricultural fertiliser (Jorgensen and Halling-Sorensen, 2000). The loads of antibiotics shed by manuring have been estimated up to kilograms per hectare (van Gool, 1993). For tetracyclines, detection at soil depths of up to 30 cm over long time periods was described by Hamscher et al. (2002). This data demonstrated that TCs not only occur in significant amounts in soil after fertilisation with liquid manure, but also persist and accumulate in the environment. This strong binding to soil-organic matter is based on the ability of the TCs to form complexes with double-charged cations, such as calcium, which occur in high concentrations in soil (Samuelsen et al., 1992). The residual concentrations of antibiotics were estimated for agricultural soils, ranging for TCs from 450 to $900 \mu\text{g kg}^{-1}$ (van Gool, 1993). In soils under conventional landfarming fertilized with manure and monitored for two years, average concentrations of up to $199 \mu\text{g kg}^{-1}$ tetracycline, $7 \mu\text{g kg}^{-1}$ chlortetracycline (Hamscher et al., 2002), and $11 \mu\text{g kg}^{-1}$ sulfadimidine (Höper et al., 2002) were detected.

Recently, Karıcı and Balcıoğlu (2009), investigated the level of antimicrobial pollution in total 17 agricultural soil and animal manure samples collected from different sampling points located in the Northern part of the Marmara region in Turkey and at least one antimicrobial compound was detected up to concentrations as high as 0.50 mg kg^{-1} in soil and 35.5 mg kg^{-1} in manure samples.

2.1.2.4. Plants. Kumar et al. (2005) and Boxall et al. (2006) argued that antibiotics may be taken up by food crops and make their way into food supply systems. The major concern about antibiotic uptake by plants is the contamination of the food supply and associated health risks. Health implications of antibiotic residues in plant-based products are largely unknown.

However; Kumar et al. (2005), Doyle (2006), and Dolliver et al. (2007) demonstrated several potential adverse impacts including allergic/toxic reactions and chronic toxic

effects as a result of prolonged low-level exposure, the development and spreading of antibiotic-resistant bacteria, and disruption of digestive system functioning.

Kumar et al. (2005) studied on cabbage (*Brassica oleracea* L.), corn, and green onion (*Allium cepa* L.) grown in manure-amended soil contaminated with antibiotics at concentrations ranging from 25 to 125 mg kg⁻¹ manure and evaluated plant taken up of chlortetracycline and tylosin. The authors found that chlortetracycline was uptaken between 0.002 and 0.017 mg kg⁻¹ fresh weight; however, tylosin was not taken up by these food crops. The authors speculated that the large size of the tylosin molecule possibly prohibited mass flow or active uptake.

Boxall et al. (2006) evaluated plant uptake of seven antibacterials in lettuce and carrot (*Daucus carota*) tissues from a sandy soil spiked at a concentration of 1 mg antibiotic per kg of soil. Florfenicol and trimethoprim were detected in lettuce leaves, whereas enrofloxacin, florfenicol, and trimethoprim were detected in carrot. Concentrations of these antibiotics ranged from approximately 3 to 38 mg kg⁻¹ fresh weight.

Recently, Dolliver et al. (2007) evaluated the plant uptake of a sulfonamide-class antibiotic, sulfamethazine, in corn (*Zea mays* L.), lettuce (*Lactuca sativa* L.), and potato (*Solanum tuberosum* L.) grown in a manure-amended soil. The treatments were 0, 50, and, 100 µg sulfamethazine per mL of manure applied at a rate of 56 000 L ha⁻¹. Results showed that sulfamethazine was taken up by all three crops, with concentrations in plant tissue ranging from 0.1 to 1.2 mg per kg dry weight. Sulfamethazine concentrations in plant tissue increased with corresponding increase of sulfamethazine in manure. Highest plant tissue concentrations were found in corn and lettuce, followed by potato. Total accumulation of sulfamethazine in plant tissue after 45 d of growth was less than 0.1 % of the amount applied to soil in manure. These results raise potential human health concerns of consuming low levels of antibiotics from produce grown on manure-amended soils which cause a risk for the contamination of water resources.

2.1.3. Environmental Fate of Antibiotics

2.1.3.1. Sorption of Antibiotics by Soil and Clay Minerals. Sorption processes strongly influence the transport, fate, and bioavailability of many organic contaminants in soil and sub-surface environments. The sorption of antibiotics is especially affected by the pH, organic matter, and minerals of soil, and distribution coefficients (K_d) of antibiotics (Thiele-Bruhn 2003). Previous studies demonstrated that tetracycline antibiotics interact strongly with clay minerals and hydrous oxides (Figueroa et al., 2004; Kulshrestha et al., 2004; Figueroa and Mackay, 2005; Gu and Karthikeyan, 2005) and, therefore, are likely to be retained in soils. Binding of TCs to divalent metal cations such as calcium or magnesium has been suggested to explain their adsorption to organic matter, minerals, and soils (Christian et al., 2003; Figueroa et al., 2004; MacKay and Canterbury, 2005; Gu et al., 2007).

The behavior of antibiotics in soil greatly depend on their adsorption–desorption characteristics, and the knowledge of these processes are important to predict their bioavailability, fate and transport mechanism through soil column into groundwater or surface water. However, studies on the adsorption of TCs are limited and have focused mainly on humic materials (Sithole and Guy, 1987a) and minerals (Sithole and Guy, 1987b; Kulshrestha et al., 2004; Figueroa et al., 2004; Turku et al., 2007; Wang et al., 2008). For those studies, cation exchange was concluded to be the primary adsorption mechanism responsible for the adsorption of TCs especially under acidic conditions, and the adsorption of TCs always decrease with increasing pH.

2.1.3.2. Transport of Antibiotics in Soil. Transport of antibiotics in the environment can depend on several factors. Chemical properties, temperature and moisture content of the soil, the timing of manure application and weather conditions can determine the overall degree of mobility of antibiotics in the environment. Other factors such as water solubility, dissociation constants, and sorption– desorption processes, as well as the stability and binding to the soils and the partitioning coefficients at various pH values can all affect the mobility of antibiotics range in the soil environment (Sarmah et al., 2006).

Rabolle and Spiild (2000) conducted packed soil column studies under saturated steady-state conditions and the relative mobilities of four antibiotics was determined. Most of the antibiotics remained in the top few centimetres of the soil column, indicating the high sorptive affinity of these compounds for the soils used; the order of mobility for the compounds followed metronidazole > olaquinox > tylosin > oxytetracycline. The study demonstrated that the risk of soil water/groundwater quality contamination by tylosin and oxytetracyclines would be much lower compared with olaquinox and metronidazole. It was also demonstrated through field studies in the UK that weak acid such as sulfonamide and OTC has high potential to be transported to surface waters (Boxall et al., 2002; Kay et al., 2005).

A study in Germany showed no clear indication of mobility of tetracycline hydrochloride on a sandy soil when applied with liquid manure (Engels and Winckler, 2004), perhaps owing to the higher sorption coefficient values for this compound (Tolls, 2001). In contrast, Aga et al. (2003) observed in soil column studies that the presence of dissolved organic matter (DOM) in liquid manure showed increased mobility for tetracycline antibiotics. Other factors that can influence the mobility of antibiotics are preferential flow via desiccation cracks and worm channels to the tile drains, as recently demonstrated in a UK field study (Kay et al., 2004).

2.1.3.3. Biodegradation and Photodegradation of Antibiotics. Gonsalves and Tucker (1977) showed that even after repeated application of oxytetracycline (OTC) in the form of drench, residues were not found below 20 cm in a Florida sandy soil. On the contrary, the residues of OTC were found at measured concentration of $>25 \mu\text{g L}^{-1}$ for at least 40 days after application; however, it declined steadily and persisted up to 18 months after application when concentration of OTC reduced to $<1 \mu\text{g L}^{-1}$ in the soil (Gonsalves and Tucker, 1977). The apparent immobilisation of OTC in the soils to a greater depth was attributed to the presence of higher percentages of clay and organic matter in the surface soils with residues of OTC bound strongly to soil particles.

Halling-Sørensen et al. (2005) found average degradation half-lives of chlortetracycline and tylosin A to vary between 25–34 days and 49–67 days in two Danish

sandy soils, respectively. These half-lives in field soils were substantially higher than the reported values for these compounds when experiment was conducted in the laboratory.

The additions of manure or sludge, containing high numbers of microorganisms, mostly result in increased biodegradation of antibiotics in soil (Ingerslev and Halling Sorensen, 2001). However, fixation of antibiotic compounds to surfaces or in pores of the soil matrix may effectively protect them from biodegradation (Samuelsen et al., 1992; Gavalchin and Katz, 1994).

It has to be noted that the results of bio- or photodegradation studies of antibiotics depend on conditions, e.g. temperature, composition of matrix etc., as demonstrated by the following examples: Gavalchin and Katz (1994) studied the degradability of seven faecal-borne antibiotics in soil and found that five antibiotics disappeared after incubation at 30 °C, while only two were eliminated when the samples are incubated at 4 °C. Tetracyclines and aminoglycosides are susceptible to photodegradation. The half-lives of oxytetracycline under investigation varied due to differences in temperature, light intensity and flow rate from one test tank to another. Fluoroquinolones are insensitive to hydrolysis and increased temperatures, but are degraded by UV light (Thiele-Bruhn, 2003).

Photodecomposition takes place mainly in surface water, since soil and sediment prevent a substance from undergoing photochemical degradation due to the lack of light in these matrices. A laboratory incubation study of OTC in marine sediment, no degradation was observed after 6 months of incubation period (Samuelsen et al., 1992). In contrast, in an earlier laboratory study by Samuelsen (1989), OTC was found to have a half-life of 30–64 days in sediment from a fish farm.

The antibacterial substance proved to be stable in sediments rather than sea water. As no mechanism of decomposition is known for tetracyclines except photodegradation (Oka et al., 1989) the substance remains in the sediment for a long period, as proved by Lunestad and Goksøyr (1990). OTC can persist for relatively long periods in sediments. For example, the half-lives in marine sediments were found to be 151 days in the top layer (0–1 cm) and more than 300 days at 5–7 cm deep (Hektoen et al., 1995).

2.1.4. Possible Effects on the Environment

Resistance genes as well as resistant bacteria in the environment are increasingly seen as an ecological problem which are already detected in different environmental compartments such as surface water, ground water, soil, and sediment (Kümmerer, 2004).

Recent publications revealed that more than 90 % of bacterial strains originated in seawater are resistant to more than one antibiotic, and 20 % are resistant at least to five (Martinez, 2003). Similarly, surface water samples from the sites near wastewater treatment plants in Australia had a significant increase of antibiotic resistant *Escherichia coli* (Watkinson et al., 2007).

Antibiotic resistance is not the only possible adverse effect of antibiotic release in environment, and they may exert ecotoxicity (Yamashita et al., 2006). Antibiotics might act, at very low concentrations, as signaling agents in microbial environments (Linares et al., 2006; Fajardo and Martinez, 2008; Fajardo et al., 2008).

Studies on representative organisms showing EC_{50} values of streptomycin, flumequine or oxytetracycline, revealed that these antibiotics could have harmful effects or even, very toxic effects as in the case of oxofloxacin for bacteria (Halling-Sørensen et al., 1998; Lalumera et al., 2004; Eguchi et al., 2004). Exposure of antibiotics, such as tylosin, oxytetracycline, chlortetracycline or erythromycine induces high toxicity to algae (Lalumera et al., 2004; Eguchi et al., 2004; Halling-Sorensen, 2000). Moreover, studies performed with sulphadimethoxine or oxytetracycline show the toxic character to invertebrates, conversely, flumequine as well as tylosin do not have toxic effects to invertebrates (Halling-Sorensen et al., 1998; Wollenberger et al., 2000). In consequence, it was suggested that sufficiently low concentrations of antibiotics could alter community structures (even microbial community) and thereby affect the food chain (Hernando et al., 2006).

2.2. Classification of Antibiotics

In human medicine, antibiotics pose the third biggest group among all pharmaceuticals making up more than 6 % of all prescriptions (Schwabe and Paffrath, 2001). In veterinary medicine, more than 70 % of all consumed pharmaceuticals are antibiotic agents (Halling-Sorensen et al., 1998). In Europe, two thirds of all pharmaceutical antibiotics are used in human medicine and one third for veterinary purposes (FEDESA, 2001). Furthermore, the mean total antibiotic consumption in Turkey increased from 16.598 to 30.960 Defined Daily Dose (DDD)/1000 inhabitant days between the years 2001 and 2005 (Karabay and Hosoglu, 2008).

The antibiotic compound classes primarily administered in veterinary medicine are tetracyclines, sulfonamides, aminoglycosides, β -lactams, and macrolides. In human medicine β -lactams, tetracyclines, and macrolides are mostly prescribed (Schwabe and Paffrath, 2001).

Antibiotics exhibit different molecular structures and diverse chemical and physical properties (Gräfe, 1992). Most antibiotics tend to ionize depending on the pH of the medium; pK_a values are associated with the different functional groups of the compounds. Ranges of physicochemical properties of important antibiotic compound classes are listed in Table 2.1 (Thiele-Bruhn, 2003).

Table 2.1. Representative pharmaceutical antibiotics and typical ranges of physicochemical properties from selected classes of antibiotics (Thiele-Bruhn, 2003).

Compound class	Molar mass g mol ⁻¹	Water solubility mg l ⁻¹	log K _{ow}	pK _a	Henry's constant Pa l mol ⁻¹
Tetracyclines chlortetracycline, oxytetracycline, tetracycline	444.5 – 527.6	230 – 52000	-1.3 – 0.05	3.3 / 7.7 / 9.3	1.7×10 ⁻²³ – 4.8×10 ⁻²²
Sulfonamides sulfanilamide, sulfadiazine, sulfadimidine, sulfadimethoxine, sulfapyridine, sulfamethoxazole	172.2 – 300.3	7.5 – 1500	-0.1 – 1.7	2 – 3 / 4.5 – 10.6	1.3×10 ⁻¹² – 1.8×10 ⁻⁸
Aminoglycosides kanamycin, neomycin, streptomycin	332.4 – 615.6	10 – 500 ^a	-8.1 – -0.8	6.9 – 8.5	8.5×10 ⁻¹² – 4.1×10 ⁻⁸
β-Lactams penicillins: ampicillin, meropenem, penicillin G; cephalosporins: cefitofur, cefotiam	334.4 – 470.3	22 – 10100	0.9 – 2.9	2.7	2.5×10 ⁻¹⁹ – 1.2×10 ⁻¹²
Macrolides erythromycin, oleandomycin, tylosin	687.9 – 916.1	0.45 – 15	1.6 – 3.1	7.7 – 8.9	7.8×10 ⁻³⁶ – 2.0×10 ⁻²⁶
Fluoroquinolones ciprofloxacin, enrofloxacin, flumequin, sarafloxacin, oxolinic acid	229.5 – 417.6	3.2 – 17790	-1.0 – 1.6	8.6	5.2×10 ⁻¹⁷ – 3.2×10 ⁻⁹
Imidazoles fenbendazole, metronidazole, oxfendazole	171.5 – 315.3	6.3 – 407	-0.02 – 3.9	2.4	2.3×10 ⁻¹⁸ – 2.7×10 ⁻¹⁰
Polypeptides avermectin, bacitracin, ivermectin, virginiamycin	499.6 – 1038	not – completely	-1.0 – 3.2		negligible – 2.8×10 ⁻²³
Polyethers monensin, salinomycin	670.9 – 751.0	2.2×10 ⁻⁶ – 3.1×10 ⁻³	5.4 – 8.5	6.4	2.1×10 ⁻¹⁸ – 1.5×10 ⁻¹⁸
Glycopeptides vancomycin	1450.7	> 1000	not soluble in octanol	5.0	negligible
Quinoxaline-derivatives olaquinox	263.3	1.0×10 ⁶	-2.2	10	1.1×10 ⁻¹⁸

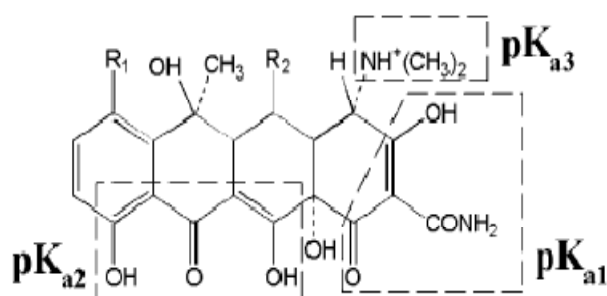
^a g l⁻¹

2.2.1. Physical and Chemical Properties of Tetracycline Antibiotics

The tetracyclines (TCs) are broad-spectrum antibacterials widely used for the therapy of infectious diseases of humans and animals. Tetracycline (TC), oxytetracycline (OTC), and chlortetracyclines (CTC) are also widely used in animal feeds to maintain health and improve growth efficiency in many countries. These chemicals are characterized by a partially conjugated four-ring structure with a carboxamide functional group (Mitscher, 1978).

As can be seen from Figure 2.2 there are three distinct acidic functional groups for tetracycline: tricarbonyl methane (pKa 3.3); dimethyl ammonium cation (pKa 9.6); and

phenolic diketone (pK_a 7.7). The multiple ionizable functional groups present in TCs suggest that at environmentally relevant pH values, they may exist as a cation (+ 0 0), zwitterion (+ - 0), or as a net negatively charged ion (+ - -) (Figuroa et al., 2004; Sassman and Lee, 2005). Therefore, it can be envisaged from these ionization schemes that in the pH regime of environmental interest (pH 4–8), the antibiotics would be dominated by the zwitterionic species and would reach maximum concentration at pH 5.5 (Figure 2.3).



Antibiotic	R ₁	R ₂	pK _{a1}	pK _{a2}	pK _{a3}
OTC	H	OH	3.57	7.49	9.88
TET	H	H	3.3	7.7	9.7
CTC	Cl	H	3.6	7.52	9.88

Figure 2.2. Molecular structure and pK_a values of tetracycline antibiotics (Figuroa et al., 2004).

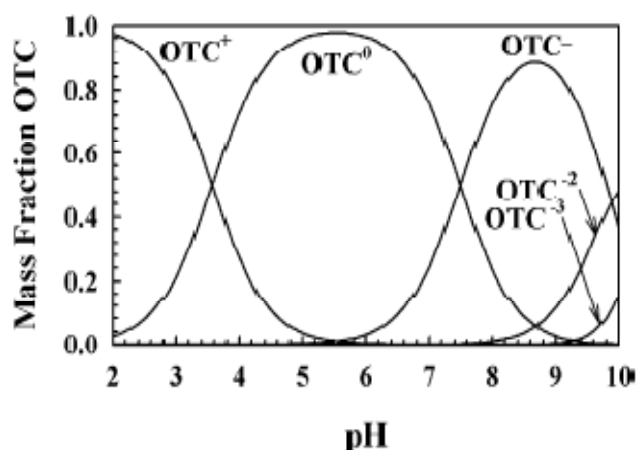


Figure 2.3. Speciation of OTC as a function of pH (Figuroa et. al., 2004).

TCs are relatively stable in acidic media, but not in alkaline conditions, and form salts in both media (Halling-Sørensen et al., 2002). They have been found to form complexes with chelating agents such as divalent metal ions and β -diketones and this property is responsible for strong binding of TCs to soil proteins and silanol groups (Oka et al., 2000).

Tetracyclines photodecomposes and can be converted to several products. Three major photodecomposition products of TC were reported as 4-dedimethylaminotetracycline, 5a, 6-anhydro-tetracyclines, and a quinine (Oka et al., 1989; Halling-Sørensen et al., 2002).

2.3. Sorption of Tetracyclines by Soils and Clay Minerals

Given the variation in the chemical nature of these antibiotics (Figure 2.3), their sorption mechanism onto soil or other environmental matrices is likely to be different. Tolls (2001) reported that K_d values for the adsorption of antibiotics to soil material and aquatic sediments vary for SAs from 0.6 to 4.9, for TCs from 290 to 1620 and for fluorquinolones (FQs) from 310 to 6310 L kg⁻¹.

Sithole and Guy (1987a) studied the interactions of tetracycline with model clay adsorbents as a function of suspension pH, ionic strength, and adsorbate concentration using Na, Ca, and dodecyltrimethylammonium modified bentonite and bentonite covered with tannic acid. The adsorption of TC on all adsorbents was explained by Langmuir isotherm, suggesting the occurrence of sorption at limited number of sites. The resultant adsorption capacity followed a decreasing order of tannic acid-clay > Ca-clay > Na-clay > DDTMA-clay, and maximum adsorptive capacity was obtained at pH 4.6–6.0. The authors postulated three mechanisms based on the interaction of each form of clay used in the study: an interaction between TC and clay due to the ion exchange between the clay surface and the protonated amine group of the TC; complexation reactions between the divalent cations on the clay and TC; and a mechanism where there is interaction between TC with the exposed aluminium ions on the edges of clay.

Sithole and Guy (1987b) investigated the adsorption of tetracycline onto humic acid and peat. In this study, Freundlich isotherm model was applied to the data. They suggested that the adsorption of tetracycline onto organic matter-rich soil or manure would depend on the pH and ionic strength of the suspension, with greater sorption occurring mainly within the pH range of 4.0–7.0, a range within the pH regime of environmental interest. It was concluded that the hydrophobic interaction of tetracycline with bentonite clays decreased its sorption and the interaction between the molecules of tetracycline and the divalent cations at the clay surface dominated the sorption process.

Rabolle and Spliid (2000) reported a laboratory sorption study for four veterinary antibiotics (metronidazole, olaquinox, oxytetracycline and tylosin) which were commonly used as growth promoters in swine production. The partitioning coefficients (K_d) of metronidazole and olaquinox ranged from 0.54 to 1.67 ml g⁻¹, while that of oxytetracycline and tylosin were a few orders of magnitude higher. None of the soil properties showed positive correlation with the estimated partitioning coefficients for the compounds, although there appeared to be some correlation for tylosin. The non-linear trend of the isotherms were clear from the reported n (slope) values, and it was more prominent for tylosin data, as the values of K_d and K_f (Freundlich's coefficient) in all four soils were several orders of magnitude difference. The authors attributed this to their inability to measure the K_d values with sufficient accuracy, citing stronger sorption affinity for tylosin molecules to the soils.

More recently, Kulshrestha et al. (2004) investigated the interaction of OTC with model clay sorbents and postulated that at lower pH values, when OTC has a net positive charge, they tend to have greater sorption affinity with cation exchange as the dominant mechanism. On the other hand in case of zwitterionic form of OTC hydrophobic mechanism prevails over other sorption mechanisms.

Figuroa and MacKay (2005) showed that there is a general trend of cationic and zwitterionic OTC species interaction with soil or sediment clay components. Furthermore, the authors suggested that antibiotic sorption interactions with clays are controlled by the ionic functional groups of the base compound structure within an antibiotic class, although there may be only little influence of other nonionic substituents on the base structure.

Further insight to the mechanisms of TC sorption by soil and its constituents was recently provided by Sassman and Lee (2005), who investigated the sorption of three TCs (TC, OTC, and CTC) in several soils varying in pH, cation exchange capacity (CEC), anion exchange capacity, clay content and type, and OC content under various background electrolyte concentrations. They concluded that several processes may influence the sorption of TCs, and pH and CEC play an important role in TC sorption.

A study by Jones et al. (2005) demonstrated a poor correlation between OC and OTC sorption on 30 soils, presumably due to the fact that CEC values and isotherms were determined at different pH values (Sassman and Lee, 2005). Since TCs exist in an environmentally relevant pH regime as cations, zwitterions, and anions, the prediction of sorption and transport of this group of antibiotics can be often complicated and difficult.

Most sorption studies also reveal that although the majority of the antibiotics used in animal production are strongly sorbed to soil and clay particles, whether they may still be biologically active and can influence the selection of antibiotic resistant bacteria in the terrestrial environment are some areas where future research should be directed (Chander et al., 2005).

2.4. Removal of Antibiotics

Generally, conventional wastewater treatment plants (WWTPs) including biological treatment processes have been shown to be ineffective in the removal of antibiotics (Glassmeyer et al., 2005; Kolpin et al., 2002; Stumpf et al., 1999).

Kümmerer et al. (1997) investigated treatment of hospital and pharmaceutical wastewater at several wastewater treatment plants in Germany. This research showed that many pharmaceuticals could not be biodegraded during conventional biological treatment, but they could be adsorbed by sewage sludge.

Some combined chemical/biological treatment processes appear to be more effective for the removal of antibiotics from wastewater. Garcia et al. (1995) used aerobic digestion

integrated with activated carbon filtration and reverse osmosis (RO) to reduce biochemical oxygen demand (BOD), chemical oxygen demand (COD), and total dissolved solids (TDS) in pharmaceutical wastewater by approximately 80 %.

Belter et al. (1973) patented an ion exchange process that used a weak-base anion exchange resin to absorb streptomycin, which could subsequently be eluted with a dilute acid solution. In a later study, Belter (1985) again used ion exchange to remove and recover the antibiotics from pharmaceutical water.

Snyder et al. (2007) studied the removal of various pharmaceuticals including antibiotics, in surface waters and wastewater treatment plant effluents in South Korea. They concluded that conventional drinking water treatment methods were relatively inefficient for contaminant removal, while efficient removal ($\approx 99\%$) was achieved by granular activated carbon (GAC). In wastewater treatment processes, membrane bioreactors (MBR) showed limited target compound removal, but were effective at eliminating hormones and some pharmaceuticals (e.g., acetaminophen, ibuprofen, and caffeine). Membrane filtration processes using reverse osmosis (RO) and nanofiltration (NF) showed excellent removal ($>95\%$) for all target analytes.

Oxidative treatment has also been shown to be a viable option for the treatment of pharmaceutical process water. Rey et al. (1999) used ozone to inactivate wastewater from pharmaceutical manufacturers of cytostatic drugs. The results showed that more than 90 % removal of the compounds was achieved after 45 min. In addition, none of the solutions of oxidized cytostatics gave positive results for the Ames test, indicating that the by-products were not mutagenic. Hofl et al. (1997) used three advanced oxidation processes ($\text{H}_2\text{O}_2/\text{ultraviolet (UV)}$, O_3/UV , and $\text{H}_2\text{O}_2/\text{Fe}^{+2}$) for the removal of adsorbable organic halogen (AOX) and COD of pharmaceutical wastewater. The results showed that under test conditions the Fenton method (i.e., $\text{Fe}^{+2}/\text{H}_2\text{O}_2$) needed the shortest reaction time, and was the most appropriate for the degradation of large amounts of COD ($>500\text{ mg L}^{-1}$). There was no significant difference between $\text{H}_2\text{O}_2/\text{UV}$ and O_3/UV processes while ozone alone caused the slowest degradation.

Balcioglu Akmehmet and Ötger (2003) applied ozonation to synthetic penicillin VK formulation wastewater. About 70 %, 40 %, and 30 % of initial COD (450 mg L^{-1}), TOC (162 mg L^{-1}), and aromaticity (0.456; absorbance at 254 nm) were removed by ozonation in one hour at an applied ozone dose of 2.96 g L^{-1} at pH 7 or 11 at 20°C . The addition of H_2O_2 improved the COD removal to 95 % at pH 7. Same group studied the ozonation of a buffered synthetic wastewater containing ceftriaxone. After 1 h of ozonation at an applied ozone dose of 2.96 g L^{-1} , 74 % of initial COD (450 mg L^{-1}) and 50 % of initial TOC (167 mg L^{-1}) was removed at pH 7. The COD reduction was slightly improved to 82% by elevating pH from 7 to 11. The addition of hydrogen peroxide also improved the COD removal. The absorbance at 254 nm in the synthetic wastewater was reduced by more than 90 %, indicating effective destruction of aromatic rings in the ceftriaxone molecules.

2.5. Regeneration of Adsorbents

The regeneration of adsorbents has become a very important issue because the spent adsorbents may be considered as a waste. Regeneration techniques of spent adsorbents can be classified into thermal and nonthermal methods.

Thermal regeneration includes hot gas or steam regeneration and thermal desorption. The reactivation of spent adsorbent is commonly considered a high-temperature process ($650\text{-}1000^\circ\text{C}$) during which the adsorption capacity is restored through desorption of the adsorbate and/or burnoff of carbonaceous residual on the adsorbent surface. The harmful adsorbates are rendered harmless by oxidation during the reactivation process. However, on-site thermal reactivation is economically feasible only for large systems that use more than 500,000 lb ($\approx 230,000 \text{ kg}$) adsorbent per year (Sontheimer et al. 1988).

Nonthermal regeneration includes solvent extraction, supercritical fluid extraction, biological regeneration, wet oxidation, chemical oxidation, and advanced oxidation. Among thermal and nonthermal regeneration methods, steam or hot gas regeneration, supercritical fluid extraction, and wet oxidation can be very effective to remove a wide variety of organic compounds, but all require high temperatures and/or high pressures (Sontheimer et al., 1988). Biological regeneration is usually slow and requires the biodegradability of adsorbed species, which is not an occurrence in many water pollutants

(Scholz and Martin, 1998). The major advantages of is that, advanced oxidation processes (AOPs) can be operated at ambient conditions and they are very effective in destroying or mineralizing a wide range of organic compounds (Blake, 1994; Liu et al. 1995).

The regeneration of adsorbents can be driven by ozone and Fenton processes as advanced oxidation processes. Hydroxyl radicals are the main oxidizing species in these processes. Molecular ozone can also react with species adsorbed onto adsorbent, thus removing them from the surface (Jans and Hoigne, 1998). Regeneration studies with ozone are usually focused on activated carbon (AC) because of its high cost property (Gomez-Serrano et. al., 2002; Chiang et. al., 2002a,b; Valdes et. al., 2002) However, ozone can modify surface properties of AC such as specific surface area, pore volume, and chemical functional groups. In particular, Valdes et al. (2002) have demonstrated that after high ozone uptake it may decrease the AC adsorptive properties because of the fixation of oxygen groups on the surface which obstruct the entrance of micropores.

Recently, Fenton-driven oxidation has been proposed for regenerating spent organic-loaded carbon by Huling et al. (2005). Two successive regeneration cycles were performed including repetitive adsorption and oxidation processes and the regeneration efficiency after two full cycles of treatment was calculated as 91 %. Although small reductions in carbon surface area and pore volume were measured, adsorption efficiency was not affected significantly.

Wang et al. (2006) studied on physical (high temperature combustion) and chemical (Fenton oxidation) regeneration of natural zeolite used as adsorbents for the removal of a basic dye, methylene blue and their efficiencies were compared. Regeneration did not fully recover the adsorption capacity of zeolite with the two techniques and the regenerated zeolites by the two techniques were similar, resulted in 60 % adsorption capacity of fresh sample.

Apart from the advantages, at least two general mechanisms could adversely affect the adsorption capacity of the regenerated adsorbent. First, oxidative treatment may detrimentally alter the chemical and physical characteristics of the adsorbent. It was established previously that reductions in surface area, microporosity, total porosity and

sorptive capacity resulted from repeated (10–15) aggressive oxidative treatments. Second, incomplete transformation of the target compounds may result in the accumulation of byproducts at sorption sites that would otherwise be available for the target compounds (Huling et al., 2005).

3. MATERIALS AND METHODS

3.1. Materials

3.1.1. Adsorbents

Unexpanded perlite, sepiolite, raw, and treated bentonite were used as natural adsorbents. Perlite and sepiolite were provided from Persan A.Ş. (İzmir) and Anadolu Endüstriyel Mineralleri San. Tic. Ltd. (Eskişehir), respectively. Bentonite, which was extracted from Reşadiye (Tokat), was prepared as adsorbent by Istanbul Technical University Faculty of Mines.

3.1.2. Oxytetracycline Hydrochloride Antibacterial Compound

Hydrochloride salt of oxytetracycline was used as a model antimicrobial compound in the adsorption experiments due to its higher solubility. Oxytetracycline hydrochloride ($C_{22}H_{24}N_2O_9 \cdot HCl$, $\geq 95\%$, crystalline) was purchased from Sigma Aldrich. Stock solution of OTC was prepared freshly in deionized water and the desired concentrations of OTC were prepared by diluting the stock solution with deionized water. The properties (Thomas et al., 2006) and chemical structure of OTC are represented in Table 3.1.

3.1.3. Other Chemicals

All other chemicals used in this study are listed in Table 3.2.

Table 3.1. Properties and chemical structure of oxytetracycline hydrochloride.

Properties	
Molecular Weight (g mol⁻¹)	496.89
CAS Number	2058-46-0
Solubility (g L⁻¹)	1
Log K_{ow}	-1.12
pK_A	3.27, 7.33, 9.11
Structure	
<p>Chemical structure of oxytetracycline hydrochloride. The structure shows a tetracycline core with a dimethylammonium group (NH(CH₃)₂⁺) and a hydrochloride counterion (HCl). Three pKa values are indicated: pKa₁ for the dimethylammonium group, pKa₂ for the phenolic diketone system, and pKa₃ for the tricarbonyl system.</p>	HCl

Table 3.2. Chemicals used in the experiments.

Chemical Name	Formula	Experiment	Supplier
Sodium Hydroxide	NaOH	pH adjustment	Riedel de Haen
Hydrochloric Acid	HCl	pH adjustment	Riedel de Haen
Citric Acid Monohydrate	$C_6H_8O_7 \cdot H_2O$	Extraction	Merck
Disodium Ethylenediamine Tetraacetate (Na ₂ EDTA)	$C_{10}H_{14}N_2Na_2O_8 \cdot 2H_2O$	Extraction	Merck
Sodium Hydrogen Phosphate	Na ₂ HPO ₄	Extraction	Merck
Sodium Chloride	NaCl	Extraction	Riedel de Haen
Magnesium Nitrate Hexahydrate	$Mg(NO_3)_2 \cdot 6H_2O$	Extraction	Merck
Oxalic Acid Dihydrate	$C_2H_2O_4 \cdot 2H_2O$	Extraction	Riedel de Haen
Methanol	CH ₃ OH	Extraction	Sigma Aldrich
Magnesium Chloride Hexahydrate	$MgCl_2 \cdot 6H_2O$	Extraction	J. T. Baker
Sodium Acetate Trihydrate	$CH_3COONa \cdot 3H_2O$	CEC* determination	Riedel de Haen
Acetic Acid Glacial	CH ₃ COOH	CEC determination	Merck
Ammonium Hydroxide	NH ₄ OH	CEC determination	Riedel de Haen
2-Propanol (isopropyl alcohol)	CH ₃ CH(OH)CH ₃	CEC determination	Merck
Iron (II) Sulfate Exsiccated	$FeSO_4 \cdot 1,5 H_2O$	Oxidation	Riedel de Haen
Hydrogen Peroxide	H ₂ O ₂ (30 %)	Oxidation	Merck

*Cation Exchange Capacity

3.2. Methods

3.2.1. Preparation of Adsorbents

Perlite and sepiolite samples were washed with deionized water for several times and subsequently dried in a drying oven at 70 °C for 2 hours and finally, they were sieved to a size range of 0 - 45 µm (325 mesh size) before keeping them in a desiccator. Bentonite was prepared by rinsing raw bentonite once and leaving in deionized water for 24 hours before the adsorption experiments.

3.2.2. Characterization of Adsorbents

3.2.2.1. Surface Area Analysis. Specific surface area, pore volume, and pore size measurements were conducted using a Quantachrome Nova Station A analyzer employing the conventional multipoint BET technique at 350 °C bath temperature and 200 °C outgas temperature. Nitrogen was used as an analysis gas.

3.2.2.2. Determination of Cation Exchange Capacity (CEC). The total cation exchange capacity of adsorbents were determined by sodium acetate method (<http://www.epa.gov/testmethods/pdfs/9081.pdf>). Adsorbent was mixed with an excess of sodium acetate solution, resulting in an exchange of the added sodium cations for the matrix cations. Subsequently, the sample was washed with isopropyl alcohol. An ammonium acetate solution was then added to replace the adsorbed sodium with the ammonium ion. The concentration of displaced sodium was then determined by atomic absorption spectroscopy (Perkin Elmer AAS 300).

CEC is calculated by the following equation:

$$\text{CEC}(\text{meq}/100\text{g}) = \frac{[\text{Na}] \times V \times \text{DF} \times 100}{m \times \text{MV}} \quad (3.1)$$

where,

[Na] = Na⁺ concentration (mg L⁻¹)

V = Volume of extract (L)

DF = Dilution factor

m = Weighed mass of adsorbent (g)

MV = Molecular weight of sodium (23 g mole⁻¹ = 23 mg meq⁻¹)

3.2.2.3. X-ray Diffraction Analysis (XRD). The crystalline phases and the basal spacing (d_{001} reflection) of adsorbents were determined by XRD analysis with a Rigaku D/MAX-2200 Ultima+/PC X-ray diffraction equipment with CuK α radiation generated at 40 kV, 40 mA, a scanning speed of 2 deg. min⁻¹ and 1.5-70 deg. scanning range. XRD analysis was also performed for the adsorbents after the adsorption of OTC (0.4 mg mL⁻¹) at pH 6.5 and subsequent lyophilization (Freeze-drying, Labconco Freezone 4.5; -54 °C; 0.050 mbar vacuum).

3.2.2.4. Fourier Transform Infrared (FTIR) Analysis. The FTIR analysis of OTC and adsorbents were recorded by Thermo Nicolet, FTIR 380 spectrometer, using a diamond ATR accessory. The FTIR spectrophotometer was set to scan in the region of 4000-500 cm⁻¹ with the resolution of 4 cm⁻¹. FTIR analysis was also performed for the adsorbents loaded with OTC that were prepared in the same manner as for XRD analysis.

3.2.2.5. Elemental Analysis. The elemental analyses (C, N, H) of adsorbents were accomplished by an elemental combustion system (Costech ECS 4010). The samples were burned in an excess of oxygen at 1700-1800 °C and the combustion products, N₂, CO₂ and H₂O, passed through a gas chromatographic (GC) separation column. Finally they were detected by a high sensitivity thermal conductivity detector (TCD). Helium was the carrier gas in the system.

3.2.2.6. Scanning Electron Microscopy (SEM) Analysis. The surface morphology of the adsorbents was investigated by SEM (Philips XL-30 ESEM-FEG/EDAX microscope). For the SEM analysis, adsorbents were mounted directly on a holder and analysis was performed at 10-25 kV electron beam accelerating voltage. Semiquantitative surface

elemental compositions of adsorbents were determined by energy dispersive X-ray spectroscopy (EDAX).

3.2.3. Batch Adsorption Tests

Batch adsorption tests were performed by using, unexpanded perlite, sepiolite, and bentonite. A volume of 7.5 mL OTC solution (115 mg L^{-1}) at desired pH, was placed in a screwed cap polyethylene tube. Accurately weighed adsorbent (10 g L^{-1}) was then added to the solution. The tubes were wrapped with aluminum foil to eliminate the photodecomposition of OTC (Halling-Sørensen et al., 2002) and agitated on a shaker (Julabo Shake Temperature SW 22) at 150 rpm for predetermined contact time at $25 \text{ }^{\circ}\text{C}$. The control experiments in the absence of sorbent were assembled in the same manner to account for possible OTC losses at different pH values. Each run was done at least in duplicate. After equilibration, adsorbents were separated from the suspension by centrifugation (Eppendorf Centrifuge 5804) at $10,000 \times g$ for 10 minutes and subsequently filtered through a $0.45 \text{ }\mu\text{m}$ membrane filter (Sartorius Minisart). The supernatant was analyzed for the OTC concentration by SHIMADZU UV-1208 spectrophotometer. The amount of the OTC adsorbed on natural materials was calculated by a mass balance relationship. The effects of pH, OTC concentration, and contact time on the adsorption efficiency were investigated in batch adsorption experiments.

The time required to attain the state of equilibrium is termed the equilibrium time and the amount of adsorption at equilibrium, q_e (mg g^{-1}), was calculated by the mass balance relationship as follows,

$$q_e = \frac{(C_0 - C_e) V}{W} \quad (3.2)$$

where C_0 and C_e are initial and equilibrium liquid phase concentrations of OTC (mg L^{-1}) respectively, V is the volume of solution (L) and W is the weight of adsorbent used (g).

3.2.4. Extraction of OTC from Adsorbent

The extraction of OTC from the surface of bentonite, which was the only adsorbent used in extraction experiments, was performed with magnesium salt solutions at different concentrations. In addition, the standard extraction solvents used in the analysis of antibiotics were applied to spent bentonite.

After adsorption tests, the samples were centrifuged and supernatant was decanted. A volume of 7.5 mL extraction solution at desired concentration and pH was added to the OTC equilibrated adsorbent and they were agitated on a shaker (Julabo Shake Temperature SW 22) at 150 rpm at 25 °C for 2 hours. Thereafter, adsorbents were separated from the suspension by centrifugation (Eppendorf Centrifuge 5804) at 10,000 x g for 10 minutes and subsequently filtered through a 0.45 µm membrane filter (Sartorius Minisart). The supernatant was analyzed for the OTC concentration by SHIMADZU UV-1208 spectrophotometer to evaluate the performance of extraction.

3.2.5. Oxidation of OTC on Adsorbents

The degradation of OTC in bentonite slurry was performed by two different oxidation processes. After the extraction of OTC from the surface of adsorbent by using $\text{Mg}(\text{NO}_3)_2$ solution, ozone and hydrogen peroxide with iron catalyst were applied to the slurry for the destruction of OTC. The oxidation processes were also applied to OTC loaded adsorbent without the application of extraction procedure.

3.2.5.1. Degradation of OTC by Ozonation Process. After the extraction of OTC from the spent bentonite, the slurry was transferred into a glass tube (15 mL) which was used as an ozonation reactor. Ozone was bubbled into the slurry through a pasteur pipette connected to an ozone generator by a teflon tubing. Teflon tubing was also used to connect it to an ozone analyzer (Ozotron 23 Ozone Analyzer). During the ozonation experiments slurry was mixed by a magnetic stirrer. The schematic diagram of experimental setup is given in Figure 3.1.

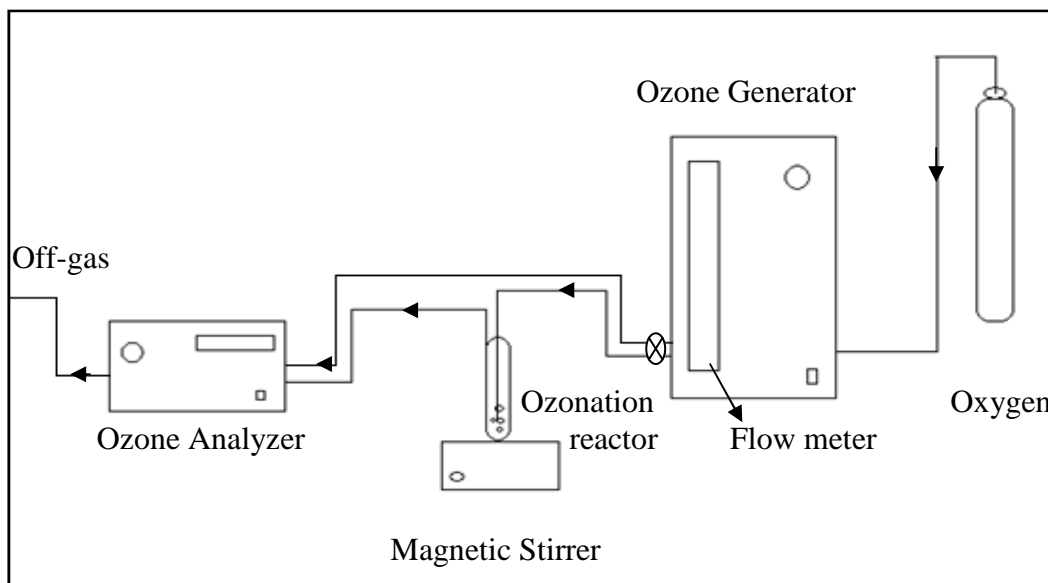


Figure 3.1. Schematic presentation of ozonation process.

Fisher OZ 500 model ozone generator was used for the production of ozone from dry and pure oxygen. The oxygen flow rate in the generator was maintained at 10 L h^{-1} and monitored with a rotameter incorporated into the ozone generator. The ozonation rate in ozone-oxygen gas mixture, introduced into the reactor with a glass pasteur pipette, was $13 \pm 2 \text{ g m}^{-3} \text{ h}$. After the ozonation, treated samples were centrifuged at $10,000 \times g$ for 10 minutes and subsequently filtered through a $0.45 \mu\text{m}$ membrane filter (Sartorius Minisart). The supernatant was analyzed for the OTC concentration by a high-performance liquid chromatography (HPLC) (Agilent 1100 Series). The efficiency of ozonation was determined by the difference in the amount of OTC in the extraction solution before and after the application of ozonation. All experiments were done in duplicate.

3.2.5.2. Degradation of OTC by Fenton Process. A 0.5 mL volume of H_2O_2 and ferrous sulphate were added to 7.5 mL of spent bentonite slurry. The initial hydrogen peroxide and the iron (II) concentration ranged from 10 mM and 1 mM to 15 mM and 150 mM , respectively to provide a $1/10$ ratio of $\text{Fe(II)}:\text{H}_2\text{O}_2$. Ferrous iron and hydrogen peroxide solutions, which were freshly prepared from stock solutions, were successively added to the slurry and the Fenton's reaction was started upon the addition of hydrogen peroxide. The samples in 15 mL screwed cap polyethylene tube were agitated on a shaker (Julabo Shake Temperature SW 22) at 150 rpm at $25 \text{ }^\circ\text{C}$ for predetermined contact time. The adsorbents were separated from the slurry by centrifugation (Eppendorf Centrifuge 5804)

at 10,000 x g for 10 minutes and subsequently filtered through a 0.45 µm membrane filter (Sartorius Minisart). The residual concentration of OTC was determined in the filtrate by HPLC analysis and the performance of the Fenton process was calculated as in the case of ozonation process. Two replicate experiments were conducted at each experimental condition.

3.2.6. Analytical Methods

3.2.6.1. Determination of Released Ions from the Adsorbents. The amount of ions released from the adsorbents were determined by placing 10 g L⁻¹ of the adsorbent into a polyethylene tube and shaking them at 150 rpm at 25 °C for 24 hours. Subsequently, adsorbents were separated from the suspension by centrifugation (Eppendorf Centrifuge 5804) at 10,000 x g for 10 minutes and finally, it was filtered through a 0.45 µm membrane filter (Sartorius, Minisart). The filtrate was analyzed for Al⁺³, Na⁺, Ca⁺, K⁺, Mg⁺², Fe⁺³, Mn⁺⁴, Cu⁺, Ti⁺⁴ and Zn⁺² ions by ICP (Inductively Coupled Plasma) (Optical Emission Spectrometer Optima 2100 DV-Perkin Elmer).

3.2.6.2. Spectrophotometric Analysis of OTC. In the adsorption tests, the concentration of OTC in the solution was quantified by UV/Vis spectrophotometer (SHIMADZU UV-1208) at a wavelength corresponding to the maximum absorbance which exhibited a shift depending upon the pH of solution. The spectra of OTC at different pH values were recorded between 354.5 – 372 nm wavelengths and a separate calibration curve was prepared for each pH value (Table A.1-Figure A.1). The initial and final antibiotic concentrations were determined by using these calibration curves. In accordance with the Lambert-Beer law, a linear relationship was found between the absorbance values and the concentrations of OTC. In the spectrophotometric measurements, dilutions were undertaken when absorbance exceeded 0.9.

3.2.6.3. HPLC Analysis of OTC. After the application of oxidation processes, the residual OTC in the solution was determined by HPLC analysis (Agilent 1100 Series) instead of UV spectroscopic analysis in order to eliminate the interferences of oxidation products. The HPLC system was equipped with a tertiary pump, a photodiode array, and an

autosampler with an automated injection system. Gradient elution was carried out with acetonitrile (solvent A) and water containing 0.1 % formic acid (solvent B) using an analytical column Eclipse XDB C18 (5 μ , 150 x 4 mm) equipped with ODS guard column. Elution started with A:B:10:90 rising linearly to 40:60 from 0 to 5 min and then returning to initial composition from 5 to 8 minutes. OTC was detected at the 360 nm wavelength with a retention time of 5.98 min. The limit of detection (LOD) for OTC was calculated as 0.8 mg L⁻¹. OTC quantification in solution was conducted by an external calibration curve (Figure A.2 - Figure A.3).

3.2.7. Error Analysis Method

In this study, a Chi-square test was used to perform an error analysis and in order to evaluate the suitability of isotherm and kinetic models to the experimental results. This test is basically the sum of the squares of the differences between the experimental data and the data obtained by calculation from the models, with each squared difference divided by the corresponding data obtained by the experiments.

The sum of square errors (SSE) is found by following equation:

$$SSE = \sum_{i=1}^m \frac{(q_{e,exp} - q_{e,calc})^2}{q_{e,exp}} \quad (3.3)$$

where $q_{e,exp}$ is the experimental data of the equilibrium capacity (mg g⁻¹), $q_{e,calc}$ is the calculated equilibrium capacity obtained by the model (mg g⁻¹). If the data from the model are similar to the experimental data, SSE will be a small number, if they are different, SSE will be a large number.

4. RESULTS AND DISCUSSION

4.1. Characterization of Virgin Adsorbents

For the characterization of adsorbents cation exchange capacity, surface area, pore volume, pore size, XRD pattern, FTIR spectra, SEM image, and elemental analysis were investigated.

4.1.1. Cation Exchange Capacity (CEC) of Virgin Adsorbents

Cation exchange capacity is one of the basic properties of natural materials which have clay content and a high adsorption of ionizable organic pollutants is expected to such adsorbents. In accordance, it is suggested that the CEC plays a key role in the adsorption of TCs, which have multiple ionizable functional groups, on clays and soils, (Sassman et al., 2005). Considering these facts, the CECs of adsorbents were determined to elucidate the role of it on OTC adsorption and the results are reported in Table 4.1.

Table 4.1. Cation exchange capacity of virgin adsorbents.

Adsorbent	CEC (meq/100g)
Perlite	21.90
Sepiolite	8.91
Bentonite	101.85

As can be seen from Table 4.1, the CECs of the investigated adsorbents varied over a wide range. These results are in consistent with those obtained in previous studies. CECs of unexpanded perlite, sepiolite, and bentonite were determined as 25.97 (Doğan et al., 1997), 8.2-30 (Lemic et. al, 2005; Sabah and Çelik, 1999; Alkan et al., 2005) and 76-106 meq/100g (Tomita and Naixian, 1990), respectively.

4.1.2. Surface Area and Porosity of Virgin Adsorbents

Surface area is another important characteristic of adsorbents and plays a key role in the adsorption of pollutants. Therefore, specific surface area (SSA), total pore volume (V_t), and pore size (D_p) of adsorbents were investigated (Table C1, C2, C3) and the results are listed in Table 4.2.

Table 4.2. Textural parameters of virgin adsorbents.

Adsorbent	SSA ^a (m ² g ⁻¹)	V _t ^b (cm ³ g ⁻¹)	D _p ^b (Å)
Perlite	11.78	0.005	20.48
Sepiolite	332	0.157	12.65
Bentonite	136.44	0.062	15.19

^aBET method

^bDubinin-Radushkevich method

Similar to CECs of adsorbents, the textural parameters given in Table 4.2 exhibited a wide variation depending upon the type of adsorbent. Usually sepiolite is characterized by large surface area and high porosity and due to these properties it was widely used in pollution control studies. In previous studies, SSAs of unexpanded perlite, sepiolite and bentonite were determined as 1.1-5.83 (Akçay et al., 1998; Koumanova and Peeva-Antova, 2002; Acemioğlu, 2005; Alkan et al., 2005), 340-426 (Rytwo et al., 2002; Özcan and Özcan, 2005) and 27.9-47.73 (Demirbaş et al., 2006; Hu et al., 2006; Anirudhan and Ramachandran, 2007) m² g⁻¹, respectively.

4.1.3. Fourier Transformed Infrared (FTIR) Surface Analysis of Virgin Adsorbents

In order to investigate the adsorbent-OTC interactions FTIR spectroscopy was used in the middle region (4000-400 cm⁻¹). Before the loading of OTC on the adsorbents FTIR spectra was recorded for each adsorbent (Figure 4.1).

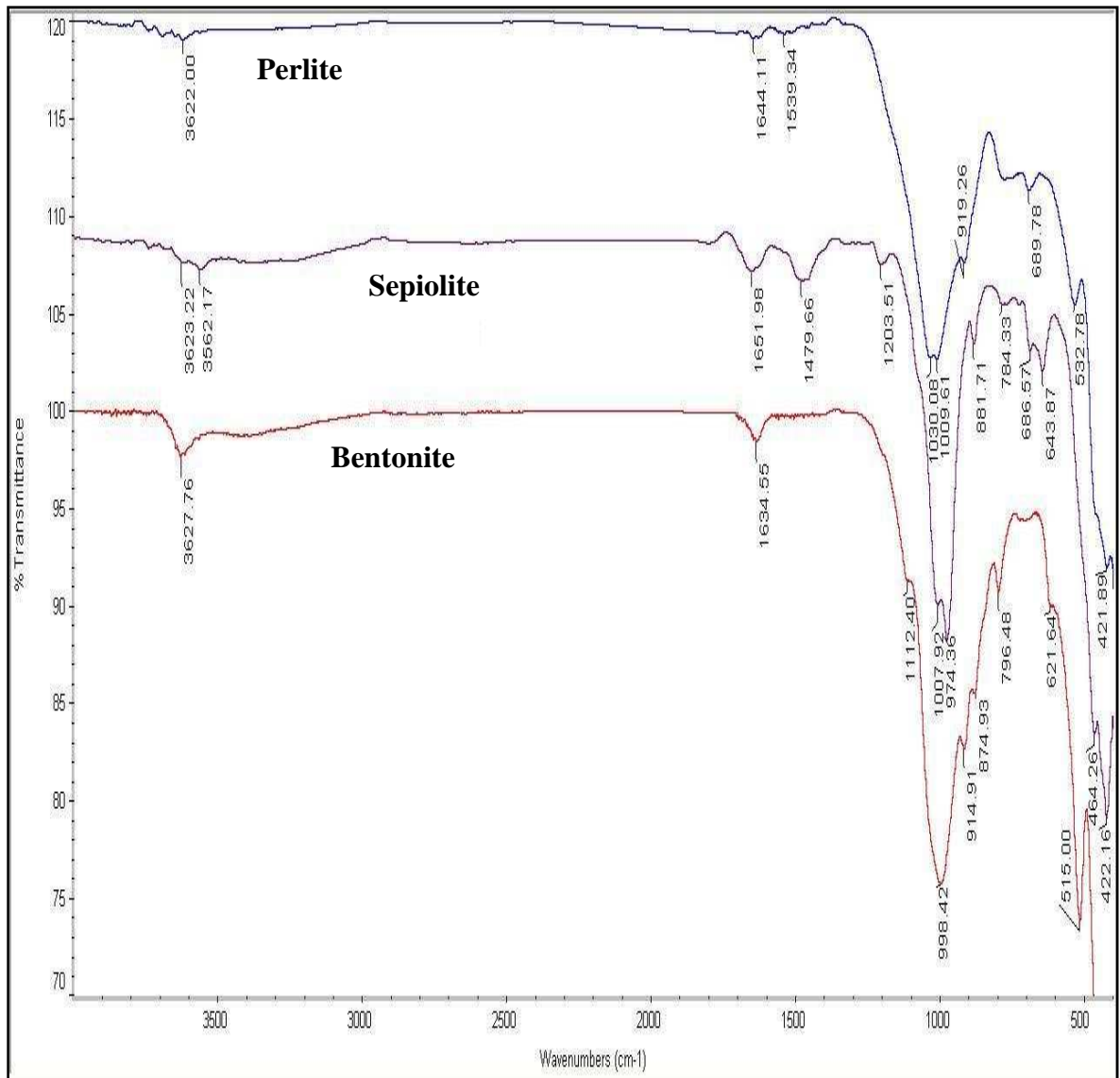


Figure 4.1. FTIR spectra of virgin adsorbents.

In the region of OH stretching vibration, all adsorbents showed bands around 3400-3600 cm^{-1} . For typical clay minerals the bands around 3620 cm^{-1} are attributed to the inner hydroxyl groups between tetrahedral and octahedral sheets. On the other hand, the bands in 1300-400 cm^{-1} region are due to Si-O stretching and bending, and O-H bending which is strongly influenced by the layering of clays. An absorption band around 1640 cm^{-1} is due to the bending vibration of adsorbed water molecule (Stuard, 2004).

4.1.4. X-ray Diffraction (XRD) Analysis of Virgin Adsorbents

The mineralogical compositions of adsorbents were investigated by XRD analysis and XRD patterns of adsorbents are illustrated in Figure 4.2- 4.3 and Figure 4.4 (Table B1, B3, B5).

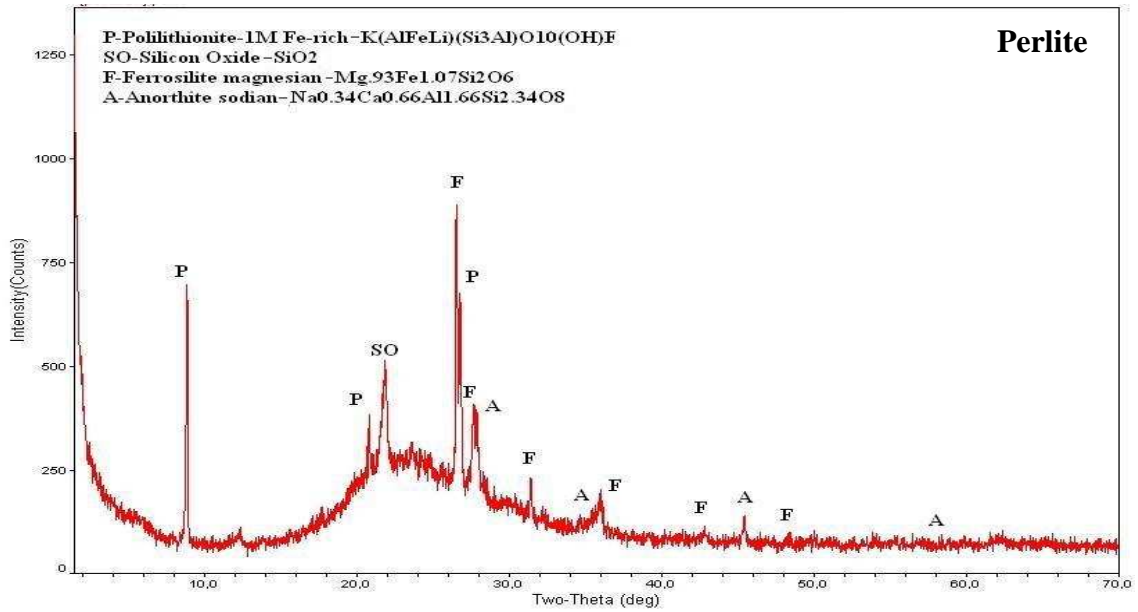


Figure. 4.2. XRD patterns of perlite.

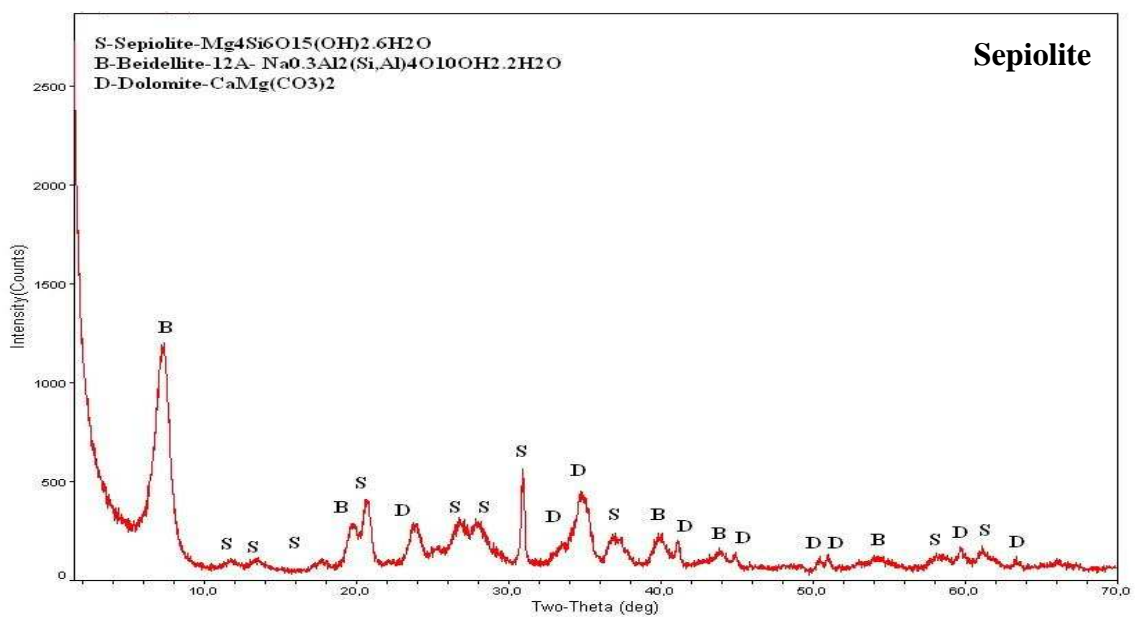


Figure. 4.3. XRD patterns of sepiolite.

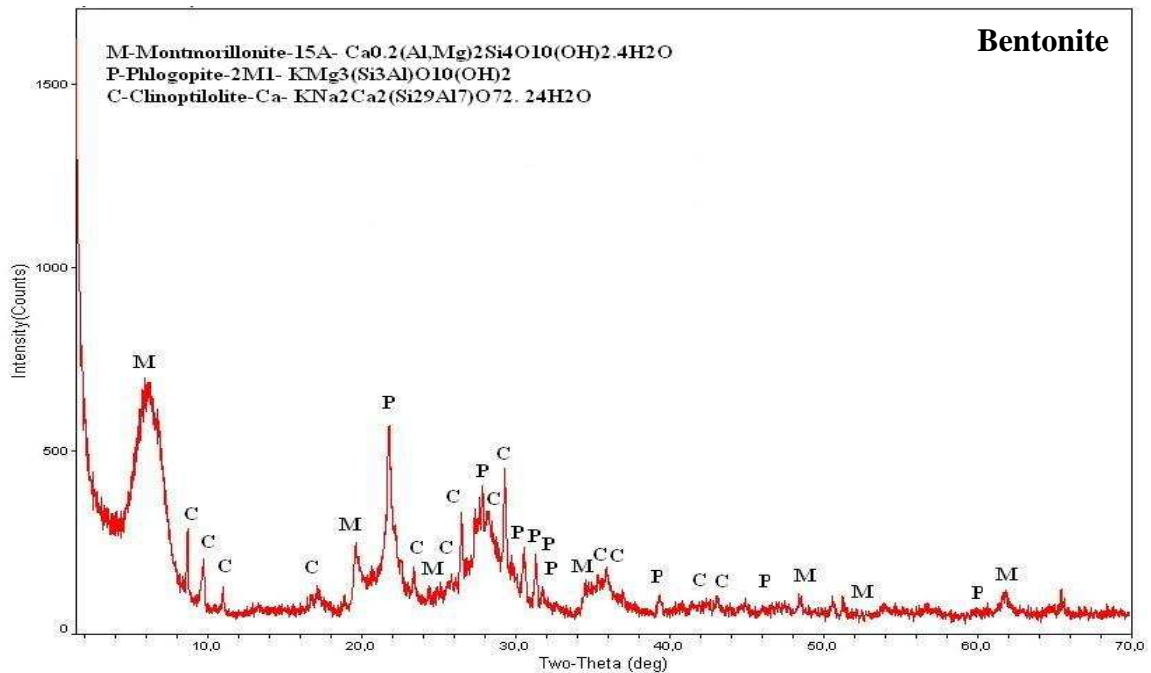


Figure 4.4. XRD pattern of bentonite.

According to the results shown in Figure 4.2 the most intense peaks of perlite were identified as Ferrosilite magnesian ($\text{Mg}_{.93}\text{Fe}_{1.07}\text{Si}_2\text{O}_6$) at $2\theta = 26.600^\circ$ (100 %) and Polilithionite-1M Fe-rich ($\text{K}(\text{AlFeLi})(\text{Si}_3\text{Al})\text{O}_{10}(\text{OH})\text{F}$) at $2\theta = 8.918^\circ$ (94.6 %).

For the sepiolite the most intense peaks (Figure 4. 3) were identified as Beidellite-12A ($\text{Na}_{0.3}\text{Al}_2(\text{Si},\text{Al})_4\text{O}_{10}\text{OH}_2 \cdot 2\text{H}_2\text{O}$) at $2\theta = 7.460^\circ$ (100 %), Dolomite ($\text{CaMg}(\text{CO}_3)_2$) at $2\theta = 31.020^\circ$ (48.8 %) and Sepiolite ($\text{Mg}_4\text{Si}_6\text{O}_{15}(\text{OH})_2 \cdot 6\text{H}_2\text{O}$) at $2\theta = 20.740^\circ$ (32.7 %).

Bentonite has three intense peaks (Figure 4.4) identified as Phlogopite-2M1 ($\text{KMg}_3(\text{Si}_3\text{Al})\text{O}_{10}(\text{OH})_2$) at $2\theta = 21.860^\circ$ (100 %), Montmorillonite-15-A ($\text{Ca}_{0.2}(\text{Al},\text{Mg})_2\text{Si}_4\text{O}_{10}(\text{OH})_2 \cdot 4\text{H}_2\text{O}$) at $2\theta = 6.180^\circ$ (60.7 %) and Clinoptilolite-Ca ($\text{KNa}_2\text{Ca}_2(\text{Si}_{29}\text{Al}_7)\text{O}_{72} \cdot 24\text{H}_2\text{O}$) at $2\theta = 27.921^\circ$ (48 %).

4.1.5. Scanning Electron Microscopy (SEM) of Adsorbents

The surface morphology of adsorbents was studied by SEM and EDAX analysis. The SEM images of perlite, sepiolite, and bentonite adsorbents are represented in Figure 4.5, Figure 4.6, Figure 4.7, respectively at five different magnification.

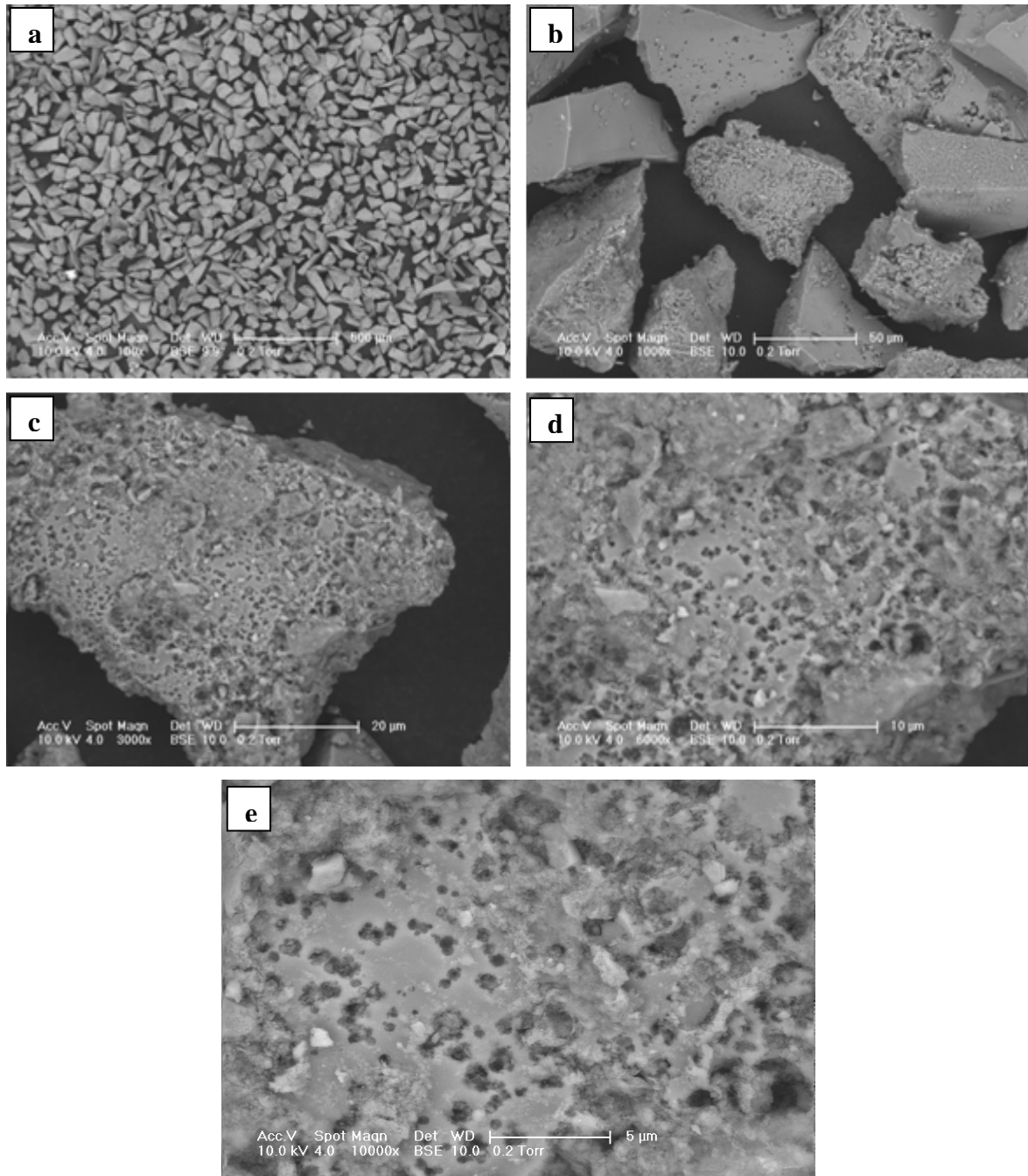


Figure 4.5. SEM images of perlite (a)100x, b)1000x, c) 3000x, d) 6000x, e) 10000x).

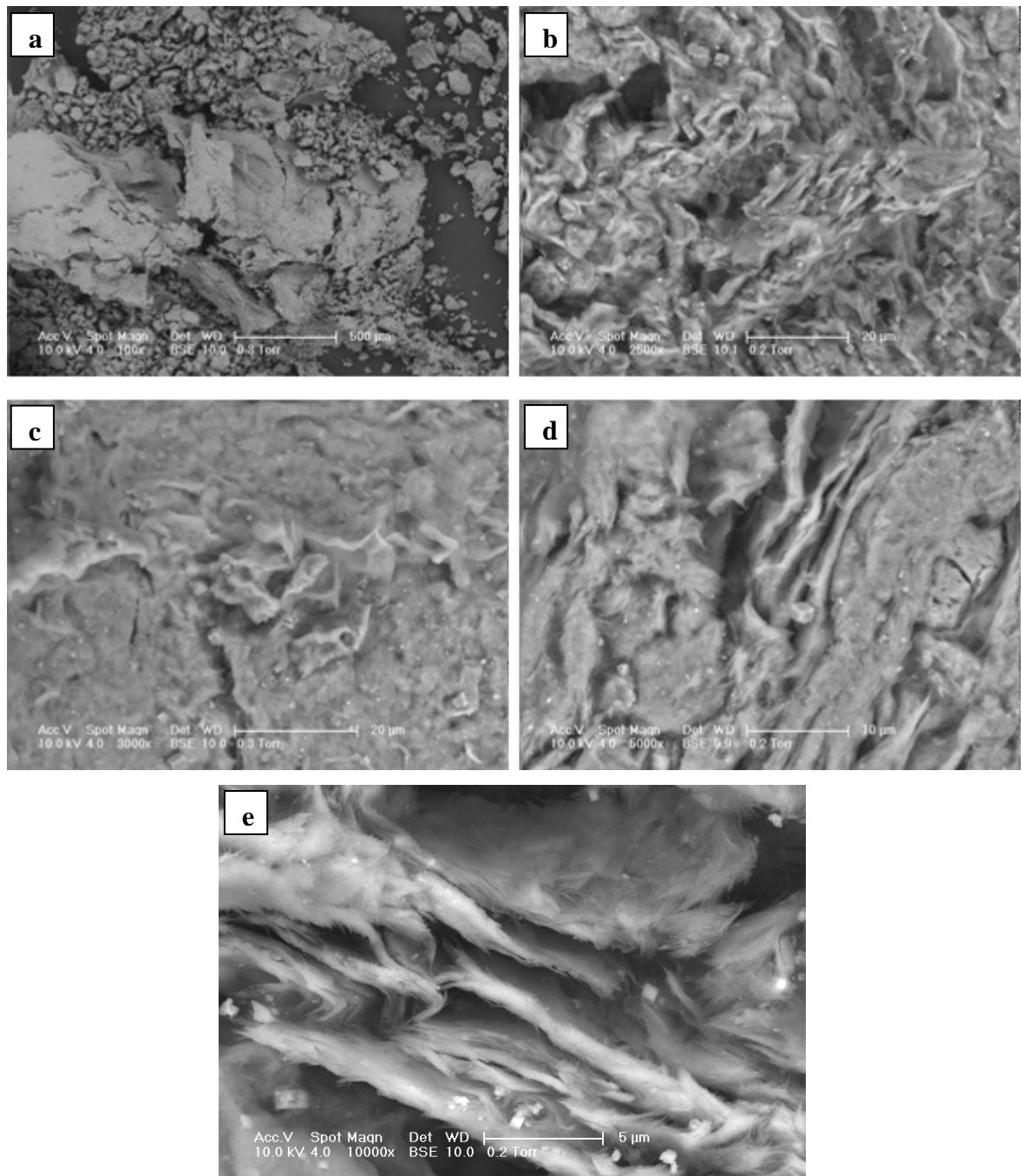


Figure 4.6. SEM images of sepiolite (a)100x, b)1000x, c) 3000x, d) 6000x, e) 10000x).

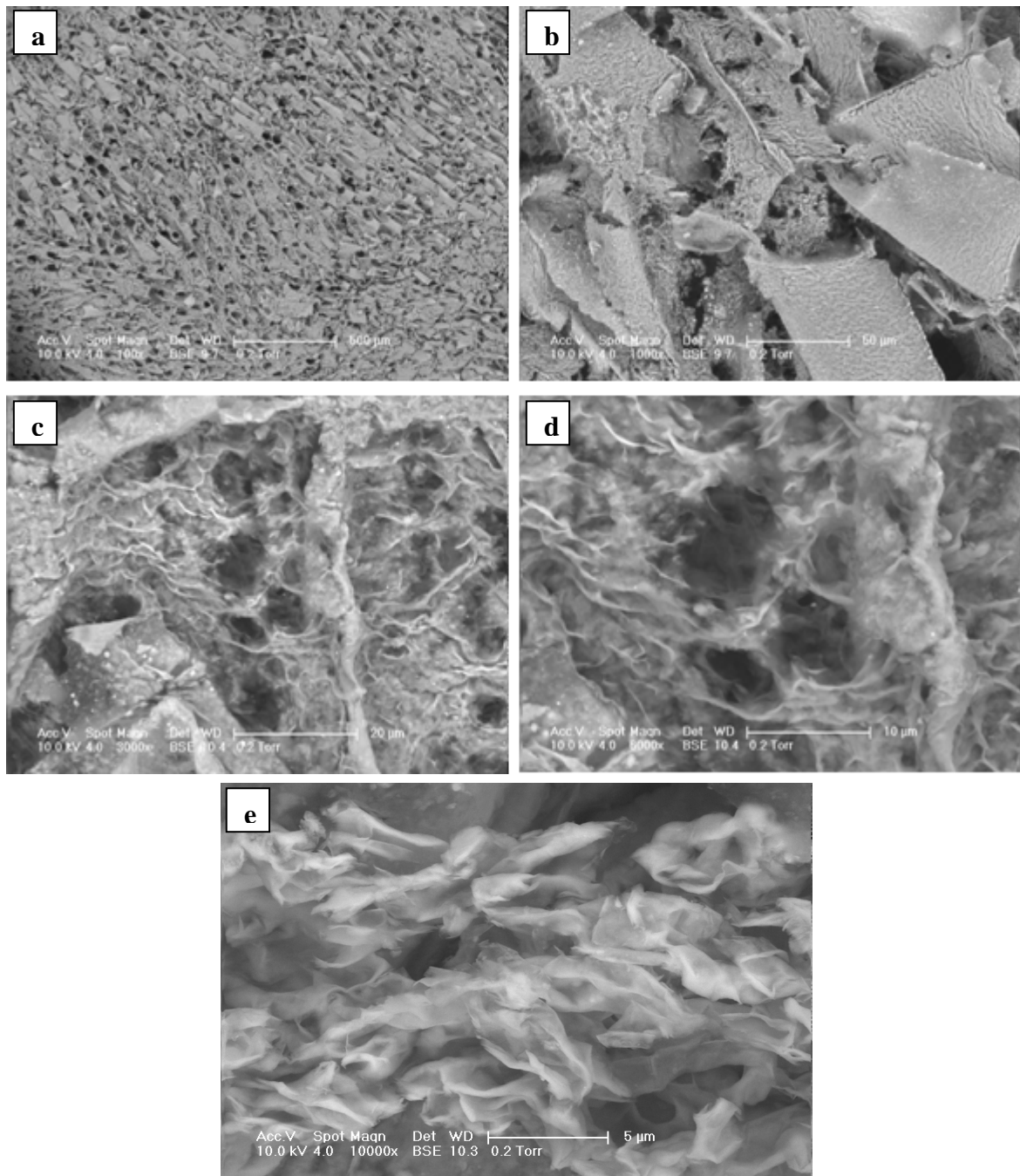


Figure 4.7. SEM images of bentonite (a)100x, b)1000x, c) 3000x, d) 6000x, e) 10000x).

As can be seen from the figures all types of adsorbents have a porous structure. While crystallites on the surface of sepiolite (Figure 4.6) can be attributed to the dolomite particles, rough surfaces of bentonite (Figure 4.7) may indicate the swelling characteristic of montmorillinite particles. Unexpanded perlite (Figure 4.5), which is a glassy volcanic

rock, seems to be dominated by an amorphous phase with inclusions of crystallites, which are supposed to be formed during the slow freezing of lava.

The EDAX analysis of adsorbents, which gave information on the semiquantitative elemental composition of them, were illustrated in Table 4.3.

Table 4.3. EDAX analysis of adsorbents.

Element (Wt %)	Perlite	Sepiolite	Bentonite
C K	16.84	16.78	18.01
O K	29.83	41.32	38.23
Na K	1.36	0.94	2.10
Mg K	1.13	11.81	2.10
Al K	12.50	3.95	9.12
Si K	21.45	22.77	24.37
K K	6.34	0.41	0.59
Ca K	1.35	1.32	0.87
Fe K	3.78	0.69	4.6
Cu K	4.96	-	-
Ti K	0.47	-	-
Total	100	100	100

All investigated adsorbents have similar silicon content. On the other hand, the magnesium content of sepiolite is remarkably high while iron and aluminium are found in lower quantities compare to the amounts detected in other adsorbents.

EDAX analysis combined with XRD results shows that most of the magnesium is originated from the presence of sepiolite and dolomite. The high iron and potassium content of perlite determined by EDAX analysis is in a good agreement with the mineralogical composition of perlite obtained by XRD analysis.

4.2. Sorption Kinetics of OTC on Adsorbents

Adsorption kinetics, which describes adsorbate uptake rate, is strongly influenced by several parameters related to the state of the adsorbent and to the physico-chemical

conditions under which adsorption is carried out. The adsorption of organic pollutants by natural materials in aqueous solution is a phenomenon with often complex kinetics due to their heterogeneous reactive surface. Since the rate of adsorption controls the residence time of adsorbate at the solid liquid interfaces, it is an important factor for the performance of adsorption process. In order to compare the adsorption efficiencies of perlite, sepiolite, and, bentonite for the sorption of OTC (initial concentration= 115 mg L^{-1}) a series batch adsorption kinetic experiments were performed at pH 6.5 and $25 \text{ }^{\circ}\text{C}$ for 28 h contact time period. Figure 4.8 shows the plot of the amount of OTC adsorbed (mg g^{-1}) against contact time for each of the adsorbent at 10 g L^{-1} concentration.

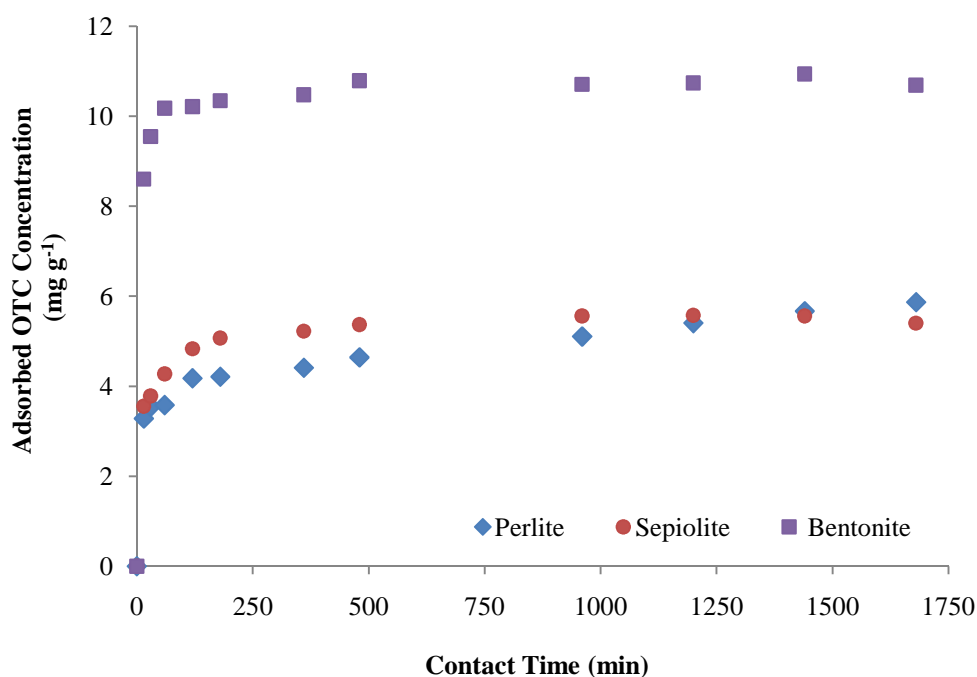


Figure 4.8. Kinetics of OTC sorption ($[\text{OTC}]_i = 115 \text{ mg L}^{-1}$; $[\text{adsorbent}] = 10 \text{ g L}^{-1}$; $\text{pH}_i = 6.5$; $25 \text{ }^{\circ}\text{C}$).

As observed from Figure 4.7, perlite and sepiolite exhibited similar performance for the adsorption of OTC at pH 6.5 although their textural properties and CECs are remarkably different (Table 4.1- Table 4.2) and about 52 % OTC removal was achieved at equilibration with these adsorbents. On the other hand, the sorption rate of OTC on bentonite was 95 %. While the adsorption equilibration value, q_e obtained for perlite and sepiolite was 5.87 and 5.56 mg g^{-1} , respectively it was 10.93 mg g^{-1} for bentonite. As

opposed to the sorption on perlite and sepiolite, there was an initially rapid and linear increase in the sorbed amount of OTC on bentonite. This rapid sorption could reflect the surface layer sorption of OTC and a marginal increase in OTC sorption, after reaching the plateau within 6 hours, could be attributed to pore diffusion.

In order to investigate the adsorption mechanism of OTC on the investigated adsorbents, pseudo-first-order, pseudo-second-order, Elovich, and intra-particle diffusion kinetic models were used to fit experimental data. The equations of these kinetic models are listed in Table 4.4.

Table 4.4. Kinetic model equations.

Kinetic Model	Equation	Linear form of equation	Plot
Pseudo-first-order	$\frac{dq_t}{dt} = k_1(q_e - q_t)$	$\log(q_e - q_t) = \log(q_e) - \frac{k_1}{2.303} t$	$\log(q_e - q_t)$ vs. t
Pseudo-second order	$\frac{dq_t}{dt} = k_2(q_e - q_t)^2$	$\frac{t}{q_t} = \frac{1}{k_2 q_e^2} + \frac{t}{q_e}$	t/q_t vs. t
Simple Elovich	$\frac{dq_t}{dt} = \alpha \exp(-\beta q_t)$	$q_t = \frac{1}{\beta} (\ln(\alpha\beta) + \ln t)$ $q_t = a + b \ln t$	q_t vs. $\ln t$
Intraparticle diffusion	$q_t = k_p \sqrt{t}$ or $q_t = k_p \sqrt{t} + C$		q_t vs. $t^{0.5}$

The pseudo-first order equation of Lagergren is generally expressed as follows:

$$\frac{dq_t}{dt} = k_1(q_e - q_t) \quad (4.1)$$

where q_e and q_t (mg g^{-1}) are the amounts of OTC sorbed on adsorbents at equilibrium and at time t , respectively, and k_1 (min^{-1}) is the rate constant of first-order sorption model.

After integration and applying boundary conditions $t=0$ to $t=t$ and $q_t=0$ to $q_t=q_t$, the integrated form of equation becomes,

$$\log(q_e - q_t) = \log(q_e) - \frac{k_1}{2.303} t \quad (4.2)$$

To evaluate suitability of the model to kinetic data of OTC the plot of $\log(q_e - q_t)$ vs. t is shown in Figure 4.9 for each of the three different adsorbents. The values of first order model equilibrium rate constants, k_1 which is the slope of each line in Figure 4.9 and the corresponding correlation coefficients are summarized in Table 4.5 together with the kinetic constants of other used models.

In most of the adsorption studies carried out with clays, the pseudo-first-order equation of Lagergren does not fit well with the whole range of contact time and is generally applicable over the initial stage of the adsorption processes (Aksu and Tezer, 2000; Chiou and Li, 2002). However, in this study, the model was applied to almost whole contact time range for perlite (1200 min) and sepiolite (960 min) whereas for bentonite (60 min) it is applicable over the initial stage.

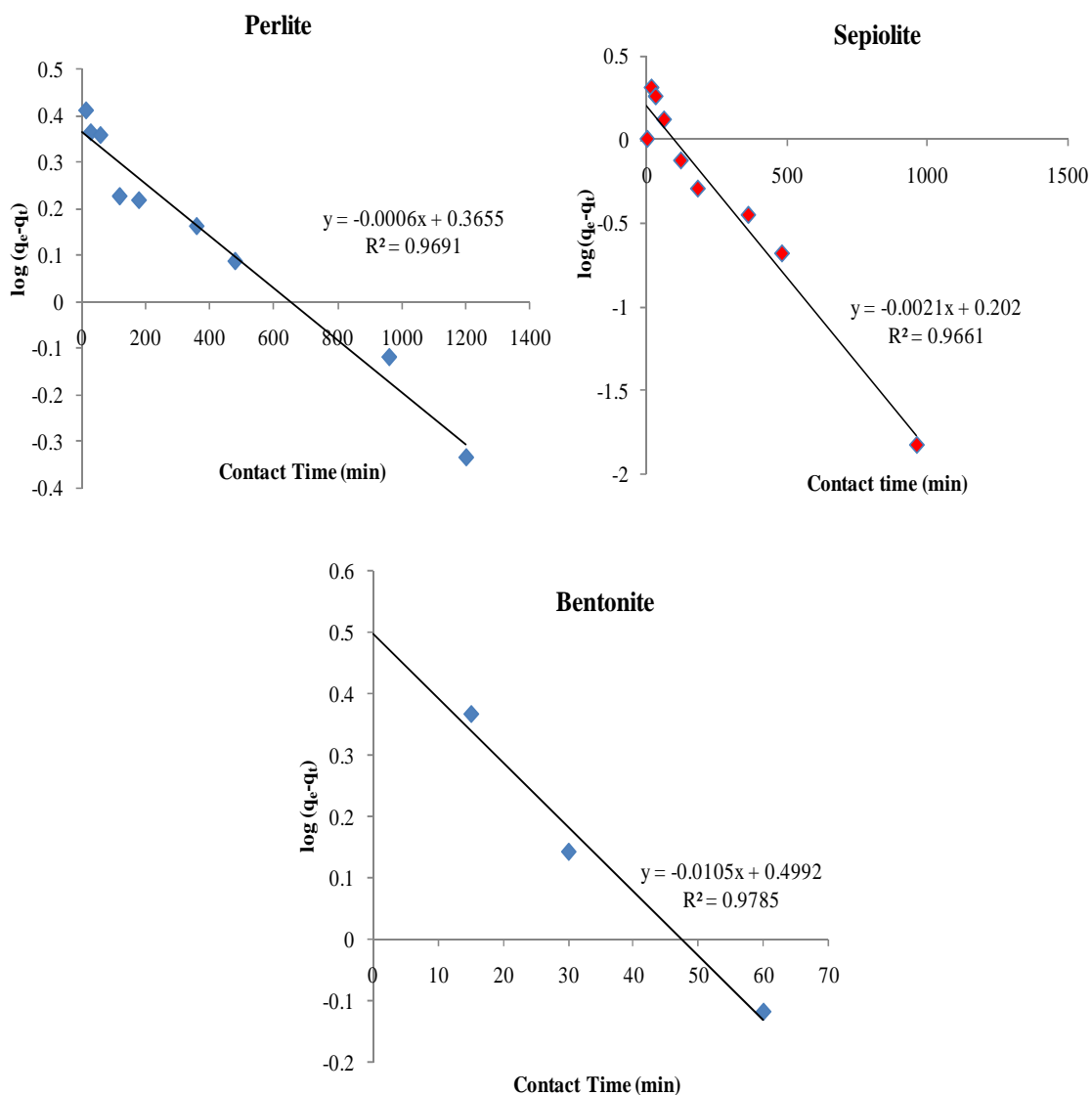


Figure 4.9. Pseudo-first-order order plots of OTC adsorption ($[OTC]_i = 115 \text{ mg L}^{-1}$; $[\text{adsorbent}] = 10 \text{ g L}^{-1}$; $\text{pH}_i = 6.5$; 25°C).

For each adsorbent the predicted values of equilibrium adsorption were calculated according to the model (Table 4.5). The conformity between experimental equilibrium adsorption and the model predicted values was expressed by SSE values. While the values of determination coefficient for the plots were in the range 0.97–0.98 the calculated sorption capacity values obtained from this kinetic model do not give reasonable values compared to the experimental sorption capacity and SSE values are noticeably high. These findings suggested that the pseudo-first-order sorption rate expression of Lagergren did not describe the sorption of OTC onto three different adsorbents.

Table 4.5. Experimental and predicted adsorption kinetics of OTC by different adsorbents.

	Adsorbent		
	Perlite	Sepiolite	Bentonite
q_e^* (exp) (mg g ⁻¹)	5.87	5.57	10.93
Pseudo-first order model			
k_1 (min ⁻¹)	1.38×10^{-3}	4.84×10^{-3}	24×10^{-3}
q_e^* (calc) (mg g ⁻¹)	2.32	1.77	3.15
R ²	0.97	0.98	0.98
SSE	16.52	>100	>100
Pseudo-second order model			
k_2 (g mg ⁻¹ min ⁻¹)	2.67×10^{-3}	1.30×10^{-2}	1.65×10^{-2}
q_e (calc) (mg g ⁻¹)	5.02	5.56	10.87
R ²	0.99	0.99	0.99
SSE	2.58	0.15	0.09
Elovich model			
a (mg g ⁻¹)	1.62	2.53	8.19
b (mg g ⁻¹ min ⁻¹)	0.53	0.43	0.38
R ²	0.94	0.93	0.82
SSE	0.10	0.08	0.09
Intraparticle diffusion model			
k_p (mg min ^{0.5} g ⁻¹)	6.63×10^{-2}	16.59×10^{-2}	39.78×10^{-2}
C	3.13	2.93	7.17
q_e (calc) (mg g ⁻¹)	5.85	8.68	22.26
R ²	0.99	0.99	0.96
SSE	0.04	9.14	48.71

* q_e (exp) = experimental data of the equilibrium capacity

q_e (calc) = calculated data of the equilibrium capacity obtained by the model

The sorption data were also analyzed in terms of pseudo-second-order mechanism by the following equation:

$$\frac{dq_t}{dt} = k_2(q_e - q_t)^2 \quad (4.3)$$

where q_e and q_t are the sorption capacity at equilibrium and at time t , respectively (mg g^{-1}), and k_2 is the rate constant of pseudo-second order sorption ($\text{g mg}^{-1} \text{min}^{-1}$). For the boundary conditions $t = 0$ to $t = t$ and $q_t = 0$ to $q_t = q_t$, the integrated form of equation becomes,

$$\frac{t}{q_t} = \frac{1}{k_2 q_e^2} + \frac{t}{q_e} \quad (4.4)$$

The slope and intercept of the plot of t/q versus t in Figure 4.10 were used to calculate the pseudo-second-order rate constant, k_2 and the predicted sorption capacities of three different adsorbents. For each adsorbent the values of equilibrium rate constant are presented in Table 4.5 together with the calculated q_e and SSE values.

As can be seen from Figure 4.10 and Table 4.5, pseudo-second-order model adequately fits the data over the entire course of the experiment with the high correlation coefficients which are above 0.99. Moreover, the experimental sorption capacities of adsorbents are close to the theoretical values estimated from the model. Hence, SSE values are remarkably lower than those obtained by the application of pseudo-first-order model. These findings reveals that the sorption process follows the pseudo-second-order model for all types of adsorbents. This result suggests that the rate limiting step of OTC adsorption on natural adsorbents was the chemisorption similar to the previous study performed by Na- and HDTMA modified zeolite (Şalcıoğlu, 2007).

According to the model, the calculated initial sorption rates ($k_2 q_e^2$) of perlite and sepiolite were 0.067 and 0.40 $\text{mg g}^{-1} \text{min}^{-1}$, respectively. Among three adsorbents used in this study, bentonite has the fastest initial sorption rate and it was found as 1.95 mg g^{-1}

min^{-1} which is noticeably higher than that of natural zeolite ($1-0.76 \times 10^{-2} \text{ mg g}^{-1} \text{ min}^{-1}$) having a larger particle size (Şalcıoğlu, 2007).

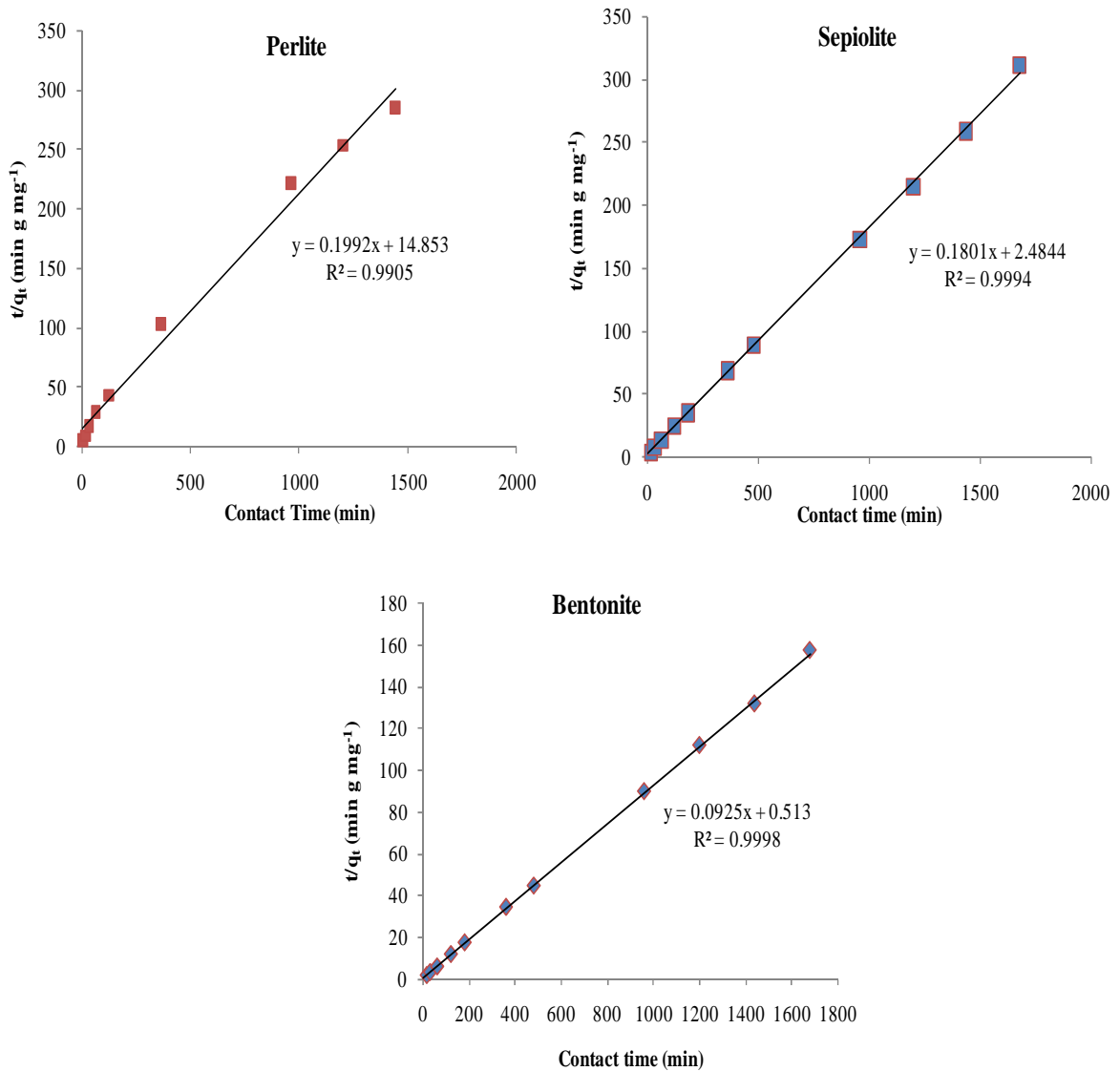


Figure 4.10. Pseudo-second-order order plots of OTC adsorption ($[\text{OTC}]_i = 115 \text{ mg L}^{-1}$; $[\text{adsorbent}] = 10 \text{ g L}^{-1}$; $\text{pH}_i = 6.5$; 25°C).

Elovich model, which has general application to chemisorption kinetics, assumes that the active sites of adsorbents are heterogeneous and exhibit different activation energy for the sorption of pollutants. In reactions involving chemisorption of adsorbates on a solid surface without the desorption of the pollutants, the rate decreases with time due to an increased surface coverage.

Elovich model is expressed by the following equation (Ho and McKay, 2004),

$$\frac{dq_t}{dt} = \alpha \exp(-\beta q_t) \quad (4.5)$$

Among the boundary conditions $t = 0$ to $t = t$ and $q_t = 0$, the integrated form of equation becomes,

$$q_t = 1/\beta (\ln(\alpha\beta) + \ln t) \quad (4.6)$$

Equation is simplified as follows:

$$q_t = a + b \ln t \quad (4.7)$$

According to the Elovich model, the slope and intercept of plot of q vs. $\ln(t)$, which is shown in Figure 4.11, were used to calculate the values of the a and b constants (Table 4.5). b ($\text{mg g}^{-1} \text{min}^{-1}$) is the initial adsorption rate constant and a (mg g^{-1}) is related to the extent of surface coverage and activated energy for the chemisorption.

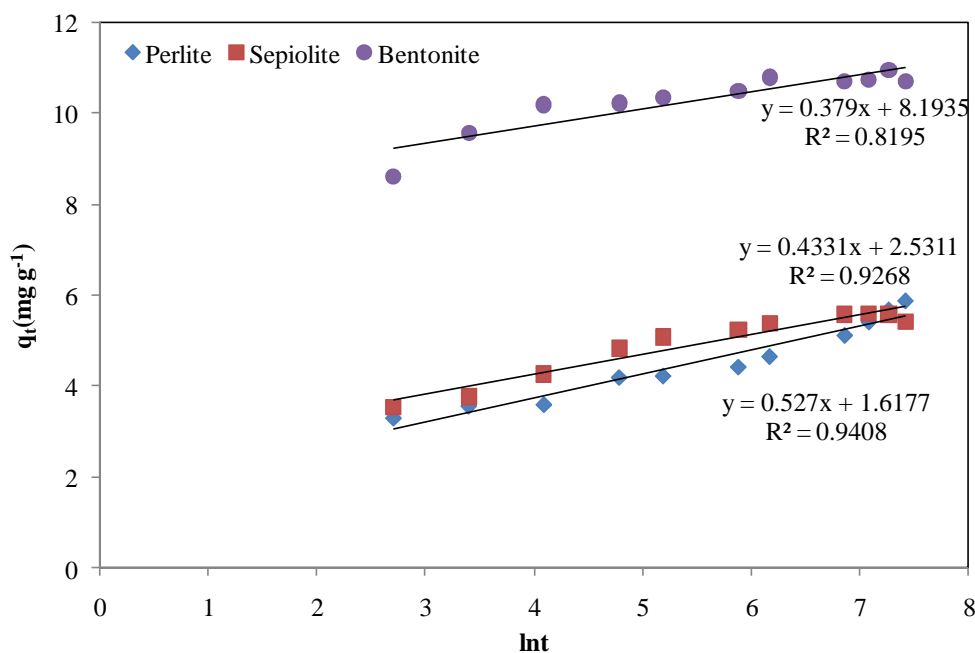


Figure 4.11. Sorption of OTC described by Elovich model ($[\text{OTC}]_i = 115 \text{ mg L}^{-1}$; $[\text{adsorbent}] = 10 \text{ g L}^{-1}$; $\text{pH}_i = 6.5$; 25°C).

The values of determination correlation coefficient for the plots were in the range 0.82–0.94. However, the calculated sorption capacity values obtained from this kinetic model fit with experimental sorption capacity and SSE values ranged from 0.08 to 0.10. These findings suggest that the sorption kinetics can be described by Elovich model. The values of “a”, Elovich model parameter for bentonite and sepiolite suggest that due to the higher pore volume of sepiolite OTC adsorption mainly occurs in the interior surface of adsorbent whereas for bentonite higher sorption is expected on the surface of adsorbent regarding the higher values of “a”.

Finally, sorption kinetic data were analyzed to determine whether intraparticle diffusion is rate limiting step in adsorption process. Many researchers have modeled intraparticle diffusion in the sorption of the organic contaminants in aqueous environment (Werth and Reinhard, 1997; Ball and Roberts, 1991). The intraparticle diffusion approach can be described by Equation 4.8 (Weber and Morris, 1963). This model suggests that the sorption process is considered to be controlled by the internal diffusion with a minor effect of the external diffusion (Khraisheh et al., 2002).

$$q_t = k_p \sqrt{t} \quad (4.8)$$

where q_t (mg g^{-1}) is the concentration of OTC sorbed at time t and k_p ($\text{mg g}^{-1} \text{min}^{-0.5}$) is the intraparticle rate constant.

The fraction of OTC uptake against square root of contact time ($t^{0.5}$) is shown in Figure 4.12. This figure reveals that the data obtained by different adsorbents exhibited multi-linearity character except those for perlite. However, none of the straight lines obtained for three different adsorbents passed through the origin (Figure 4.12). It was suggested that this occurs when external diffusion is dominant and intraparticle diffusion is not a rate-limiting step (Poots et al., 1976). In such cases, following equation is used to describe the model.

$$q_t = k_p \sqrt{t} + C \quad (4.9)$$

C is the intercept and the values of C give an idea about the thickness of boundary layer (Table 4.5), i.e. the larger the intercept the greater is the boundary layer effect (Amin, 2009). The smallest C value was obtained for sepiolite which has the largest pore volume. The intraparticle diffusion equation was fitted for the data obtained within 60 min contact time for bentonite, and 180 min for sepiolite whereas model was applied in whole time interval studied for perlite. This period, when a linear relationship was obtained, was the gradual adsorption stage where intraparticle diffusion started.

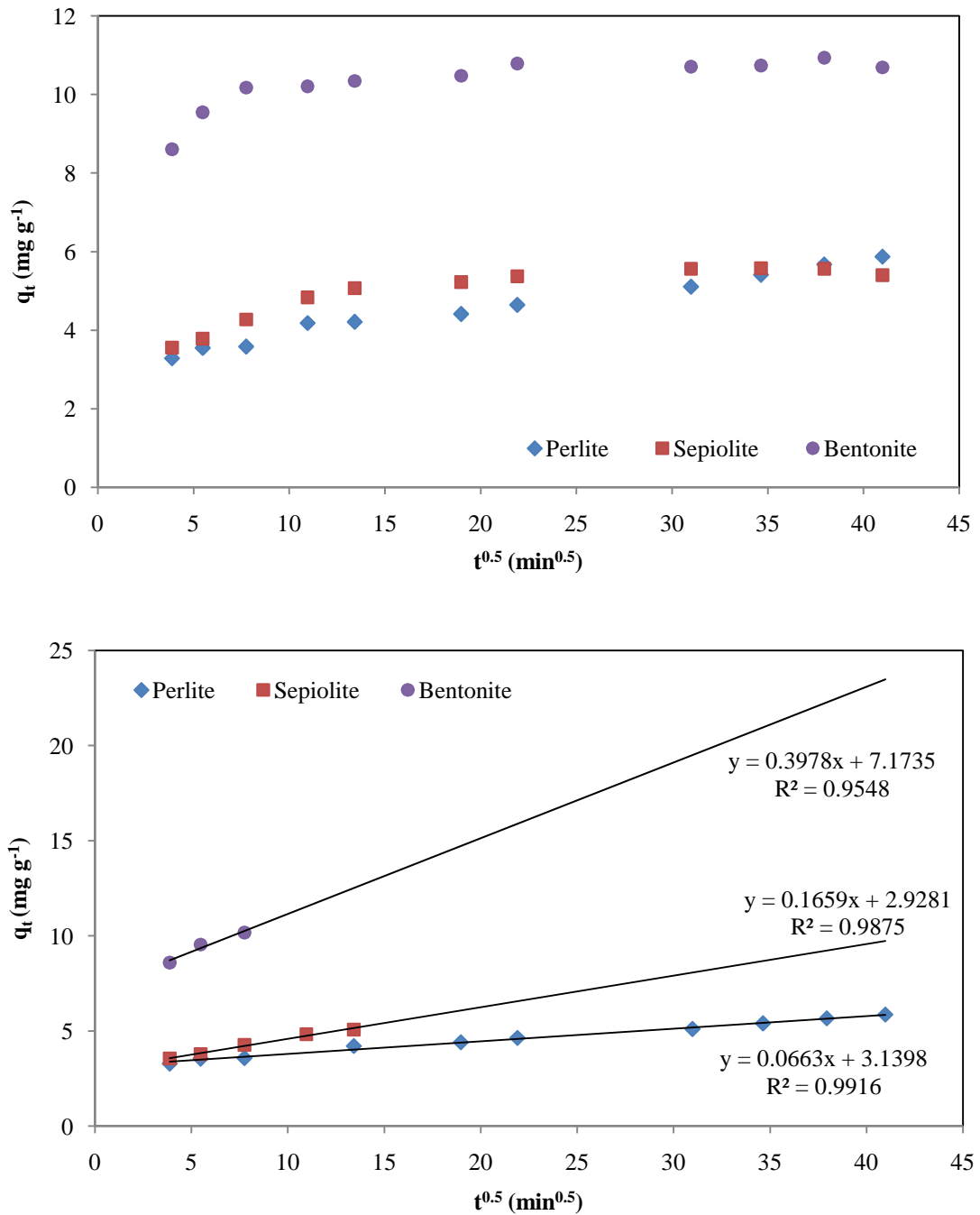


Figure 4.12. Intraparticle diffusion model plot of OTC adsorption ($[OTC]_i = 115 \text{ mg L}^{-1}$; $[\text{adsorbent}] = 10 \text{ g L}^{-1}$; $\text{pH}_i = 6.5$; $25 \text{ }^\circ\text{C}$).

The results indicate that particle diffusion is involved in the sorption of OTC on adsorbents but it is not the only rate-limiting mechanism and that some other mechanisms can be involved.

Figure 4.13 compares the experimental (symbols) and predicted (lines) q_t values for all types of adsorbents. As can be seen from the figure pseudo-second-order and Elovich model best fit to all adsorbents whereas intraparticle diffusion model only fits to perlite for the whole contact time period.

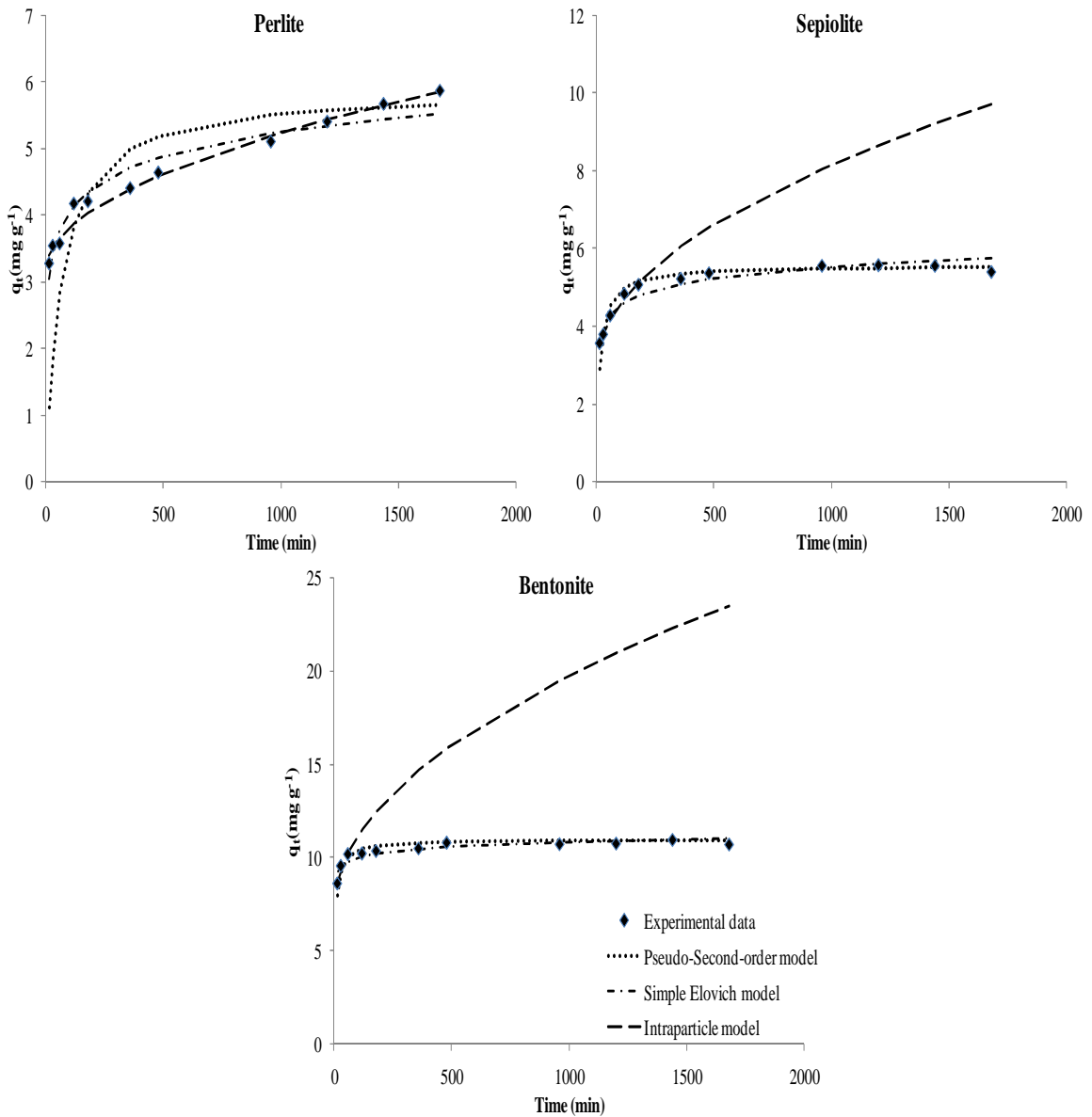


Figure 4.13. Comparison of experimental and estimated sorption kinetics of OTC.

4.3. Equilibrium Modeling

The batch adsorption equilibrium experiments of OTC onto perlite, sepiolite, and bentonite were conducted at 25 °C and pH 6.5 by the using various concentrations of antibiotic ranged from 0.03-0.4 mg mL⁻¹. Considering the results of previous kinetic experiments, 24 h was selected as equilibration time. The amount of OTC adsorbed per unit mass of clay, q_e (mg g⁻¹) was correlated with liquid phase concentration at equilibrium, C_e (mg L⁻¹) using different adsorption isotherm models. The equilibrium data which is known as adsorption isotherm, can describe how adsorbate interacts with adsorbent and so they can provide critical information on the capacity of the adsorbent. Langmuir, Freundlich, Temkin, and Redlich–Peterson models, which are the most frequently used two- and three-parameter equations in the literature, were applied to the equilibrium experimental data.

The Langmuir isotherm model, which indicates the monolayer coverage of the homogeneous surface of a adsorbent and negligible interaction of adsorbed molecules, is given by the following equation,

$$q_e = \frac{qK_L C_e}{1 + K_L C_e} \quad (4.10)$$

where C_e (mg L⁻¹) is the equilibrium concentration of the adsorbate in the aqueous solution, q_e (mg g⁻¹) is the equilibrium adsorption capacity of adsorbent, q and K_L are Langmuir constants related to maximum adsorption capacity and energy of adsorption, respectively.

The Freundlich isotherm model is an empirical equation that encompasses the heterogeneity of the adsorption sites and the exponential distribution of sites and their energies. In general, the Freundlich equation gives better correlation between theoretical and experimental data for natural adsorbents. Freundlich isotherm is expressed by equation 4.11.

$$q_e = K_F \times C_e^n \quad (4.11)$$

where K_F ($\text{mg g}^{-1})(\text{L mg}^{-1})^n$ and n are the Freundlich constants which indicate adsorption capacity and intensity, respectively.

The Temkin isotherm model is used to explain adsorption on heterogenous surfaces and assumes that the heat of adsorption of all the molecules decreases linearly with coverage due to adsorbent-adsorbate interactions (Temkin, 1940). Temkin isotherm equation is given by the following equation,

$$q_e = \frac{RT}{b} \ln(K_T C_e) \quad (4.12)$$

where $RT/b = B_1$ and B_1 is related to the heat of adsorption, T is the absolute temperature in K° , R is the universal gas constant, $8.314 \text{ J mol}^{-1} \text{ K}^{-1}$, K_T the equilibrium binding constant (L mg^{-1}) (Table 4.7).

The Redlich–Peterson equation which is given by Equation 4.13, incorporates with the features of the Langmuir and Freundlich,

$$q_e = \frac{K_{RP} C_e}{1 + a C_e^\beta} \quad (4.13)$$

where K_{RP} (L g^{-1}), a (L mg^{-1}), and β are Redlich–Peterson isotherm parameters. The exponent β varies between 1 and 0 (Redlich and Peterson, 1959).

In Table 4.6 the equations of Langmuir, Freundlich, Temkin, and Redlich Peterson isotherm models and their linearized forms are summarized.

Table 4.6. Adsorption isotherms equations.

Isotherm	Equation	Linear form of equation	Plot
Freundlich	$q_e = K_F \times C_e^n$	$\log q_e = n \log C_e + \log K_F$	$\log q_e$ vs. $\log C_e$
Langmuir	$q_e = \frac{qK_L C_e}{1 + K_L C_e}$	$\frac{C_e}{q_e} = \frac{C_e}{q} + \frac{1}{K_L q}$	C_e/q_e vs. C_e
Temkin	$q_e = B_1 \ln(K_T C_e)$	$q_e = B_1 \ln K_T + B_1 \ln C_e$	q_e vs. $\ln C_e$
Redlich-Peterson	$q_e = \frac{K_{RP} C_e}{1 + a C_e^\beta}$	$\ln \left(K_{RP} \frac{C_e}{q_e} - 1 \right) = \ln a + \beta \ln C_e$	$\ln[(K_{RP} C_e/q_e) - 1]$ vs. $\ln C_e$

The experimental equilibrium data of OTC on three different adsorbents are given in Figure 4.14 as a plot of equilibrium solid phase concentration, q_e , versus equilibrium liquid phase concentration C_e . The figure also indicates the predicted data (lines) by four different isotherm models. The parameters of the models obtained by using the linearizing forms of equations are listed in Table 4.6. The applicability of models is judged by the correlation coefficients of linearized data and SSE values which were calculated with the predicted and the experimental values of sorption capacity are represented in Table 4.7.

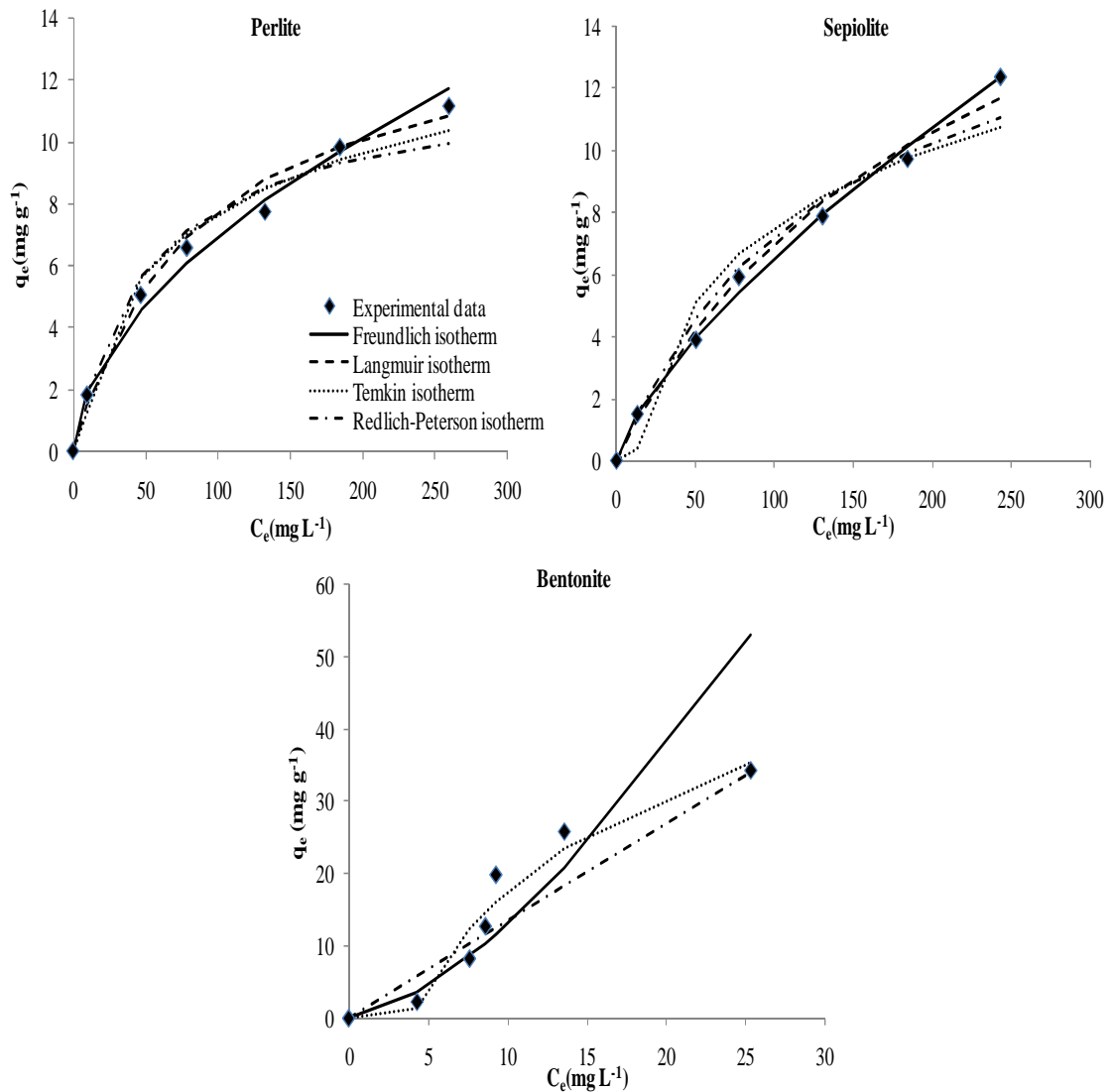


Figure 4.14. Comparison of experimental and estimated sorption isotherms of OTC. ($[OTC]_i = 30 - 400 \text{ mg L}^{-1}$; $[\text{adsorbent}] = 10 \text{ g L}^{-1}$; $pH_i = 6.5$; 25°C ; $t = 24 \text{ h}$).

As can be seen from Figure 4.14, the sorption capacity of all investigated adsorbents increased with increasing OTC concentration. The initial concentration provides an important driving force to overcome all mass transfer resistances.

Table 4.7. Adsorption isotherm parameters.

	Adsorbent		
	Perlite	Sepiolite	Bentonite
Freundlich Isotherm			
n	0.55	0.72	1.51
$K_F (\text{mg g}^{-1})(\text{L mg}^{-1})^n$	0.55	0.24	0.40
R^2	0.99	0.99	0.84
SSE	0.14	0.06	15.97
Langmuir Isotherm			
$K_L (\text{L mg}^{-1})$	0.012	0.005	-0.025
q (mg g^{-1})	14.29	21.74	-32.26
R^2	0.97	0.93	0.19
SSE	0.23	0.14	24.32
Temkin Isotherm			
B_1	2.77	3.56	19.23
$K_T (\text{L mg}^{-1})$	0.16	0.08	0.25
R^2	0.96	0.92	0.94
SSE	0.42	1.60	3.64
Redlich-Peterson isotherm			
K (L g^{-1})	0.22	0.12	4.50
a (L mg^{-1})	0.02	0.01	2.36
β	1	1	0
R^2	0.99	0.95	0.33
SSE	0.35	0.33	10.94

According to the magnitude of SSE, the adsorption equilibrium data of perlite and sepiolite can be satisfactorily described by Freundlich isotherm whereas the adsorption equilibrium data of bentonite can be explained by Temkin isotherm.

Negative values for the Langmuir isotherms parameters as given in Table 4.7 indicate the inadequacy of the isotherm model to explain the adsorption process.

The conformity of the data to the Freundlich equation suggests that heterogeneity in the surface and pores of adsorbent played a role in the adsorption. For perlite and sepiolite the adsorption intensity $n < 1$ indicates favorable adsorption. K_F implies the adsorption capacity of the adsorbent which is higher for perlite than that for sepiolite.

The data of bentonite fitted with Temkin isotherm indicates that the adsorption can be characterized by a uniform distribution of the bonding energies, up to some maximum binding energy.

4.4. Effect of pH on Sorption

Since the pH can affect both the speciation of OTC (Figure 2.3) and the surface charge of adsorbent the effect of this parameter on the adsorption of OTC ($[OTC]_i = 115 \text{ mg L}^{-1}$) was investigated over a wide pH range (2-10.5) and the results were evaluated by both distribution coefficient (K_d) and OTC removal percentage. The distribution coefficient and removal efficiency of OTC were calculated by Equation 4.14 and 4.15, respectively,

$$K_d = \frac{q_e}{C_e} \quad (4.14)$$

$$\text{OTC Removal (\%)} = \frac{C_0 - C_e}{C_0} \times 100 \quad (4.15)$$

K_d = distribution coefficient (L g^{-1} or L kg^{-1}),

q_e = adsorbed OTC concentration (mg g^{-1}),

C_e = equilibrium OTC concentration (mg L^{-1}),

C_0 = initial OTC concentration (mg L^{-1}).

The sorption of OTC on adsorbents is illustrated as a function of initial pH in Figure 4.15 and the equilibrium pH values are also listed in this figure.

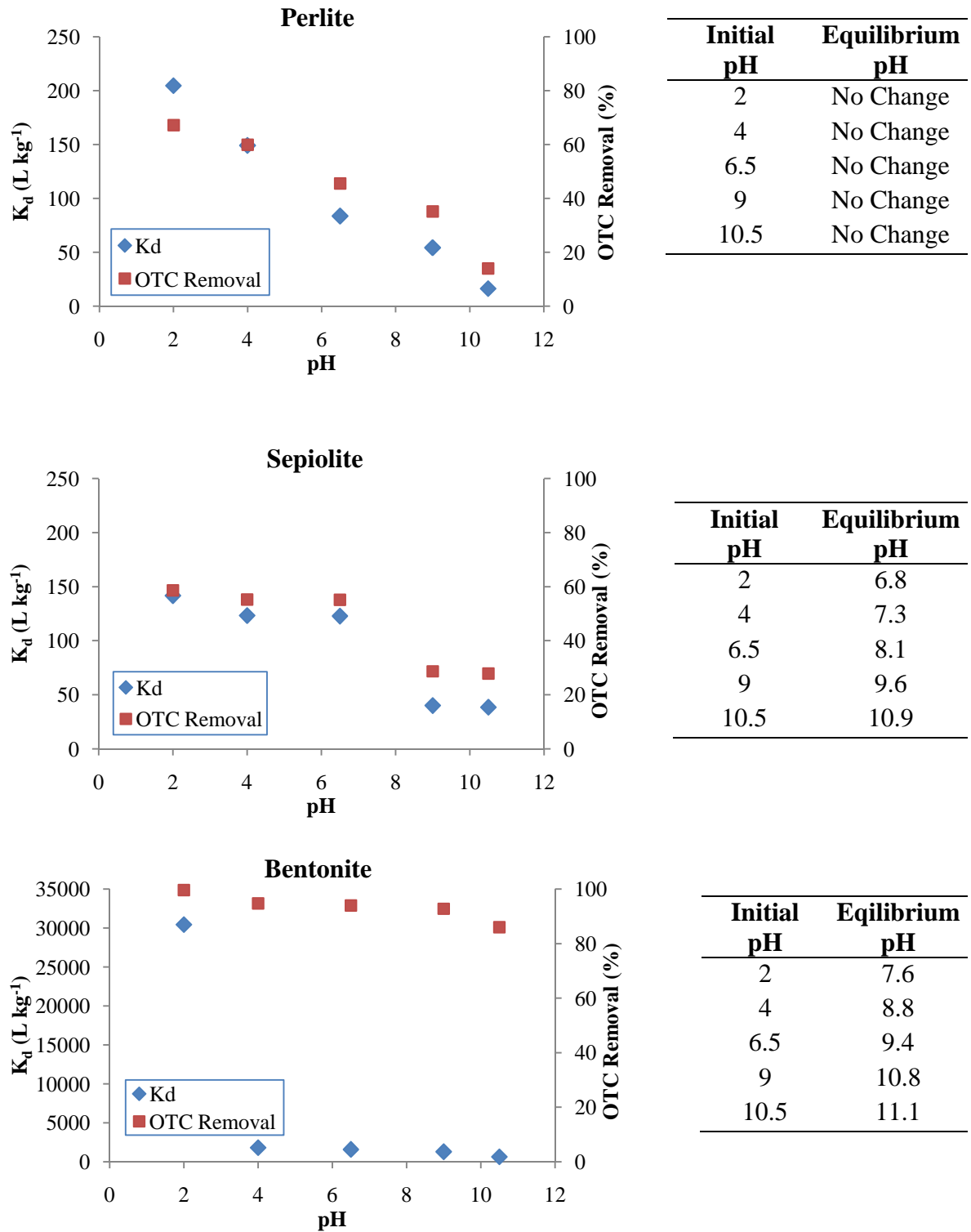


Figure 4.15. Effect of pH on the sorption of OTC.

As stated in figure the pH of perlite slurry did not exhibit any variation during the equilibration period of OTC. Maximum OTC sorption onto perlite occurred at pH 2 was 67.16 %. From a previous study it is known that perlite is negatively charged at a pH range of 3–11 (Doğan et al., 1997). Therefore, this is well expected result since the association of OTC cations with negatively charged perlite could take place as the pH of the solution becomes lower. On the other hand, as the pH value of solution increased, the sorption of OTC decreased due to the repulsion between anionic antibiotic and negatively charged perlite surface. By increasing the pH from 2 to 10.5, K_d decreased from 204.5 to 16.2 L kg⁻¹ and OTC removal decreased from 67.2 to 13.9 % (Figure 4.15). This result obtained at alkaline pH suggests that electrostatic attraction plays a significant role in the sorption of OTC.

As opposed to perlite, the pH values of bentonite and sepiolite slurry showed a noticeable increase at acidic pHs. However, similar to perlite, the maximum OTC sorption onto sepiolite and bentonite occurred when the initial pH of slurry was acidic. The isoelectrical point of sepiolite was reported as 6.6 and 6.3 by Alkan et al. (2005) and Kara et al. (2003), respectively. Considering this value and the pK_{a1} value of OTC (Table 3.1) it is expected to be both sepiolite and OTC have negative charge above pH 9.11 value. Accordingly, the lower sorption of OTC on sepiolite was observed at alkaline pH values.

For the adsorption on bentonite although by increasing the initial pH from 2 to 10.5 K_d decreased from 30,420 to 638 L kg⁻¹, OTC removal did not change significantly, it decreased from 99.7 to 86 % similar to the results of the previous study where OTC removal by natural zeolite decreased from 91 to 82 % (Şalcıoğlu, 2007). This result suggests that the sorption of OTC on bentonite occurred not only by electrostatic attraction but also other mechanisms such as cation bridging (Figuera et al., 2004).

4.5. Released Ions from Adsorbents

Tetracyclines have a number of potential metal binding sites and the ability of tetracyclines to form complexes with di- and trivalent cations has long been known (MacKay and Canterbury, 2005). This ability, which is most strongly pronounced for

hydrophilic tetracyclines (mainly tetracycline and oxytetracycline), can be important in the sorption process since cation exchange mechanism was suggested as a major sorption mechanism for TCs on clays. Therefore, the released ions from the adsorbent surface were investigated by the experiments carried out with 10 g L^{-1} adsorbent and 115 mg L^{-1} OTC without pH adjustment at room temperature. Additionally, experiments were performed in the absence of OTC. The concentrations of various released cations from adsorbents were detected during 24 hr period. The concentrations of Al^{+3} , Na^{+} , Ca^{+} , K^{+} , Mg^{+2} , Fe^{+3} , Mn^{+4} , Cu^{+} , Ti^{+4} and, Zn^{+2} ions exhibited an increasing trend by increasing the contact time. In Figure 4.16 only the ions which have concentration higher than 0.1 mg L^{-1} are illustrated.

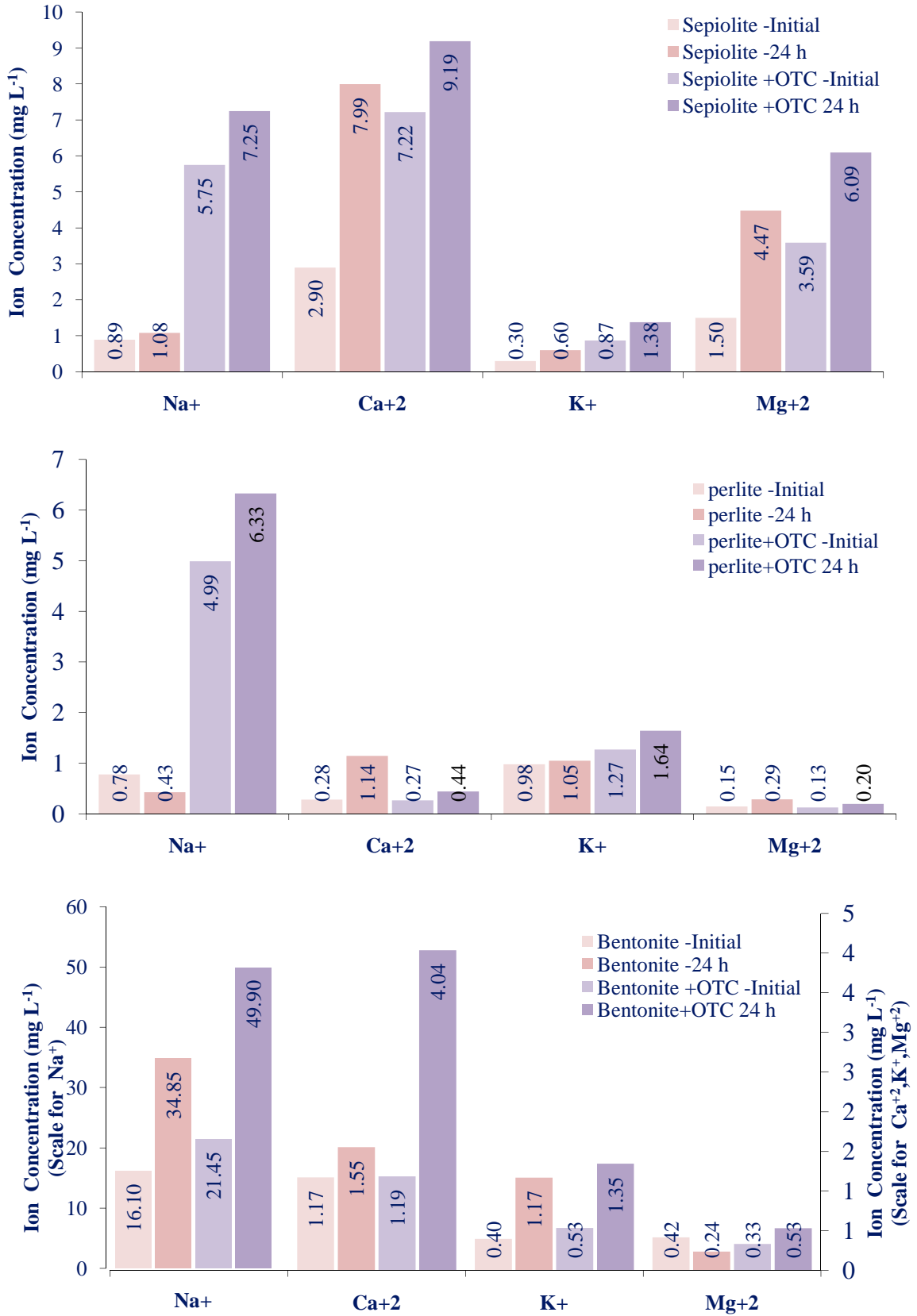
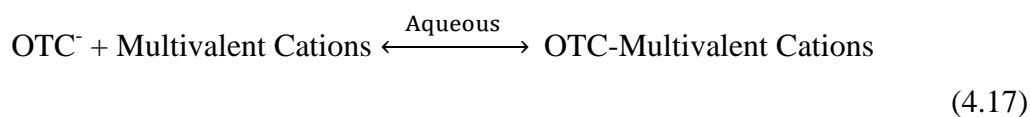
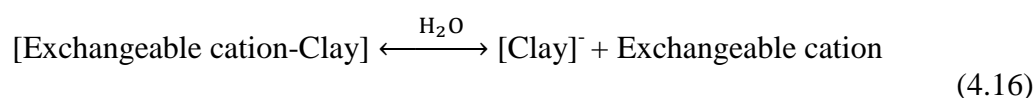


Figure 4.16. Release of cations from adsorbents (mg L^{-1}) initial pH=7.

From the figure, it is obvious that in the absence of OTC there is significantly high Na^+ release from bentonite and remarkable amount of Ca^{2+} and Mg^{2+} release from sepiolite. The presence of Ca^{2+} and Mg^{2+} ions in the aqueous solution is important because they tend to form soluble complexes with OTC which can adversely affect the adsorption of antibiotic.

In the presence of OTC, the higher release of Na^+ from all adsorbents could be attributed to the OTC adsorption by ion exchange mechanism. This suggestion is in a good agreement of high sorption capacity of bentonite having the highest CEC. The lower adsorption of OTC on sepiolite can be due to formation of the soluble complexes with the released Ca^{2+} and Mg^{2+} ions. On the other hand, OTC can form bridges with the cations on the adsorbents and hence its adsorption can be increased as suggested by Figueroa et al. (2004). Following equations can be suggested as possible reactions occurred during adsorption of OTC.



4.6. Properties of Spent Adsorbents

Some of the characteristics of the spent adsorbents were determined and compared with those of virgin adsorbents.

4.6.1. XRD Analysis of Spent Adsorbents

The XRD patterns of adsorbents (Table B2, B4, B6) interacted with OTC are shown in Figure 4.17. By the adsorption of OTC the variations of the basal spacings (d_{001}) of each adsorbent are listed in Table 4.8.

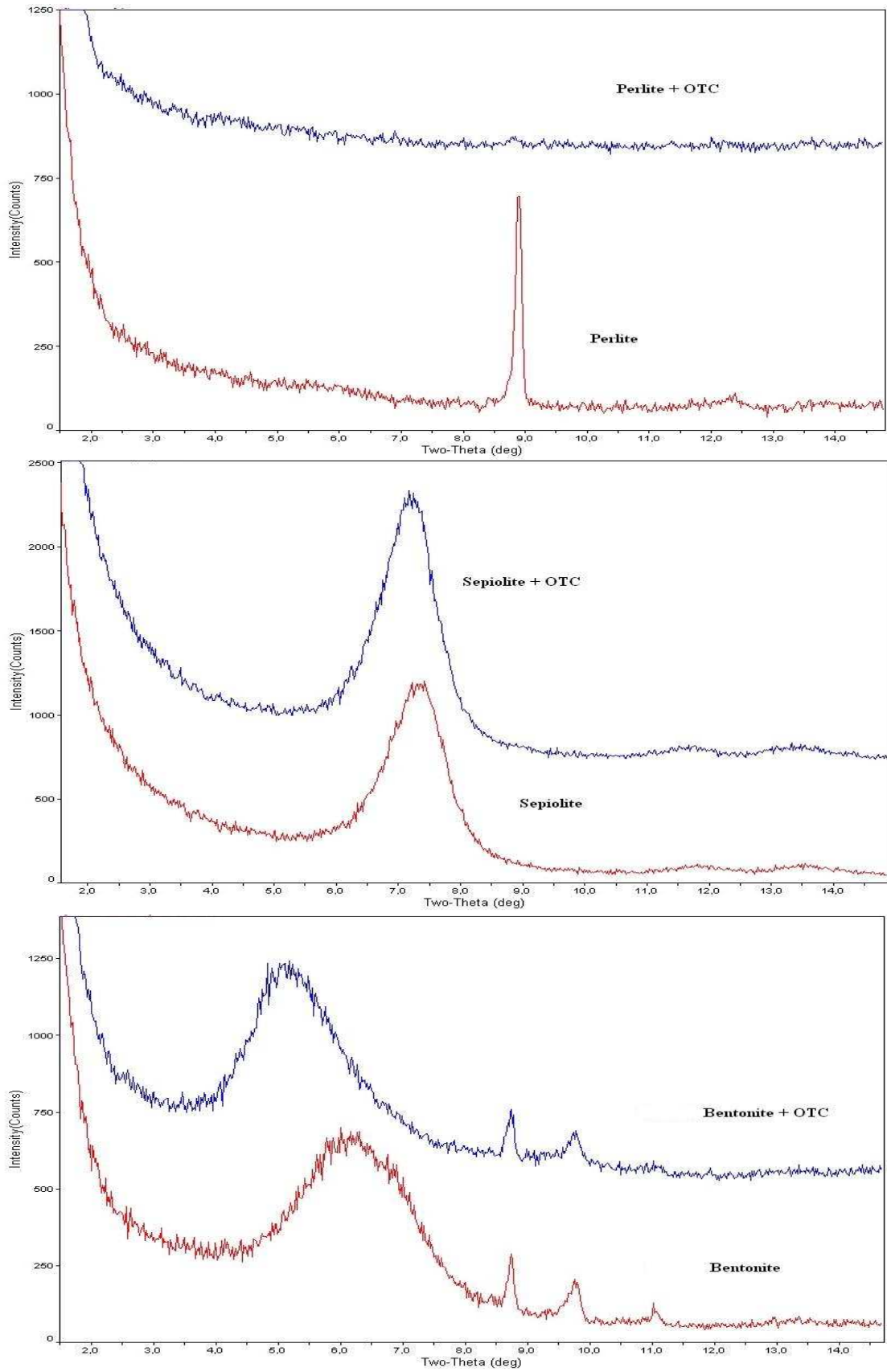


Figure 4.17. XRD patterns of virgin and spent adsorbents.

Table 4.8. Interlayer spacings (d_{001}) of virgin and spent adsorbents.

Adsorbent	d_{001} (Å)	
	Before Adsorption	After adsorption
Perlite	9.91	-
Sepiolite	11.84	12.27
Bentonite	14.29	17.25

As illustrated in table, there is an increase in the interlayer spacing of adsorbents (d_{001}) except for perlite. After the adsorption of OTC the d_{001} peak of perlite disappearance and this is probably due to the structural change of it (Figure 4.17). When the internal adsorption occurs the c -axis spacing (d_{001}), which is unique for swelling clays, sepiolite and bentonite adapts to the intercalated OTC molecule which has 8.3 Å dimension (Kulshrestha et al., 2004). Therefore, after the adsorption of OTC, the observed increase in the basal spacing (d_{001}) of adsorbents is relative to that of dehydrated form would be attributed to the dimensions of the adsorbed oxytetracycline molecule. The larger initial interlayer spacing and the higher increase in d_{001} value of bentonite are in a good agreement with the higher adsorption capacity of it.

4.6.2. FTIR Analysis of Spent Adsorbents

FTIR spectra of each spent adsorbent were determined to figure out the new bands indicating the OTC adsorption on the adsorbents and they were compared with the spectra of OTC which is given in Figure 4.18.

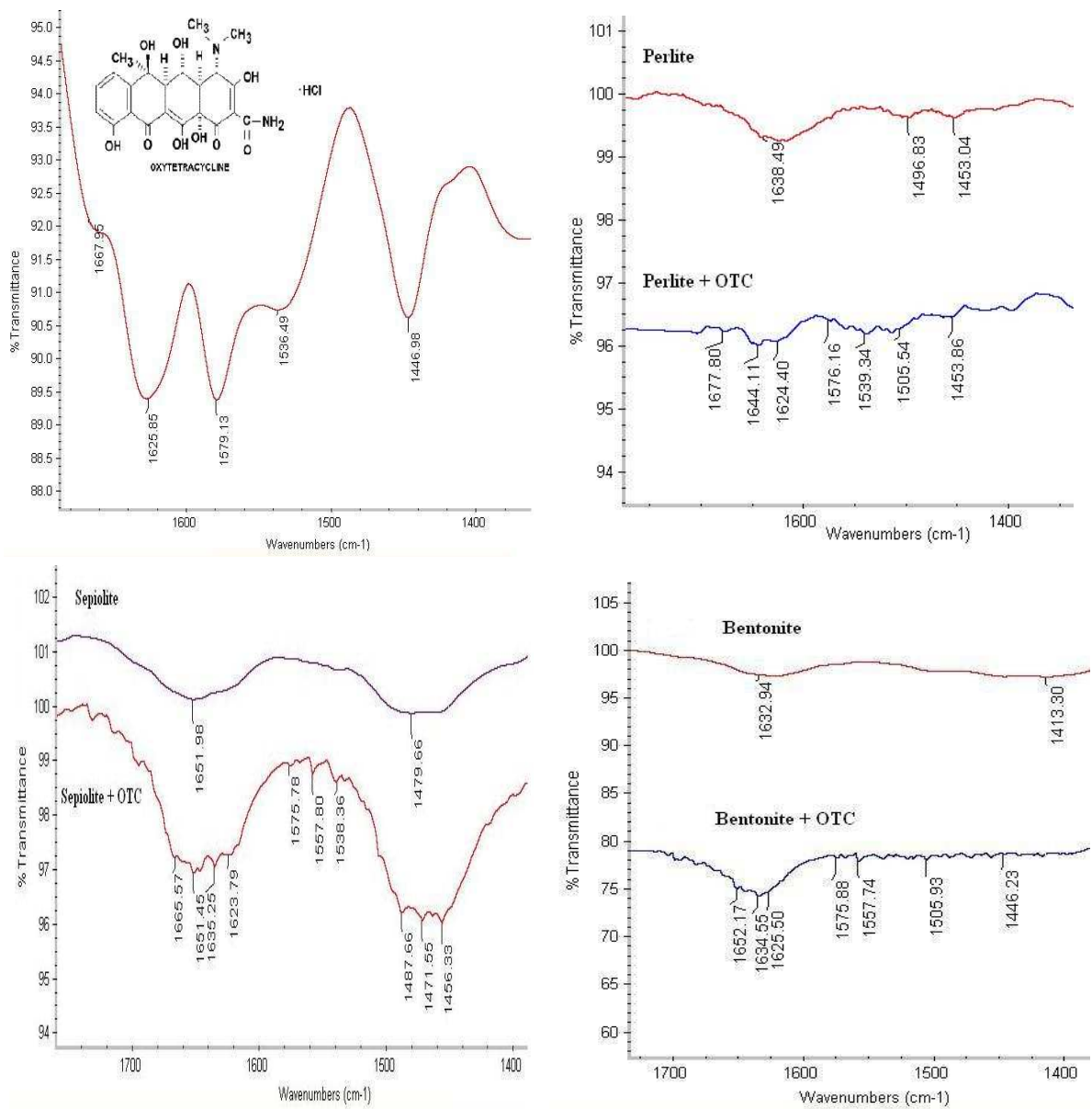


Figure 4.18. FTIR spectra of OTC and adsorbents before and after adsorption ($[OTC]_i = 400 \text{ mg L}^{-1}$).

As can be seen from the FTIR analysis of OTC a series of characteristic bands can be identified between 1400 and 1700 cm^{-1} . The characteristic bands of OTC at 1625 and 1579 cm^{-1} correspond to aromatic alkane and amide II band, respectively. A band at 1446 cm^{-1} is attributed to CH_3 bending in OTC (Kulshrestha et al., 2004; Gu and Karthikeyan, 2005).

Although significantly high amount of OTC adsorbed, its presence is not easily identified on the adsorbents. However, the most intense band of OTC (1625 cm^{-1}) is

observed on the OTC loaded perlite at 1624.40 cm^{-1} , sepiolite at 1623.79 cm^{-1} , and bentonite at 1625.50 cm^{-1} . The second intense band of OTC (1579 cm^{-1}) is observed on OTC loaded perlite at 1576.16 cm^{-1} , sepiolite at 1575.78 cm^{-1} , and bentonite at 1575.88 cm^{-1} .

4.6.3. Elemental Analysis of Adsorbents Before and After Adsorption

The elemental analyses of adsorbents were performed in order to investigate the variation in the carbon content after the adsorption of OTC and the results are tabulated in Table 4.9.

Table 4.9. Elemental content of adsorbents before and after the adsorption of OTC.

Adsorbent	Carbon	Nitrogen
	Weight (%)	
Perlite	0.079	0.008
Perlite After Adsorption	0.461	0.017
Sepiolite	1.294	0.048
Sepiolite After Adsorption	2.163	0.135
Bentonite	0.964	0.060
Bentonite After Adsorption	2.312	0.256

From the Table 4.9 it can be observed that there is an increase in carbon and nitrogen content of the adsorbents after adsorption. The higher increase in the carbon and nitrogen amounts was observed for bentonite which is in a good agreement with higher OTC adsorption capacity of it.

4.7. Regeneration of Spent Bentonite

To make the adsorption process economic regeneration studies can be applied to the spent adsorbent. Regeneration was investigated for only bentonite among the investigated

adsorbents because of its high adsorption capacity. The regeneration of bentonite to degrade the adsorbed OTC was performed either by direct application of oxidation (ozonation and Fenton processes) or by extraction followed by oxidation.

4.7.1. Extraction of OTC from Spent Bentonite

In order to enhance the efficiency of subsequent oxidative regeneration, the desorption of OTC from the spent bentonite was studied. Various extraction solutions including magnesium salt, McIlvaine buffer, and NaCl in methanol were used for the desorption of OTC from soil, manure, and food in previous studies which are listed in Table 4.10. Actually, none of these solutions are considered for the regeneration purposes and McIlvaine buffer is known as an efficient extraction solvent for the analysis of TC antibiotics sorbed on solid matrixes.

Table 4.10. Desorption of OTC by various extraction solutions.

Extraction Solvent	Ingredients	Reference
NaCl Solution	1 M NaCl / 1 M Oxalic Acid / Methanol (25:25:50)	Sassman and Lee, 2005
McIlvaine	0.2 M Citric acid / 0.4 M Na ₂ HPO ₄ (90:60) / 0.1 M Na ₂ EDTA / Methanol (25:25:50)	Blackwell et. al, 2004
MgCl ₂	1 M MgCl ₂	Figuroa and Mackay, 2005
Mg(NO ₃) ₂	1 M Mg(NO ₃) ₂	Uslu and Balçioğlu, 2009

Considering high performances of the extraction solvents for the desorption of TC antibiotics listed in table, these solutions at concentrations mentioned in table were applied to the spent bentonite for two hours period and the efficiency of extraction is determined by the following equation,

$$\text{OTC Extraction (\%)} = \frac{C_{\text{aq}}}{C_{\text{A}}} \times 100$$

(4.19)

C_{A} = adsorbed OTC concentration (mg L^{-1} or mM),

C_{aq} = aqueous OTC concentration after extraction (mg L^{-1} or mM).

In Figure 4.19 the extraction efficiencies of magnesium salts solutions are compared with those obtained by the other solvents presented in Table 4.10.

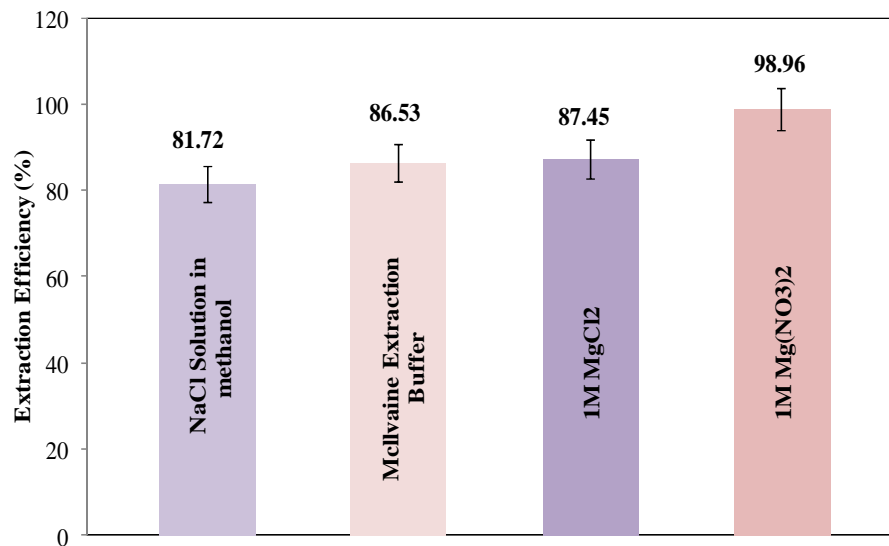


Figure 4.19. OTC extraction efficiency of different solutions.

As can be seen from the Figure 4.19, $\text{Mg}(\text{NO}_3)_2$ has the highest OTC desorption efficiency (98.96 %) for the spent bentonite. This result can be explained by the formation of a complex between OTC and magnesium ions in the liquid phase (Schmitt and Schneider, 2000, Uslu and Balcioğlu, 2009). Therefore, $\text{Mg}(\text{NO}_3)_2$ was selected as an extraction solution for the spent bentonite.

In order to investigate the effect of Mg(II) concentration, the desorption experiments were carried out with different concentrations of $\text{Mg}(\text{NO}_3)_2$ in the concentration range of 0.1M - 2M at two different initial pH values (Figure 4.20).

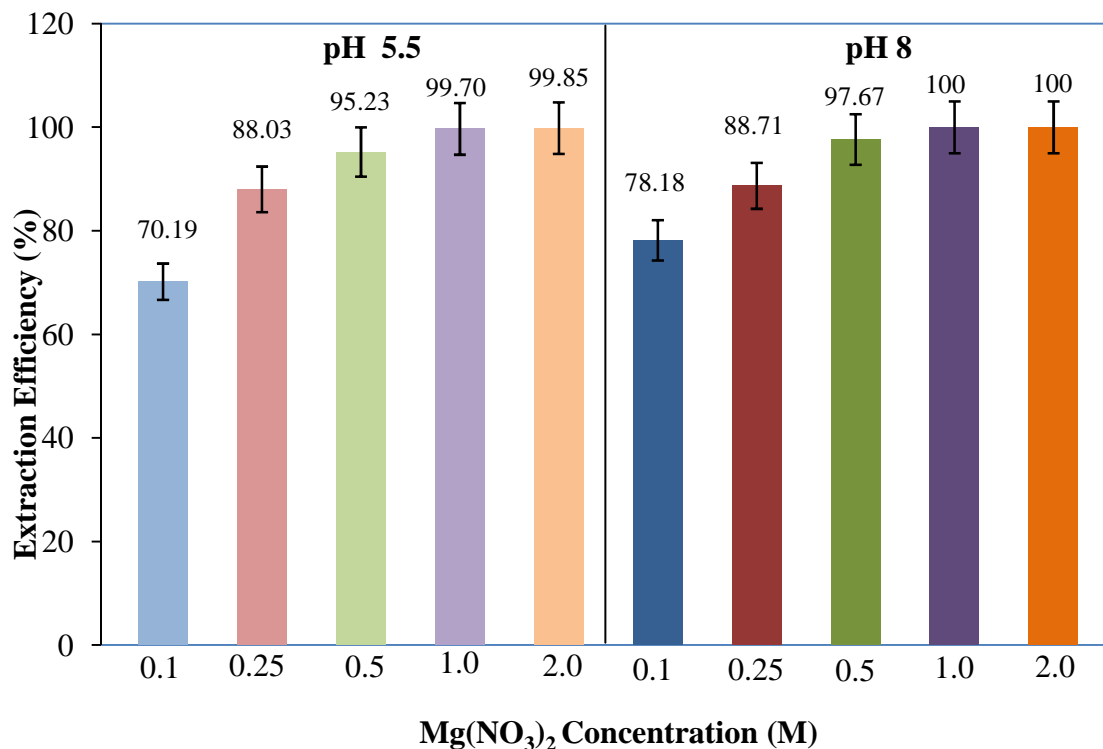


Figure 4.20. Effect of $\text{Mg}(\text{NO}_3)_2$ on extraction efficiency of OTC from bentonite.

As can be seen from Figure 4.20, the extraction efficiency of OTC gradually increases with increasing concentration of Mg(II) solution at both pH. On the other hand, increasing the pH of the extraction solution to a value of 8 did not remarkably affect the performance of extraction. Although a higher complex formation potential is expected at alkaline pH value about 95% OTC removal from the surface of spent bentonite was achieved by 0.5 M $\text{Mg}(\text{NO}_3)_2$ at pH_i 5.5 which was already obtained without any pH adjustment.

4.7.2. Ozonation of OTC on Spent Bentonite

For the degradation of OTC adsorbed on bentonite, ozone was applied directly to the spent bentonite and after the extraction of OTC from bentonite by using 0.5 M $\text{Mg}(\text{NO}_3)_2$. Various applied ozone doses (2.5, 7.5, 12.75, 24.75 and 37.5 mg min^{-1}) were used in

oxidations experiments and OTC removal efficiency of ozone before and after the extraction is illustrated as a function of treatment time in Figure 4.21. OTC removal efficiency of direct ozonation was calculated by a mass balance relationship after extraction.

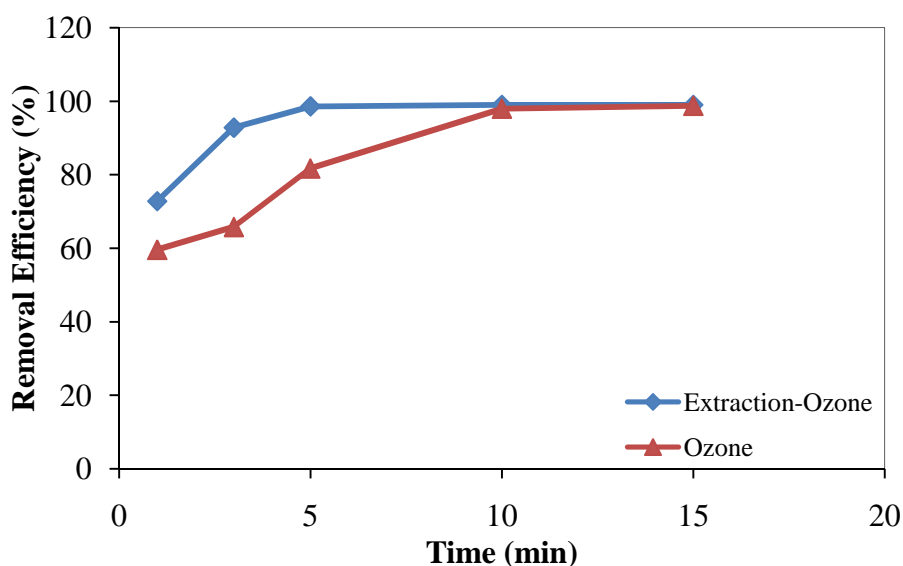
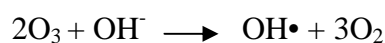


Figure 4.21. Comparison of OTC removal efficiency of ozone before and after extraction. ($\text{pH}_i = 6.5$)

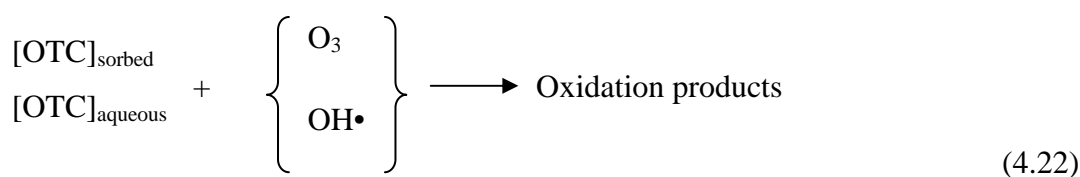
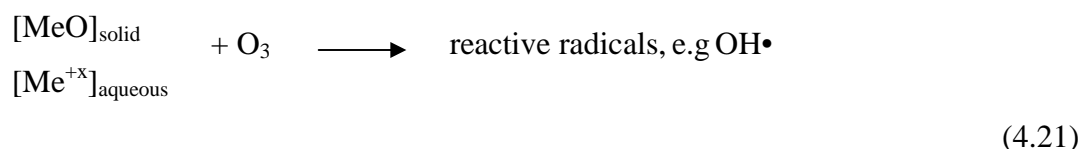
It can be seen from the figure that 98.6 % removal of OTC was achieved within 5 minutes (applied ozone dose = $12.75 \text{ mg min}^{-1}$) when ozone was applied after the extraction of OTC from the bentonite. However, 15 minutes (applied ozone dose = 37.5 mg min^{-1}) was required to obtain the same treatment efficiency when ozone was directly applied to the spent bentonite without extraction.

While the initial pH of slurry before the ozonation was 8.1, it was 7.8 after the application of extraction. At these pH values as well as molecular ozone hydroxyl radicals ($\text{OH}\bullet$) produced by the catalytic decomposition of ozone with hydroxyl ions (Langlais, 1991) can be responsible for the degradation of OTC (Equation 4.20).



(4.20)

Hydroxyl radicals in the slurry can also be produced by both homogeneous and heterogeneous metal catalyzed decomposition reactions of ozone (e.g. Balcioğlu and Moral, 2008). It was revealed that various metal oxides, MeO, (e.g. Al₂O₃, Fe₂O₃, FeOOH) can act as heterogeneous catalyst for the production of hydroxyl radicals (Kasprzyk-Hordern et al., 2006; Beltran et al., 2005; Park et al., 2004). Although the effect of catalyst is not well documented in heterogeneous catalytic ozonation for the degradation of pollutants three different reaction pathways have been speculated (1) chemisorption of ozone on catalyst can produce reactive oxidative species that can oxidize pollutants in the aqueous phase of slurry, (2) adsorbed pollutant on catalyst surface can be oxidized by either ozone or hydroxyl radicals in aqueous phase, and (3) adsorption of both pollutant and ozone on catalyst surface and subsequent reactions between them (Kasprzyk-Hordern et al., 2006). Due to the release of metal ions from the surface of bentonite (Figure 4.21) homogeneous catalytic reaction could also be responsible for the oxidation of OTC in the liquid phase of the slurry. Subsequently, reactions (4.21) and (4.22) can be suggested for the oxidation of OTC in the slurry of bentonite.



After the regeneration of the spent bentonite by ozonation, the d_{001} value of bentonite was determined and compared with that of virgin one. The d_{001} peak of the bentonite tends to return to its virgin mode by the application of ozone. d_{001} value of virgin bentonite was 14.29 and by the adsorption of OTC it increased to 17.25 Å. Subsequent regeneration resulted in a d_{001} value of 15.17 Å.

4.7.3. Fenton Oxidation of OTC on Spent Bentonite

The degradation of OTC was also performed by Fenton oxidation and this process was applied to the spent bentonite at Fe(II)/H₂O₂ molar ratio of 1/10 with varying H₂O₂ doses (H₂O₂ = 50-150 mM) for one hour treatment period. Considering the release of some cations from the surface of the bentonite that might cause the decomposition of hydrogen peroxide and the production of reactive radicals, oxidation experiments were also carried out without the addition of iron catalyst (Figure 4.22). OTC removal efficiency of Fenton process was calculated in a similar way as in the case of ozonation process.

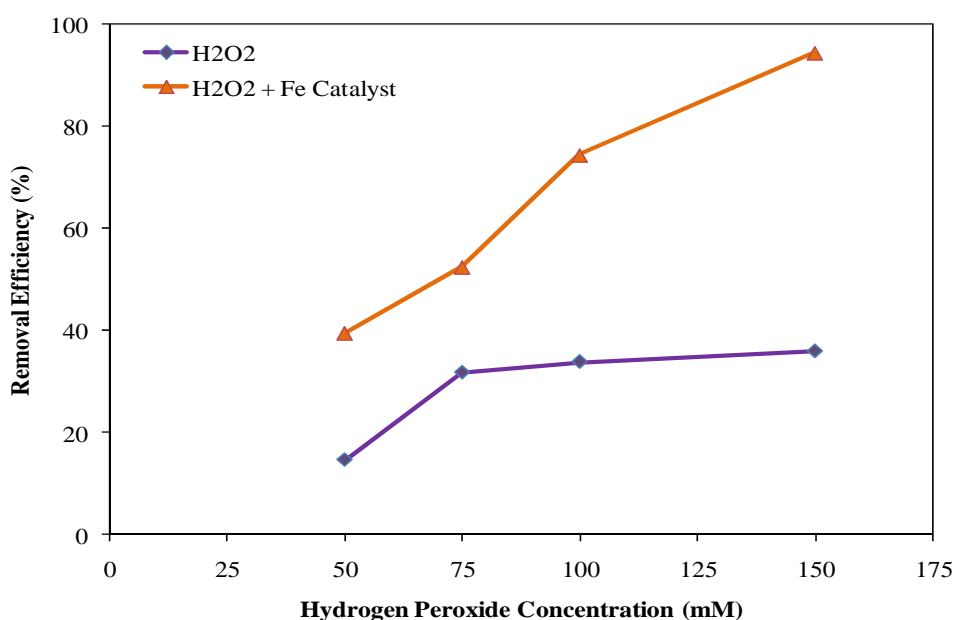


Figure 4.22. Effect of hydrogen peroxide concentration and Fe catalyst on the OTC removal efficiency (Fe(II)/ H₂O₂ =1/10; treatment period=60 min).

As it is obvious from Figure 4.22 that Fe catalyst amendment drives up the OTC removal efficiency of hydrogen peroxide due to the reaction of iron catalyst with H₂O₂ (Walling, 1975).

The degradation of OTC without the addition of iron catalyst can indicate that the reaction of H₂O₂ with the indigeneous iron released into the solution from the bentonite could produce reactive radicals or heterogenous Fenton process could be responsible for the production of reactive radicals similar to heterogeneous catalytic ozonation (Xu et al.,

2009). The following reactions could be proposed for the production of hydroxyl radicals in the solution.

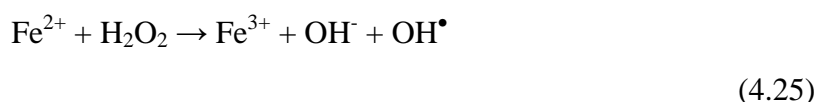
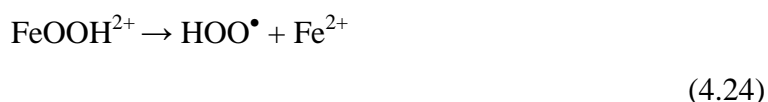
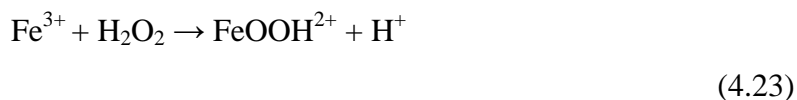


Figure 4.22 also indicates that an increase in H_2O_2 concentration resulted in a higher degradation of OTC and 94 % OTC removal was achieved with 150 mM H_2O_2 / 15 mM Fe (II). However, in the absence of the external addition of iron a limited degradation of OTC was attained with 150 mM H_2O_2 .

Similar to the ozonation treatment, Fenton process was also applied after the extraction of OTC from spent bentonite and the results were compared with those obtained by direct application of oxidation process in extended treatment time period (Figure 4.23). In order to differentiate the effect of extraction on the overall removal of OTC both 75 mM and 150 mM hydrogen peroxide dose were used in Fenton reagent.

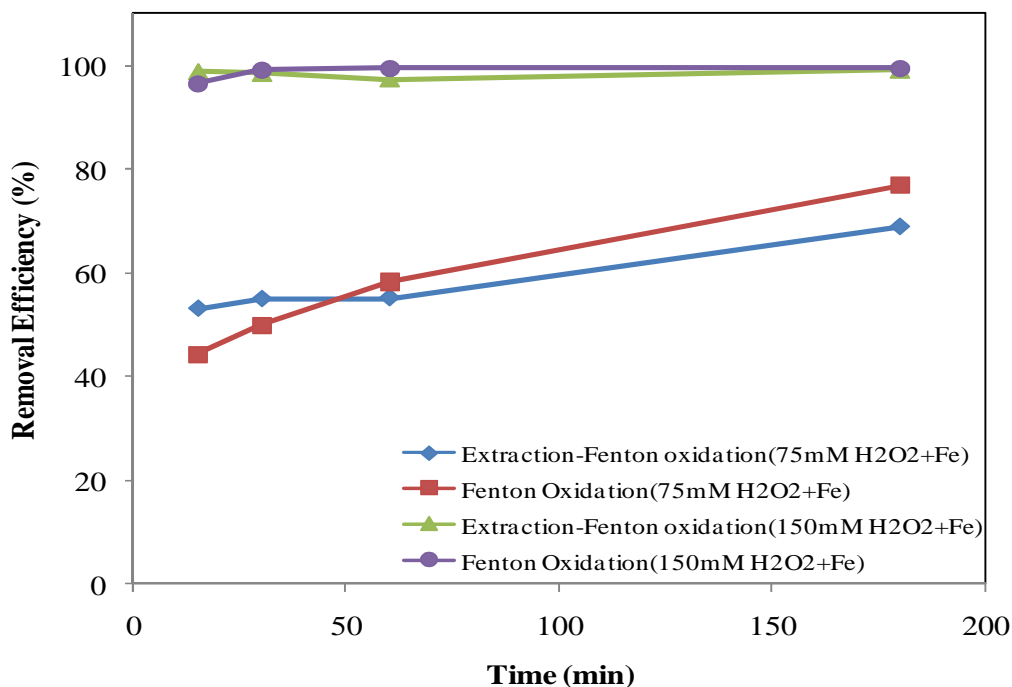


Figure 4.23. Comparison of OTC removal efficiency of Fenton process before and after extraction.

At high hydrogen peroxide dose the effect of extraction was not differentiated whereas at 75 mM H₂O₂ dose a positive effect of the pretreatment was observed for the overall removal of OTC and by the progress of oxidation this effect decreased probably due to the exchange of available Fe (II) ions on bentonite surface.

It is known that Fenton process efficiency is closely related to the solution pH (Walling, 1975) and optimal pH value of Fenton process for most of the pollutants found in aqueous phase are between 2 and 4 where higher iron solubility occurs. On the other hand, recent studies exhibited the catalytic effect of immobilized iron on the hydrogen peroxide for the production of reactive oxidative species (Kan and Huling, 2009) and the oxidation of sorbed pollutants on solid matrixes does not require highly acidic conditions due to the catalytic effect of minerals (Uslu and Balcioglu, 2009). In this study, the addition of Fenton's reagent to the slurry of the spent bentonite resulted in an initial pH value of 4.5 and 3.5 for 75 mM and 150 mM hydrogen peroxide dose, respectively. In order to clarify the effect of pH on Fenton treatment with 75 mM H₂O₂ a further decrease of initial pH to 3.5 was provided by the acidification of slurry (Figure 4.24).

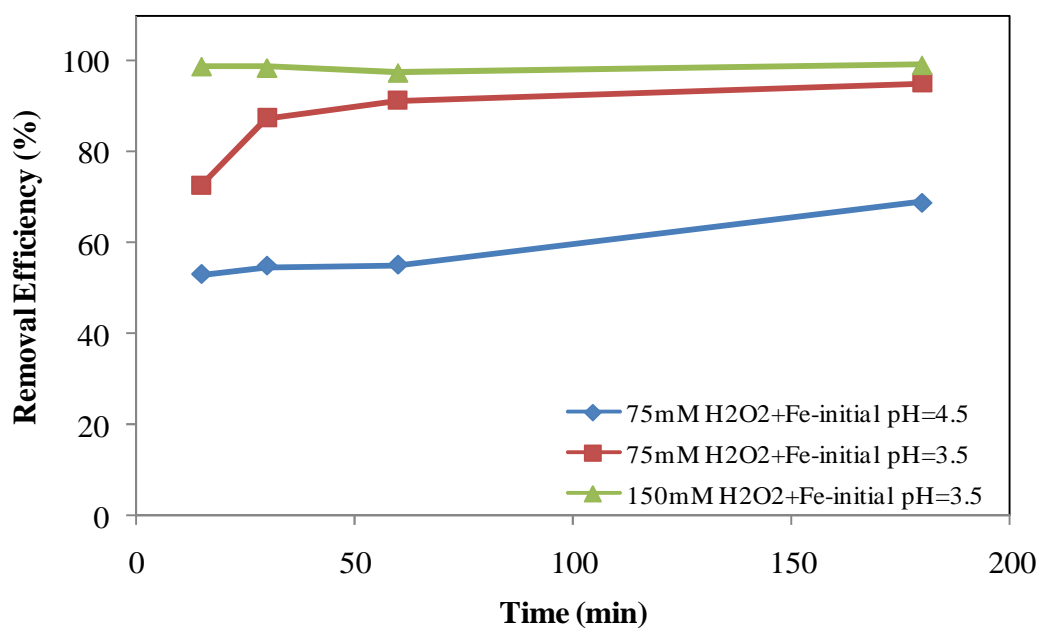


Figure 4.24. Effect of pH on Fenton process.

From the figure it can be concluded that the adjustment of the initial pH to 3.5, increased the removal efficiency of Fenton treatment (75 mM H₂O₂ / 7.5mM Fe catalyst) from 69 to 95 % within 180 min. However, almost the same OTC degradation efficiency was achieved with 150 mM H₂O₂ / 15 mM Fe catalyst within 30 min.

5. CONCLUSION

In the scope of this research the sorption of OTC to three natural adsorbents and the oxidation of spent adsorbent were investigated. The following findings highlight the major results of the study.

- Among the investigated adsorbents bentonite has the highest adsorption equilibrium value of OTC due to its highest CEC. Monovalent ions which have lower complexation constants with OTC were the major exchangeable ions of bentonite and this reduced the formation probability of soluble OTC-metal complexes consequently, the highest sorption was obtained for this adsorbent. Although sepiolite has about 30 times higher surface area and pore volume compare to perlite adsorption equilibrium values of OTC for sepiolite and perlite are close to each other indicating that the surface area and pore volume are not the controlling adsorptive factors.
- Considering EDX and ICP determinations, the lower sorption of OTC could be attributed to the formation of soluble metal/antibiotic complexes in aqueous phase formed by the release of calcium and magnesium ions from sepiolite whereas the higher sorption could be due to surface complexes formed on the perlite through the cation bridging of aluminum and iron with OTC.
- It is thus presumed that OTC was adsorbed on each adsorbent primarily via CEC and cation bridging mechanisms.
- The sorption of OTC on perlite, sepiolite, and bentonite was nonlinear and the experimental equilibrium adsorption data of OTC were tested for the Langmuir, Freundlich, Temkin and Redlich-Peterson isotherms. Consequently, the adsorption isotherms of OTC on perlite and sepiolite are well described with Freundlich model whereas only Temkin isotherm describes the adsorption of OTC on bentonite.
- Among the four kinetic models tested, pseudo-second-order and Elovich models best describe the reaction kinetics of all adsorbents indicating that the rate limiting step of OTC

adsorption is a chemical sorption process and the adsorbents have highly heterogeneous sorptive sites.

- For each adsorbent the OTC sorption at the different experimental pHs was quite different in magnitude but the adsorption was diminished considerably by the deprotonation of OTC for all adsorbents. The adsorption efficiencies of OTC on perlite and sepiolite decreased from 67.2 to 13.9 % and 58.60 to 27.79 % by increasing pH from 2 to 10.5, respectively. Adsorption on bentonite was not affected remarkably by pH variation and it decreased from 99.7 to 86 % by increasing pH from 2 to 10.5. Considering the all results, bentonite can be suggested as a promising adsorbent for OTC.
- Subsequent oxidation of spent bentonite via Fenton and ozone driven mechanisms resulted in high amount of OTC degradation. The increasing dose of oxidant both in Fenton and ozone treatments increased the degradation of OTC.
- The pretreatment of spent bentonite by magnesium salt extraction reduced the ozone dose required for the destruction of OTC whereas it did not affect the performance of Fenton process. Sequential application of extraction and ozone oxidation with an applied ozone dose of $12.75 \text{ mg min}^{-1}$ provided 98.6 % OTC degradation.
- Oxidative radicals produced by the reaction of indigenous iron content of bentonite with hydrogen peroxide provided the limited oxidation of OTC. The addition of iron at Fe(II) / H_2O_2 molar ratio of 1/10 and the acidification of spent bentonite slurry to pH 3.5 resulted in 95 % OTC degradation with 75 mM H_2O_2 . Consequently, an efficient destruction of sorbed OTC could be obtained by these chemical oxidation processes.

REFERENCES

- Acemioğlu, B., 2005. Batch kinetic study of sorption of methylene blue by perlite. *Chemical Engineering Journal*, 106, 73–81.
- Aga, D.S., Goldfish, R., Kulshrestha, P., 2003. Application of ELISA in determining the fate of tetracyclines in land-applied livestock wastes. *Analyst*, 128, 658–662.
- Ahmaruzzaman, M., 2008. Adsorption of phenolic compounds on low-cost adsorbents: A review. *Advances in Colloid and Interface Science*, 143, 48–67.
- Akçay, H., Kiliç, S., Karakaş, R., 1998. Preparation of a chromatographic solid support on the basis of perlite and separation of uranium on a TBP-loaded perlite column. *Journal of Radioanalytical and Nuclear Chemistry*, 230, 12, 83-89.
- Aksu, Z., Tezer, S., 2000. Equilibrium and kinetic modelling of biosorption of Remazol Black B by *Rhizopus arrhizus* in a batch system: effect of temperature. *Process Biochemistry*, 36, 431–439.
- Alder, A.C., Mc Ardell, C.S., Golet, E.M., Ibric, S., Molnar, E., Nipales, N.S., 2001. “Occurrence and fate of fluoroquinolone, macrolide, and sulfonamide antibiotics during wastewater treatment and in ambient waters in Switzerland.” in *Pharmaceuticals and personal care products in the environment: Scientific and regulatory issues*, Daughton CG and Jones-Lepp T.L. (Eds.), American Chemical Society, 56-69, ACS Symposium Series 791, Washington, DC.
- Alkan, M., Demirbaş, Ö., Doğan, M., 2005. Electrokinetic properties of sepiolite suspensions in different electrolyte media. *Journal of Colloid Interface Science*, 281, 240–248.

Amin, N.K., 2009. Removal of direct blue-106 dye from aqueous solution using new activated carbons developed from pomegranate peel: Adsorption equilibrium and kinetics, *Journal of Hazardous Material*, 165, 52-62.

Anirudhan, T.S., Ramachandran, M., 2007. Surfactant-modified bentonite as adsorbent for the removal of humic acid from wastewaters. *Applied Clay Science*, 35, 276–281.

Babel, S., Kurniawan, T.A., 2003. Low-cost adsorbents for heavy metal uptake from contaminated water: A review. *Journal of Hazardous Materials B97*, 219-243.

Balcioğlu Akmeahmet, I., Ötker, M., 2003. Treatment of pharmaceutical wastewater containing antibiotics by O₃ and O₃/ H₂O₂ processes. *Chemosphere*, 50, 85–95.

Balcioğlu Akmeahmet, I., Moral, Ç.K., 2008. Homogenous and heterogenous catalytic ozonation of pulp bleaching effluent. *Journal of Advanced Oxidation Technologies*, 11, 543-550.

Ball, W.P., Roberts, P.V., 1991. Long-term sorption of halogenated organic chemicals by aquifer material. 2. Intraparticle diffusion. *Environmental Science and Technology*, 25, 1237–1249.

Barnes, K.K., Kolpin, D.W., Furlong, E.T., Zaugg, S.D., Meyer, M.T., Barber, L.B., 2008. Pharmaceuticals and other organic wastewater contaminants in ground water. *Science of the Total Environment*, 65, 192–200.

Belter, P.A., 1985. Ion Exchange Recovery of Antibiotics. In Cooney, C.L., Humphrey, A.E. (Eds.), *Comprehensive Biotechnology, Volume 2, The Principles of Biotechnology: Engineering Considerations*, 473–480, Pergamon Press Ltd., New York.

Belter, P. A., Cunningham, F.L., Chen, J.W., 1973. Development of a recovery process for Novobiocin. *Biotechnology and Bioengineering*, 15, 533-549.

Beltran, F.J., Rivas, F.J., Montero-De-Espinosa, R., 2005. Iron type catalysts for the ozonation of oxalic acid in water. *Water Research*, 39, 3553-3564.

Berger, K., Petersen, B., Buning-Pfaue, H., 1986. Persistence of drugs occurring in liquid manure in the food chain. *Archive für Lebensmittelhygiene*, 37, 99–102.

Blackwell, P.A., Holten Lutzhoft, H.C., Ma, H.P., Halling-Sorensen, B., Boxall, A.B.A., Kay, P., 2004. Ultrasonic extraction of veterinary antibiotics from soils and pig slurry with SPE clean-up and LC-UV and fluorescence detection. *Talanta*, 64, 1058-1064.

Blake, D. M., 1994. Bibliography of Work on the Photocatalytic Removal of Hazardous Compounds from Water and Air. National Renewable Energy Laboratory, Golden, Colorado.

Boxall, A.B.A., Blackwell, P., Cavallo, R., Kay, P., Tolls, J., 2002. The sorption and transport of a sulfonamide antibiotic in soil systems. *Toxicology Letters*, 131, 19–28.

Boxall, A.B.A., Johnson, P., Smith, E.J., Sinclair, C.J., Stutt, E., Levy, L.S., 2006. Uptake of veterinary medicines from soils into plants. *Journal of Agricultural and Food Chemistry*, 54, 2288–2297.

Campagnolo, E.R., Hohanson, K.R., Karpati, A., Rubin, C.S., Kolpin, D.W., Meyer, M.T., Esteban, J.E., Currier, R.W., Smith, K., Thu, K.M., McGeehin, M., 2002. Antimicrobial residues in animal water and water resources proximal to large-scale swine and poultry feeding operations. *Science of the Total Environment*, 299, 89–95.

Capone, D.G., Weston, D.P., Miller, V., Shoemaker, C., 1996. Antibacterial residues in marine sediments and invertebrates following chemotherapy in aquaculture. *Aquaculture*, 145, 55–75.

Chander, Y., Kumar, K., Goel, S.M., Gupta, S.C., 2005. Antibacterial activity of soil-bound antibiotics. *Journal of Environmental Quality*, 34, 1952–1957.

Chiang, H.L., Chiang, P.C., Huang, C.P., 2002a. Ozonation of activated carbon and its effects on the adsorption of VOCs exemplified by methylethylketone and benzene. *Chemosphere*, 47, 267–75.

Chiang, H.L., Huang, C.P., Chiang, P.C., 2002b. The surface characteristics of activated carbon as affected by ozone and alkaline treatment. *Chemosphere*, 47, 257–65.

Chiou, M.S., Li, H.Y., 2002. Equilibrium and kinetic modelling of adsorption of reactive dye on crosslinked chitosan beads. *Journal of Hazardous Materials B*, 93, 233–248.

Christian T., Schneider R.J., Färber H.A., Skutlarek D., Meyer M.T., Goldbach H.E., 2003. Determination of antibiotic residues in manure, soil, and surface waters. *Acta Hydrochimica et Hydrobiologica*, 31, 36–44.

Crini, G., 2006. Non-conventional low-cost adsorbents for dye removal: A review. *Bioresource Technology*, 97, 1061-1085.

Daughton, C.G., Jones-Lepp, T. (Eds.), 2001. Pharmaceuticals and personal care products in the environment: scientific and regulatory issues. Symposium Series 791, American Chemical Society, Washington DC.

Daughton, C.G., Ternes, T.A., 1999. Pharmaceuticals and personal care products in the environment: agents of subtle change? *Environmental Health Perspectives*, 107, 907–938.

Demirbas, A., Sari, A., Isildak, Ö., 2006. Adsorption thermodynamics of stearic acid onto bentonite. *Journal of Hazardous Materials B*, 135, 226–231.

Diaz-Cruz, M.S., Lopez de Alda, M.J., Barceló, D., 2003. Environmental behavior and analysis of veterinary and human drugs in soils, sediments and sludge. *Trends in Analytical Chemistry*, 22, 340–351.

Doğan, M., Alkan, M., and Çakir, Ü., 1997. Electrokinetic properties of perlite. *Journal of Colloid and Interface Science*, 192, 114-118.

Dolliver, H., Kumar, K., Gupta, S., 2007. Sulfamethazine uptake by plants from manure-amended soil. *Journal of Environmental Quality*, 36, 1224–1230.

Doyle, M.E., 2006. Veterinary drug residues in processed meats: Potential health risk. Food Research Institute, University of Wisconsin- Madison Briefings.

Eguchi, K., Nagase, H., Ozawa, M., Endoh, Y.S., Goto, K., Hirata, K., Miyamoti, K., Yoshimura, H., 2004. Evaluation of antimicrobial agents for veterinary use in the ecotoxicity test using microalgae. *Chemosphere*, 57, 1733–1738.

Engels, H., Winckler, C., 2004. Mobility of tetracycline-hydrochloride in lysimeters with humous sandy soil. In: Program abstract of SETAC Euro 14th Annual Meeting, 18–22 April 2004.

Fajardo, A., Martinez-Martin, N., Mercadillo, M., Galan, J.C., Ghysels, B., Matthijs, S., Cornelis, P., Wiehlmann, L., Tümmeler, Baquero, F., Martinez, J.L., 2008. The neglected intrinsic resistome of bacterial pathogens. *Public Library of Science*, 3, e1619, 1-6.

FEDESA, 2001. Antibiotic use in farm animals does not threaten human health. Press release, Visby, Sweden, 2001.

Figueroa, R.A., Leonard, A., Mackay, A.A., 2004. Modeling tetracycline antibiotic sorption to clays. *Environmental Science and Technology*, 38, 476-483.

Figueroa, R.A., Mackay, A.A., 2005. Sorption of oxytetracycline to iron oxides and iron oxide-rich soils. *Environmental Science and Technology*, 39, 6664–6671.

Focazio, M.J., Kolpin, D.W., Barnes, K.K., Furlong, E.T., Meyer, M.T., Zaugg, S.D., Barber, L.B., Thurman, E.M., 2008. A national reconnaissance for pharmaceuticals and other organic wastewater contaminants in the United States: II) Untreated drinking water sources. *Science of the Total Environment*, 402, 201-216.

Frick, E.A., Henderson, A.K., Moll, D.M., Furlong, E.T., Meyer, M.T., 2001. Presence of Pharmaceuticals in Wastewater Effluent and Drinking Water, Metropolitan Atlanta, Georgia, July-September 1999. Proceedings of the 2001 Georgia Water Resources Conference, Athens, GA; Carl Vinson Institute of Government, The University of Georgia: 282.

Garcia, A., Rivas, H. M., Figueroa, J. L., and Monroe, A. L., 1995. Case history: Pharmaceutical wastewater treatment plant upgrade SmithKline Beecham pharmaceuticals company. *Desalination*, 102, 255–263.

Gavalchin, J., Katz, S.E., 1994. The persistence of fecal-borne antibiotics in soil. *Journal of AOAC International*, 77, 481–485.

Glassmeyer, S.T., Furlong, E.T., Kolpin, D.W., Cahill, J.D., Zaugg, S.D., Werner, S.L., Meyer, M.T., Kryak, D.D., 2005. Transport of chemical and microbial compounds from known wastewater discharges: potential for use as indicators of human fecal contamination. *Environmental Science and Technology* 39, 5157-5169.

Gomez-Serrano, V., Alvarez, P.M., Jaramillo, J., Beltran, F.J., 2002. Formation of oxygen complexes by ozonation of carbonaceous materials prepared from cherry stones. I. Thermal effects. *Carbon*, 40, 513–22.

Gonsalves, D., Tucker, D.P.H., 1977. Behaviour of oxytetracycline in Florida citrus and soils. *Archives of Environmental Contamination and Toxicology*, 6, 515– 523.

Grafe, U., 1992. *Biochemie der Antibiotika: Struktur-Biosynthese-Wirkmechanismus*. Spektrum Akademischer Verlag, Heidelberg-Berlin-New York.

Gu, C., Karthikeyan, K.G., Sibley, S.D., Pedersen, J.A., 2007. Complexation of the antibiotic tetracycline with humic acid. *Chemosphere*, 66, 1494–1501.

Gu, C., Karthikeyan, K.G., 2005. Interaction of tetracycline with aluminium and iron hydrous oxides. *Environmental Science and Technology*, 39, 2660–2667.

Haller, M.Y., Muller, S.R., McArdell, C.S., Alder, A.C., Suter, M., 2001. Quantification of veterinary antibiotics (sulfonamids and trimethoprim) in animal manure by liquid chromatography–mass spectrometry. *The Journal of Chromatography A* 952, 111–120.

Halling-Sørensen, B., Nielsen, N., Lansky, P.F., Ingerslev, F., Hansen, L., Lützhøft, H.C., Jørgensen, S.E., 1998. Occurrence, fate and effects of pharmaceutical substances in the environment-A review. *Chemosphere* 36, 357–394.

Halling Sorensen, 2000. Algal toxicity of antibacterial agents used in intensive farming, *Chemosphere*, 40, 731 – 739.

Halling-Sørensen, B., 2001. Inhibition of aerobic growth and nitrification of bacteria in sewage sludge by antibacterial agents. *Archives of Environmental Contamination and Toxicology*, 40, 451-460.

Halling-Sørensen, B., Sengeløv, G., Tjørnelund, J., 2002. Toxicity of tetracyclines and tetracycline degradation products to environmentally relevant bacteria, including selected tetracycline-resistant bacteria. *Archives of Environmental Contamination and Toxicology*, 44, 7–16.

Halling-Sørensen, B., Jacobsen, A., Jensen, J., Sengeløv, G., Vaclavik, E., Ingerslev, F., 2005. Dissipation and effects of chlortetracycline and tylosin in two agricultural soils: a field-scale study in southern Denmark. *Environmental Toxicology and Chemistry, SETAC*, 24, 802-10.

Hamscher, G., Abu-Quare, S., Sczesny, S., Höper, H., Nau, H., 2000. Determination of tetracyclines in soil and water samples from agricultural areas in lower Saxony. In *Proceedings of the EuroResidue IV Conference*; van Ginkel, L.A., Ruiter, A., Eds.; EuroResidue IV Conference: Veldhoven, The Netherlands, 522-526.

Hamscher, G., Sczesny, S., Höper, H., Nau, H., 2002. Determination of persistent tetracycline residues in soil fertilized with liquid manure by high-performance liquid

chromatography with electrospray ionization tandem mass spectrometry. *Analytical Chemistry* 74, 1509-1518.

Heberer, T., Stan, H.J., 1996. Occurrence of polar organic contaminants in Berlin drinking water. *Vom Wasser*, 86, 19–31.

Hektoen, H., Berge, J.A., Hormazabal, V., Yndestad, M., 1995. Persistence of Antibacterial Agents in Marine Sediments. *Aquaculture*, 133, 175-184.

Hernando, M.D., Mezcuca, M., Fernández-Alba, A.R., Barceló, D., 2006. Environmental risk assessment of pharmaceutical residues in wastewater effluents, surface waters and sediments. *Talanta*, 69, 334-342.

Hirsch, R., Ternes, T., Haberer, K., Kratz, K.L., 1999. Occurrence of antibiotics in the aquatic environment. *Science of the Total Environment*, 225, 109–118.

Ho, Y.S., McKay, G., 2004. Sorption of copper(II) from aqueous solution by peat. *Water, Air, and Soil Pollution*, 158, 77-97.

Hofl, C., Gerhard, S., Specht, O., Wurdack, I., Wabner, C., 1997. Oxidative degradation of AOX and COD by different advanced oxidation processes: A comparative study with two samples of pharmaceutical wastewater. *Water Science and Technology*, 35, 257–264.

Höper, H., Kues, J., Nau, H., and Hamscher, G., 2002. Eintrag und Verbleib von Tierarzneimittelwirkstoffen in Böden. *Bodenschutz*, 4, 141-148.

Hu, Q. H., Qiao, S. Z., Haghseresht, F. , Wilson, M. A., Lu, G. Q. 2006. Adsorption Study for Removal of Basic Red Dye Using Bentonite. *Industrial and Engineering Chemistry Research*, 45, 733-738.

Huang, C.H., Renew, J.E., Smeby, K.L., Pinkston, K., Sedlak, D.L., 2001. Assessment of potential antibiotic contaminants in water and preliminary occurrence analysis. *Water Research*, 120, 30-40.

Huling, S.G., Jones, P.K., Ela, W.P., Arnold, R.G., 2005. Fenton-driven chemical regeneration of MTBE-spent GAC. *Water Research*, 39, 2145–2153.

Ikehata, K., Naghashkar, N.J., El-Din, M.G., 2006. Degradation of aqueous pharmaceuticals by ozonation and advanced oxidation processes: A review. *Ozone: Science and Engineering*, 28, 6, 353–414.

Ingerslev, F., Halling-Sorensen, B., 2000. Biodegradability properties of sulfonamides in activated sludge. *Environmental Toxicology and Chemistry*, 19, 2467–2473.

Ingerslev, F., Halling-Sorensen, B., 2001. Biodegradability of metronidazole, olaquinox and tylosin and formation of tylosin degradation products in aerobic soil-manure slurries. *Ecotoxicology and Environmental Safety*, 48, 311-320.

Jacobsen, P., Berglund, L., 1988. Persistence of oxytetracycline in sediments from fish farms. *Aquaculture*, 70, 365-370.

Jans, U., Hoigne, J., 1998. Activated carbon and carbon black catalyzed transformation of aqueous ozone into OH-radicals. *Ozone Science Engineering*, 20, 67–90.

Jones, A.D., Bruland, G.L., Agrawal, S.G., Vasudevan, D., 2005. Factors influencing the sorption of oxytetracycline to soils. *Environmental Toxicology Chemistry*, 24, 761–770.

Jorgensen, S.E., Halling-Sorensen, B., 2000. Drugs in the environment. *Chemosphere*, 40, 691–699.

Kan, E., Huling, S.G., 2009. Effects of temperature and acidic pre-treatment on Fenton-driven oxidation of MTBE-spent granular activated carbon. *Environmental Science and Technology*, 43, 1493-1499.

Kara, M., Yuzer, H., Sabah, E., Çelik, M.S., 2003. Adsorption of cobalt from aqueous solution onto sepiolite. *Water Research*, 37, 224–232.

Karabay, O., Hosoglu, S., 2008. Increased antimicrobial consumption following reimbursement reform in Turkey. *Journal of Antimicrobial Chemotherapy*, 61, 1169–1171.

Karçı, A., Balcıoğlu Akmehmet, I., 2009. Investigation of the tetracycline, sulfonamide, and fluoroquinolone antimicrobial compounds in animal manure and agricultural soils in Turkey, *Science and Total Environment*, doi:10.1016/j.scitotenv.2009.04.047.

Kasprzyk-Hordern, B., Raczek-Stanislawiak, U., Swietlik, J., Nawrocki, J., 2006. Catalytic ozonation of natural organic matter on alumina. *Applied Catalysis B: Environmental*, 62, 345-358.

Kay, P., Blackwell, P.A., Boxall, A.B.A., 2005. Transport of veterinary antibiotics in overland flow following the application of slurry to arable land. *Chemosphere*, 59, 951–959.

Khraisheh, M.A.M., Al-Degs, Y.S., Allen, S.J. Ahmad, M.N., 2002. Elucidation of controlling steps of reactive dye adsorption on activated carbon. *Industrial and Engineering Chemistry Research*, 41, 1651–1657.

Kim, S.C., Carlson, K., 2007. Quantification of human and veterinary antibiotics in water and sediment using SPE/LC/MS/MS. *Analytical and Bioanalytical Chemistry*, Volume: 387, 4, 1301-1315.

Kolpin, D.W., Furlong, E.T., Meyer, M.T., Thurman, E.M., Zaugg, S.D., Barber, L.B., Buxton, H.T., 2002. Pharmaceuticals, hormones, and other organic wastewater contaminants in US Streams, 1999–2000: A National Reconnaissance. *Environmental Science and Technology*, 36, 1202–1211.

Koumanova, B., Peeva-Antova, P., 2002. Adsorption of *p*-chlorophenol from aqueous solutions on bentonite and perlite. *Journal of Hazardous Materials A*, 90, 229–234.

Krapac, I.G., Koike, S., Meyer, M.T., Snow, D.D., Chou, S-FJ., Mackie, R.I., Roy, W.R., Chee-Sanford, J.C., 2004. Long-term Monitoring of the Occurrence of Antibiotic Residues

and Antibiotic Resistance Genes in Groundwater near Swine Confinement Facilities. In Proceeding of the 4th International Conference on Pharmaceuticals and Endocrine Disrupting Chemicals in Water. Minneapolis, National Groundwater Association, 158–172.

Krapac, I.G., Koike, S., Meyer, M.T., Snow, D.D., Chou, S.F.J., Mackie, R.I., Roy, W.R., Chee-Sandford, J.C., 2005. Long-term monitoring of the occurrence of antibiotic residues and antibiotic resistance in groundwater near swine confinement facilities. Report of the CSREES Project 2001- 35102-10774.

Kulshrestha, P., Giese, R.F., Aga, D.S., 2004. Investigating the molecular interaction of oxytetracycline in clay and organic matter: insights on factors affecting its mobility in soil. *Environmental Science and Technology*, 38, 4097–4105.

Kumar, K., Gupta, S.C., Baidoo, S.K., Chander, Y., Rosen, C.J., 2005. Antibiotic uptake by plants from soil fertilized with animal manure. *Journal of Environmental Quality*, 34, 2082–2085.

Kümmerer, K., Hartmann, T. S., Meyer, M., 1997. Biodegradability of the antitumour agent ifosfamide and its occurrence in hospital effluents and communal sewage. *Water Research*, 31, 2705–2710.

Kümmerer, K., Al-Ahmad, A., Mersch-Sundermann, V., 2000. Biodegradability of some antibiotics, elimination of the genotoxicity and affection of wastewater bacteria in a simple test. *Chemosphere* 40, 701–707.

Kümmerer K., 2001a. *Pharmaceuticals in the Environment*, Springer-Verlag Berlin.

Kümmerer, K., 2001b. Drugs in the environment: emission of drugs, diagnostic aids and disinfectants into wastewater by hospitals in relation to other sources-A review. *Chemosphere* 45, 957–969.

Kümmerer, K., 2004. Resistance in the environment. *Journal of Antimicrobial Chemotherapy*, 54, 311–320.

Lalumera, G.M., Calamari, D., Galli, P., Castiglioni, S., Crosa, G., Fanelli, R., 2004. Preliminary investigation on the environmental occurrence and effects of antibiotics used in aquaculture in Italy. *Chemosphere*, 54, 661–668.

Langlais, B., Reckhow, D., Brink, D.R. *Ozone in water treatment: application and engineering*. USA: Lewis Publishers; 1991.

Lemic, J., Tomasevic-Canovic, M., Djuricic, M., Stanic, T., 2005. Surface modification of sepiolite with quaternary amines. *Journal of Colloid and Interface Science*, 292, 11–19.

Linares, J.F., Gustafsson, I., Baquero, F., Martinez, J.L., 2006. Antibiotics as intermicrobial signaling agents instead of weapons. *Proceedings of the National Academy of Sciences USA*, 103, 19484-19489.

Lindsey, M.E., Meyer, M., Thurman, E.M., 2001. Analysis of trace levels of sulfonamide and tetracycline antimicrobials, in groundwater and surface water using solid-phase extraction and liquid chromatography/mass spectrometry. *Analytical Chemistry*, 73, 4640–4646.

Liu, J.B., Crittenden, J.C., Hand, D.W., Perram, D.L., 1995. Removal and destruction of organic contaminants in water using adsorption, steam regeneration, and photocatalytic oxidation-pilot study. *Journal of the Air and Waste Management Association*, 49, 951-958.

Lunestad, B.T., Goksøyr, J., 1990. Reduction in the antibacterial effect of oxytetracycline in sea water by complex formation with magnesium and calcium. *Disease of Aquatic Organisms*, 9, 67–72.

MacKay, A.A., Canterbury, B., 2005. Oxytetracycline sorption to organic matter by metalbridging. *Journal of Environmental Quality*, 34, 1964–1971.

Martinez, J.L., 2003. Recent advances on antibiotic resistance genes. In *Recent Advances in Marine Biotechnology. Molecular Genetics of Marine Organisms*, 10, 13-32.

Mitscher, L.A., 1978. The chemistry of the tetracycline antibiotics. *Medicinal Research Series*, Volume 9, 330. MerceL-Dekker Inc., New York.

Oka, H., Ikai, Y., Kawamura, N., Yamada, M., Harada, K., Ito, S., Suzuki, M., 1989. Photodecomposition products of tetracyclines in aqueous solutions. *Journal of Agricultural and Food Chemistry*, 37, 226-231.

Oka, H., Ito, Y., Matsumoto, H., 2000. Chromatographic analysis of tetracycline antibiotics in foods. *The Journal of Chromatography A*, 882, 109–133.

Özcan, A., Özcan, A.S., 2005. Adsorption of Acid Red 57 from aqueous solutions onto surfactant-modified sepiolite. *Journal of Hazardous Materials B*, 125 , 252–259.

Park, J-Sup., Choi, H., Cho, J., 2004. Kinetic decomposition of ozone and para-chlorobenzoic acid (pCBA) during catalytic ozonation. *Water Research*, 38, 2285-2292.

Pearson, M., Inglis, V., 1993. A sensitive microbioassay for the detection of antibacterial agents in the aquatic environment. *Journal of Fish Diseases*, 16, 255–260.

Poots, V., McKay, G., Healy, J.J., 1976. The removal of acid dye from effluent using natural adsorbents: peat. *Water Research*, 10, 1061-1066.

Rabolle, M., Spliid, N.H., 2000. Sorption and mobility of metronidazole, olaquinox, oxytetracycline and tylosin in soil. *Chemosphere*, 40, 715-722.

Redlich, O., Peterson, D.L., 1959. A useful adsorption isotherm, *Journal of Physical Chemistry*, 63, 1024-1026.

Rey, R.P., Padron, A.S., Leon, P.L., Pozo, M.M., Baluja, C., 1999. Ozonation of cytostatics in water medium. Nitrogen bases. *Ozone Science Engineering*, 21, 69–77.

Richardson, M.L., Bowron, J.M., 1985. The fate of pharmaceutical chemicals in the environment. *Journal of Pharmacy and Pharmacology*, 37, 1–12.

Rytwo, G., Tropp, D., Serban, C., 2002. Adsorption of diquat, paraquat and methyl green on sepiolite: experimental results and model calculations. *Applied Clay Science*, 20, 273–282.

Sabah, E., Çelik, M.S., 1999. Sepiyolit : Özellikleri ve Kullanım Alanları. 3.Endüstriyel Hammaddeler Sempozyumu/14-15 Ekim 1999, İzmir, Türkiye.

Samuelsen, O.B., 1989. Degradation of oxytetracycline in seawater at two different temperatures and light intensities, and the persistence of oxytetracycline in the sediment from a fish farm. *Aquaculture*, 83, 7–16.

Samuelsen, O.B., Torsvik, V., Ervik, A., 1992. Long-range changes in oxytetracycline concentration and bacterial resistance towards oxytetracycline in a fish farm sediment after medication. *Science of the Total Environment*, 114, 25–36.

Sarmah, A.K., Meyer, M.T., Boxall, A.B.A., 2006. A global perspective on the use, sales, exposure pathways, occurrence, fate and effects of veterinary antibiotics (VAs) in the environment. *Chemosphere*, 65, 725–759.

Sassmann, S., Lee, L.S., 2005. Sorption of three tetracyclines by several soils: assessing the role of pH and cation exchange. *Environmental Science and Technology*, 39, 7452–7459.

Schmitt, M.O., Schneider, S., 2000. Spectroscopic investigation of complexation between various tetracyclines and Mg^{2+} or Ca^{2+} . *Physical Chemistry Community*, 3, 42–55.

Scholz, M., Martin, R.J., 1998. Control of bio-regenerated granular activated carbon by spreadsheet modelling. *Journal of Chemical Technology and Biotechnology*, 71, 253–61.

Schwabe, U., and Paffrath, D., 2001. *Arzneiverordnungs-Report 2001*. Springer Verlag, Heidelberg, Berlin.

Sithole, B.B., Guy, R.G., 1987a. Models for chlortetracycline in aquatic environments. I. Interaction with bentonite clay systems. *Water, Air, Soil Pollution*, 32, 303–314.

Sithole, B.B., Guy, R.G., 1987b. Models for tetracycline in aquatic environments. II. Interaction with Humic Substances. *Water, Air, Soil Pollution*, 32, 315–321.

Snyder, A., Kim, D., Cho, J., Kim, S., Vanderford, J., 2007. Occurrence and removal of pharmaceuticals and endocrine disruptors in South Korean surface, drinking, and waste waters. *Water Research*, 41, 1013 – 1021.

Sontheimer, H., Crittenden, J.C., Summers, R.C., 1988. *Activated Carbon for Water Treatment*. American Water Works Association Research Foundation, Denver, U.S.A.

Stan, H.J., Heberer, T., 1997. Pharmaceuticals in the aquatic environment. *Dossier Water Analysis*, 25, 20–23.

Stuard, B., 2004. *Infrared Spectroscopy: Fundamentals and Applications*, John Wiley & Sons, Incorporated, UK.

Stumpf, M., Ternes, T.A., Wilken, R.D., Rodrigues, S.V., Baumann, W., 1999. Polar drug residues in sewage and natural waters in the state of Rio de Janeiro, Brazil. *Science of the Total Environment*, 225, 135-141.

Şalcıoğlu, A., 2007. Sorption of tetracycline antibiotics on natural and modified zeolite. M.S. Thesis. Boğaziçi University.

Temkin, M.I., Pyzhev, V., 1940. Kinetic of ammonia synthesis on promoted iron catalyst. *Acta Physicochimica URSS*, 12, 327-356.

Ternes, T.A., 1998. Occurrence of drugs in German sewage treatment plants and rivers. *Water Research*, 32, 3245–3260.

Thiele-Bruhn, S., 2003. Pharmaceutical antibiotic compounds in soils-A review. *Journal of Plant Nutrition and Soil Science*, 166, 145–167.

Thomas, L., Wouter, A.G., Tolls, J., 2006. The effect of pH and ionic strength on the sorption of sulfachloropyridazine, tylosin, and oxytetracycline to soil. *Environmental Toxicology and Chemistry*, 25, 904-11.

Tolls, J., 2001. Sorption of veterinary pharmaceuticals in soils: A review. *Environmental Science and Technology*, 35, 3397–3406.

Tomita, K., Naixian, Z. , 1990. Some Natural Na-bentonites in China. *Earth Science and Biology*, 23, 1-8.

Turku, I., Sainio, T., Paatero, E., 2007. Thermodynamics of tetracycline adsorption on silica. *Environmental Chemistry Letters*, 5, 225–228.

Uslu, M.Ö., Balcıoğlu Akmehmet, I., 2009. Comparison of the ozonation and Fenton process performances for the treatment of antibiotic containing manure. *Science of the Total Environment*, 407, 3450–3458.

Valdes, H., Sanchez-Polo, M., Rivera-Utrilla, J., Zaror, C.A., 2002. Effect of ozone treatment on surface properties of activated carbon. *Langmuir*, 18, 211, 1–6.

Van Gool, S., 1993. Possible effects on the environment of antibiotic residues in animal manure. *Tijdschr Diergeneeskd*, 118, 8-10.

Walling, C., 1975. Fenton's reagent revisited. *Accounts of Chemical Research*, 8, 125–131.

Wang, Y.J., Zhou, D.M., Sun, R.J., Cang, L., Hao, X.Z., 2006. Cosorption of zinc and glyphosate on two soils with different characteristics. *Journal of Hazardous Materials* 137, 76–82.

Wang, Y.J., Jia, D.A., Sun, R.J., Zhu, L., Zhou, D.M., 2008. Adsorption and cosorption of tetracycline and Cu on montmorillonite. *Environmental Science and Technology*, 42, 3254–3259.

Watkinson, A.J., Micalizzi, G.R., Bates, J.R., Costanzo, S.D., 2007. Novel method for rapid assessment of antibiotic resistance in *Escherichia coli* isolates from environmental waters by use of a modified chromogenic agar. *Applied and Environmental Microbiology*, 73, 2224–2229.

Watts, C.D., Craythorne, B., Fielding, M., Killops, S.D., 1982. Nonvolatile organic compounds in treated waters. *Environmental Health Perspectives*, 46, 87–89.

Weber, W.J., Morris, J.C., 1963. Kinetics of adsorption on carbon from solution, *Journal of the Sanitary Engineering Division*, 89, 31–59.

Werth, C.J., Reinhard, M., 1997. Effects of Temperature on Trichloroethylene Desorption from Silica Gel and Natural Sediments. 2. Kinetics. *Environmental Science and Technology*, 31, 697–703.

Wollenberger, L., Halling-Sorensen, B., Kusk, K.O., 2000. Acute and chronic toxicity of veterinary antibiotics to *Daphnia magna*. *Chemosphere*, 40, 723–730.

Xu., H., Prasad, M., Liu, Y., 2009. Schorl: A novel catalyst in mineral-catalyzed Fenton-like system for dyeing wastewater discoloration. *Journal of Hazardous Materials* 165, 1186–1192.

Yamashita, N., Yasojima, M., Nakada, N., Miyajima, K., Komori, K., Suzuki, Y., Tanaka, H., 2006. Effects of antibacterial agents, levofloxacin and clarithromycin, on aquatic organisms. *Water Science and Technology*, 53, 65–72.

Yang, S., Carlson, K., 2003. Evolution of antibiotic occurrence in a river through pristine, urban, and agricultural landscapes. *Water Research*, 37, 4645–4656.

Zhu, J., Snow, D., Cassada, D.A., Monson, S.J., Spalding, R.F., 2001. Analysis of oxytetracycline, tetracycline, and chlortetracycline in water using solid phase extraction and liquid chromatography–tandem mass spectrometry. *Journal of Chromatography A*, 928, 177–186.

<http://www.epa.gov/testmethods/pdfs/9081.pdf>

APPENDIX A

Calibration Curves and HPLC Chromatogram of OTC

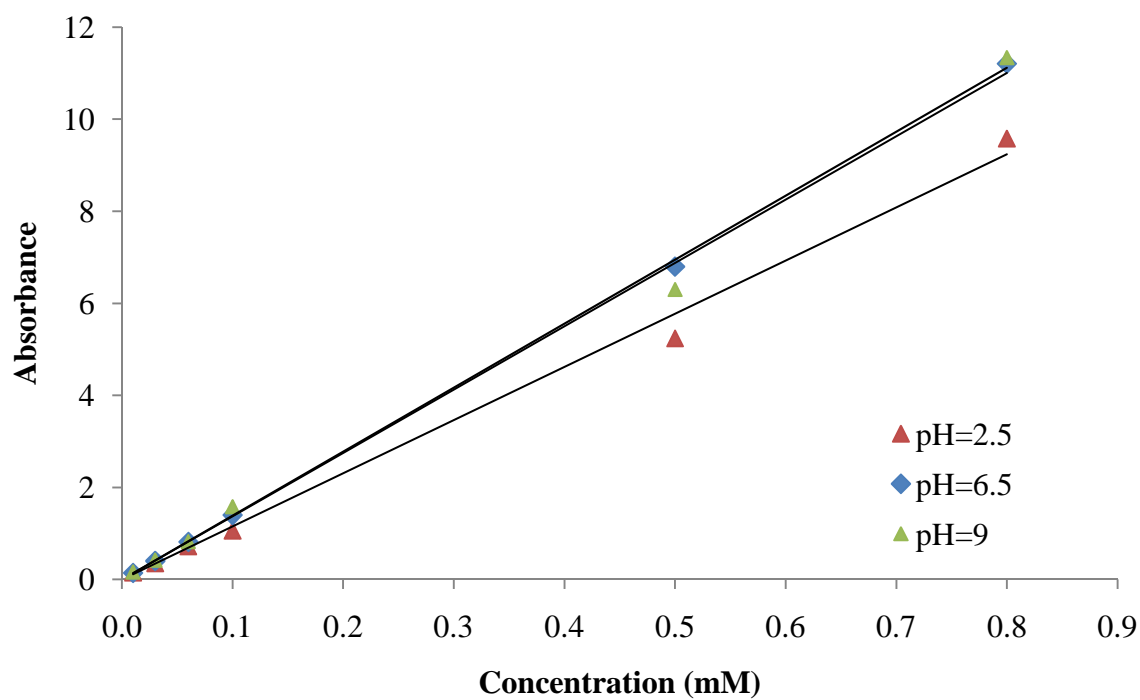


Figure A. 1. Calibration curves of OTC at different pH values.

Table A.1. Maximum absorption peak and extinction coefficient of OTC at different pH values.

pH	λ (nm)	ϵ (R^2)
2.5	355.5	11.55 (0.994)
6.5	358	13.89 (0.999)
9	372	13.76 (0.995)

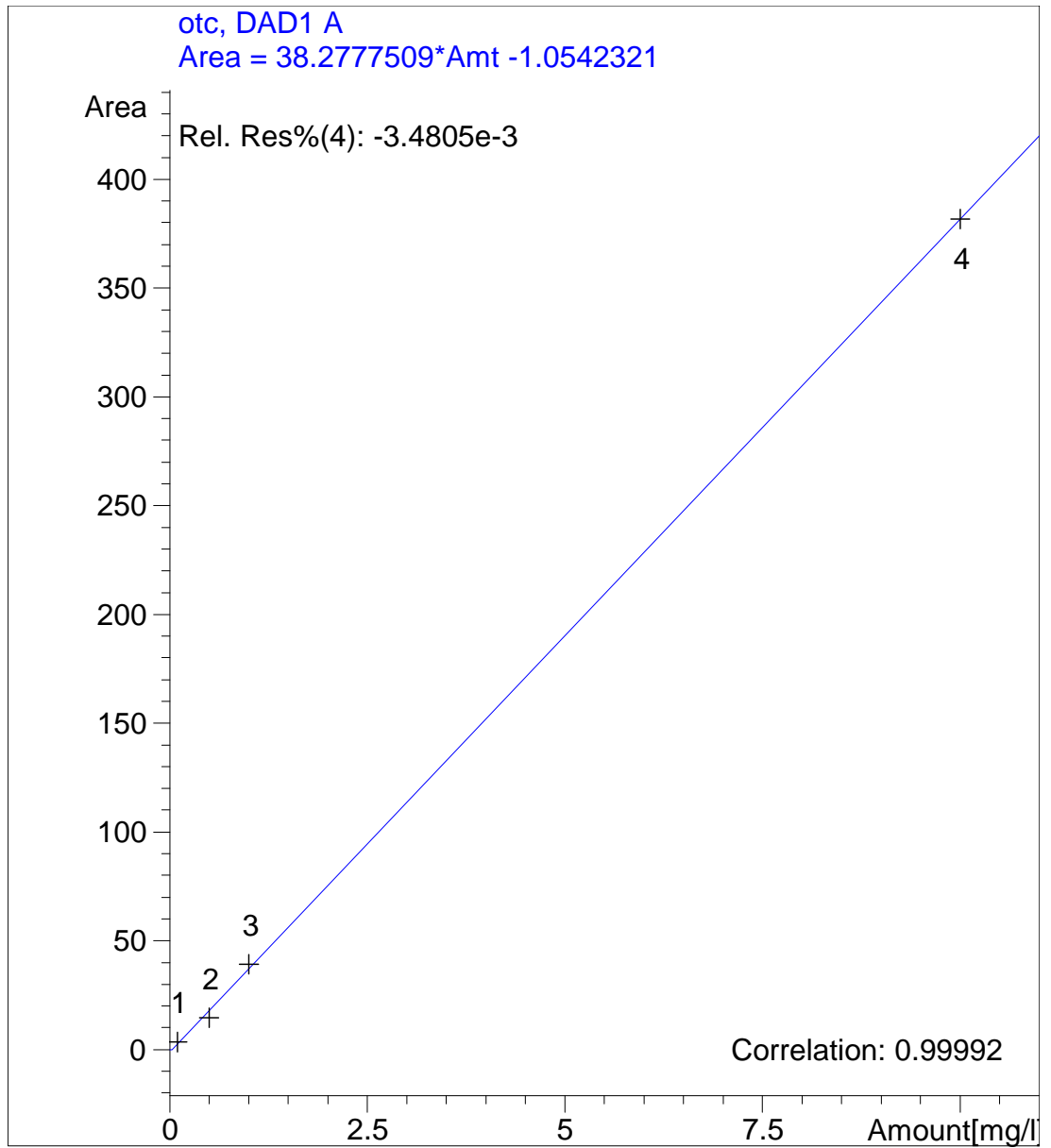


Figure A.2. HPLC calibration curve of OTC.

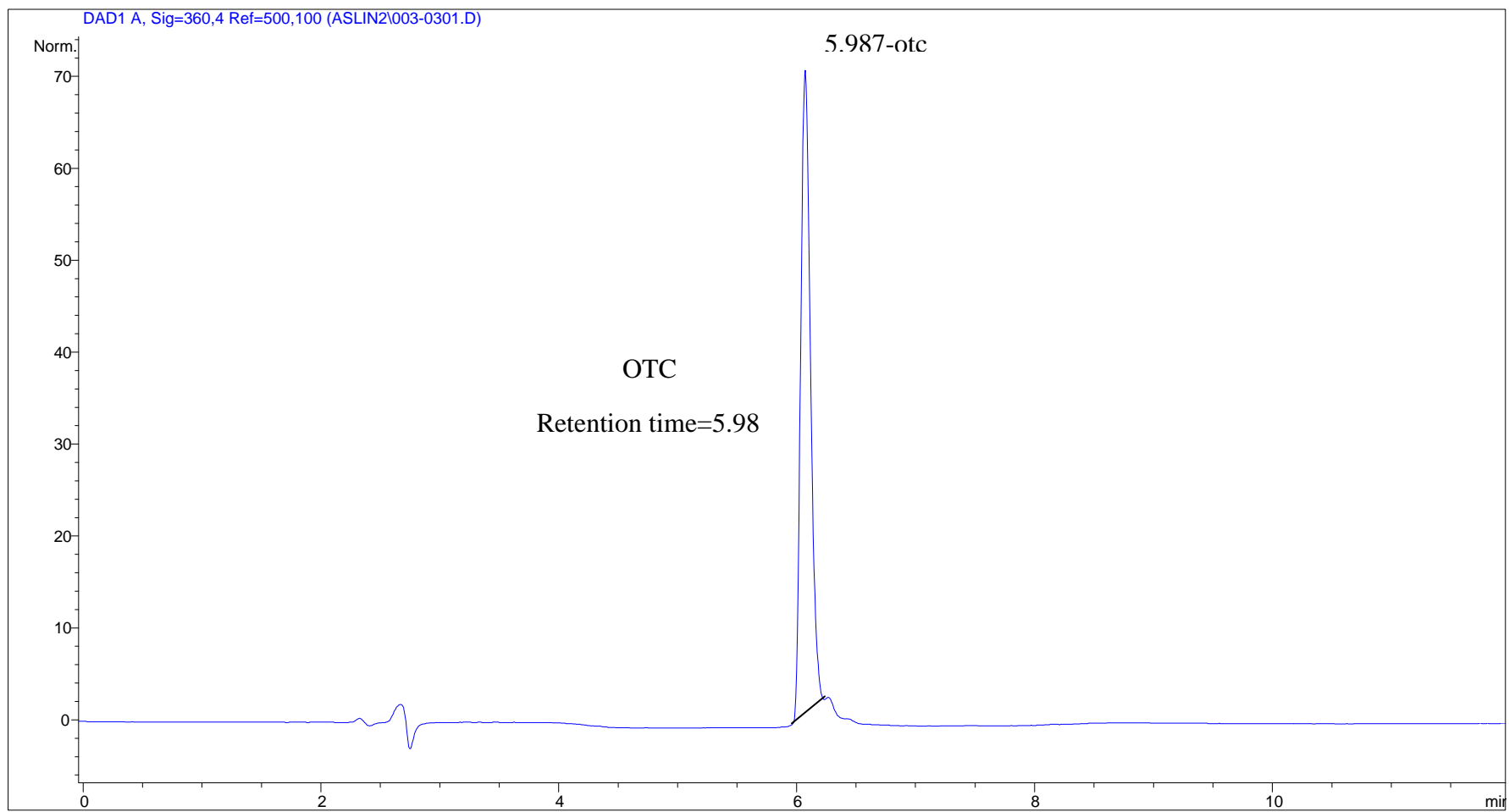


Figure A.3. Representative chromatogram of OTC.

APPENDIX B

Interlayer Spacings and Peak Intensities of Adsorbents

Table B.1. Interlayer spacings and peak intensities of virgin perlite.

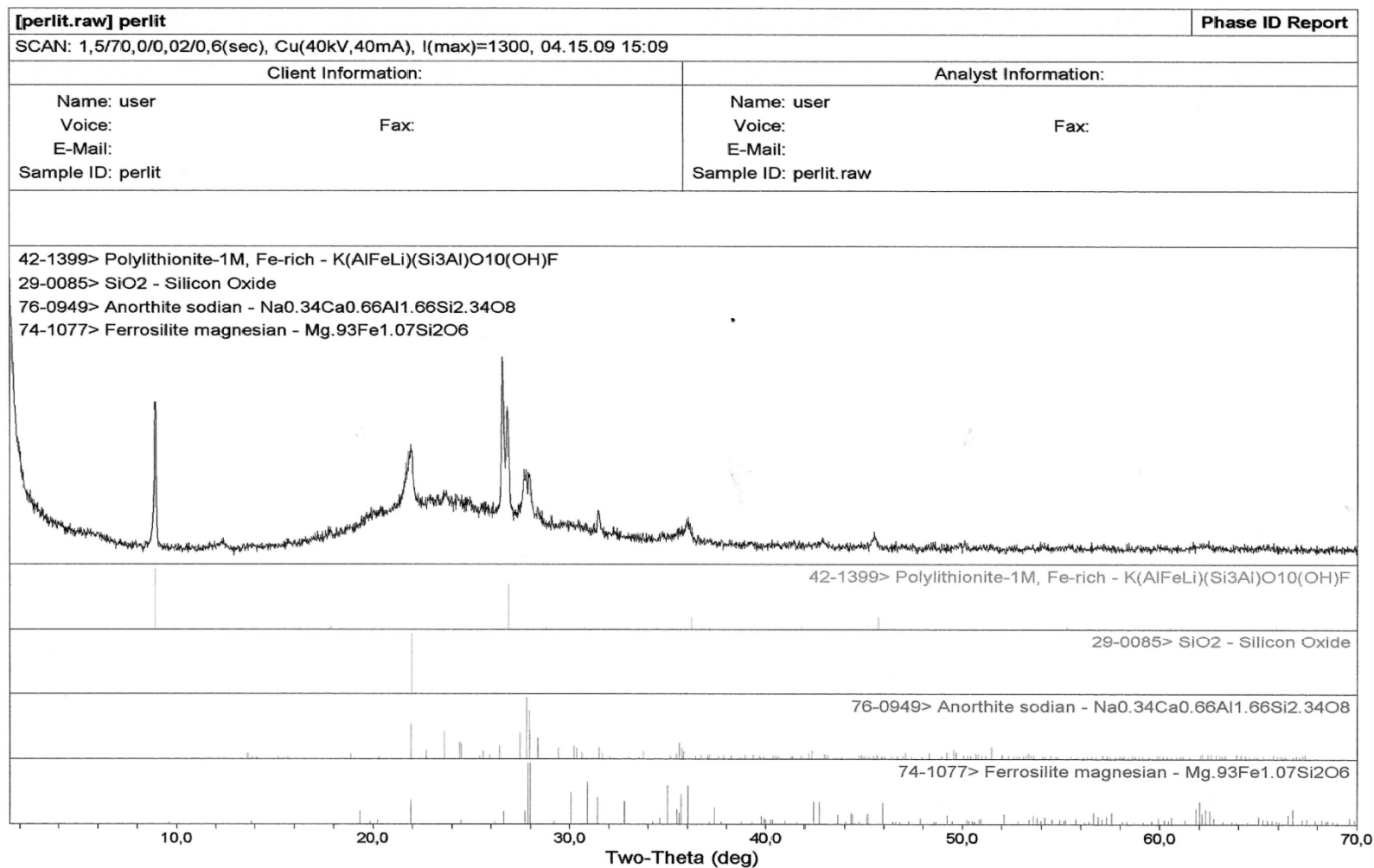


Table B.1. Continued.

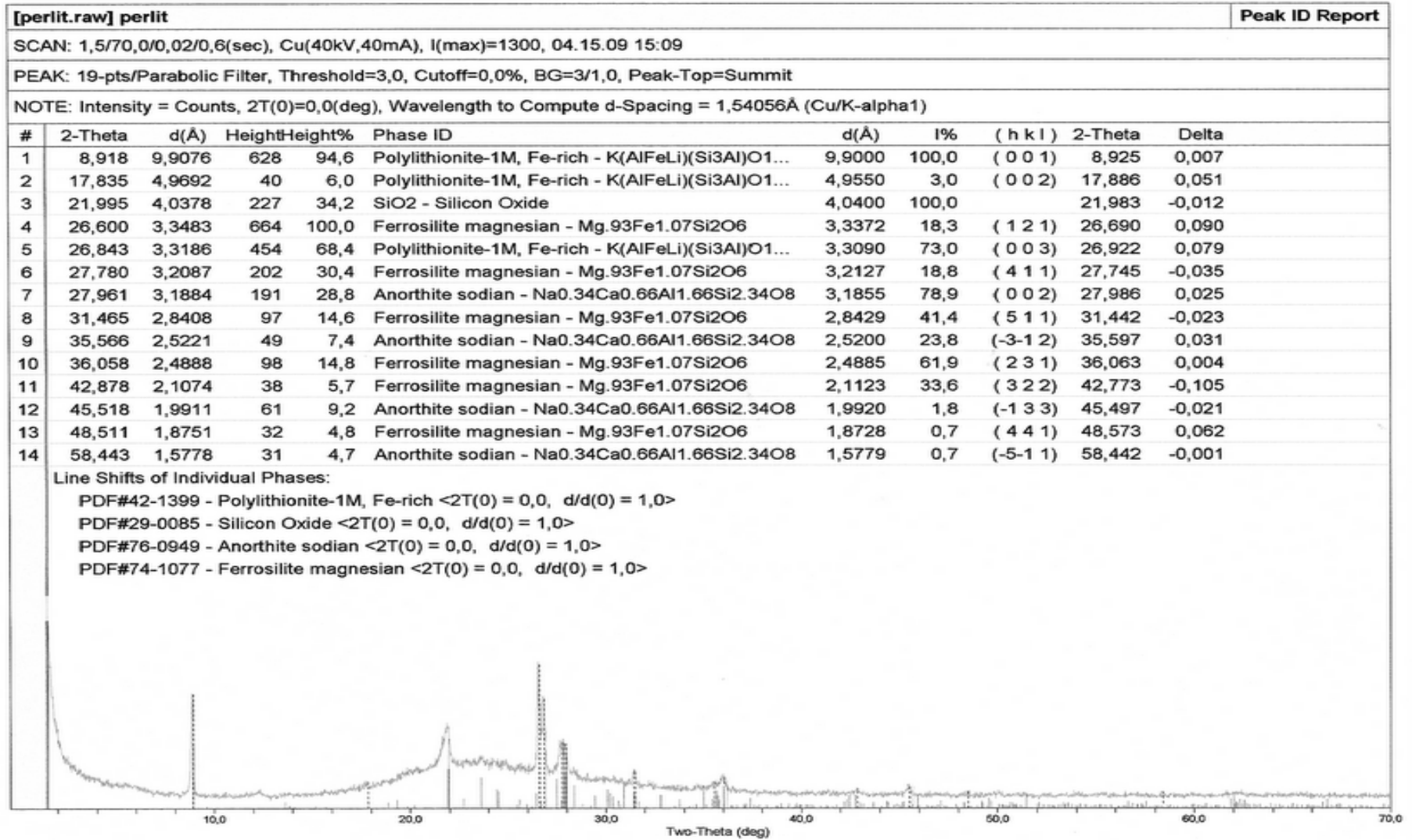


Table B.2. Interlayer spacings and peak intensities of spent perlite.

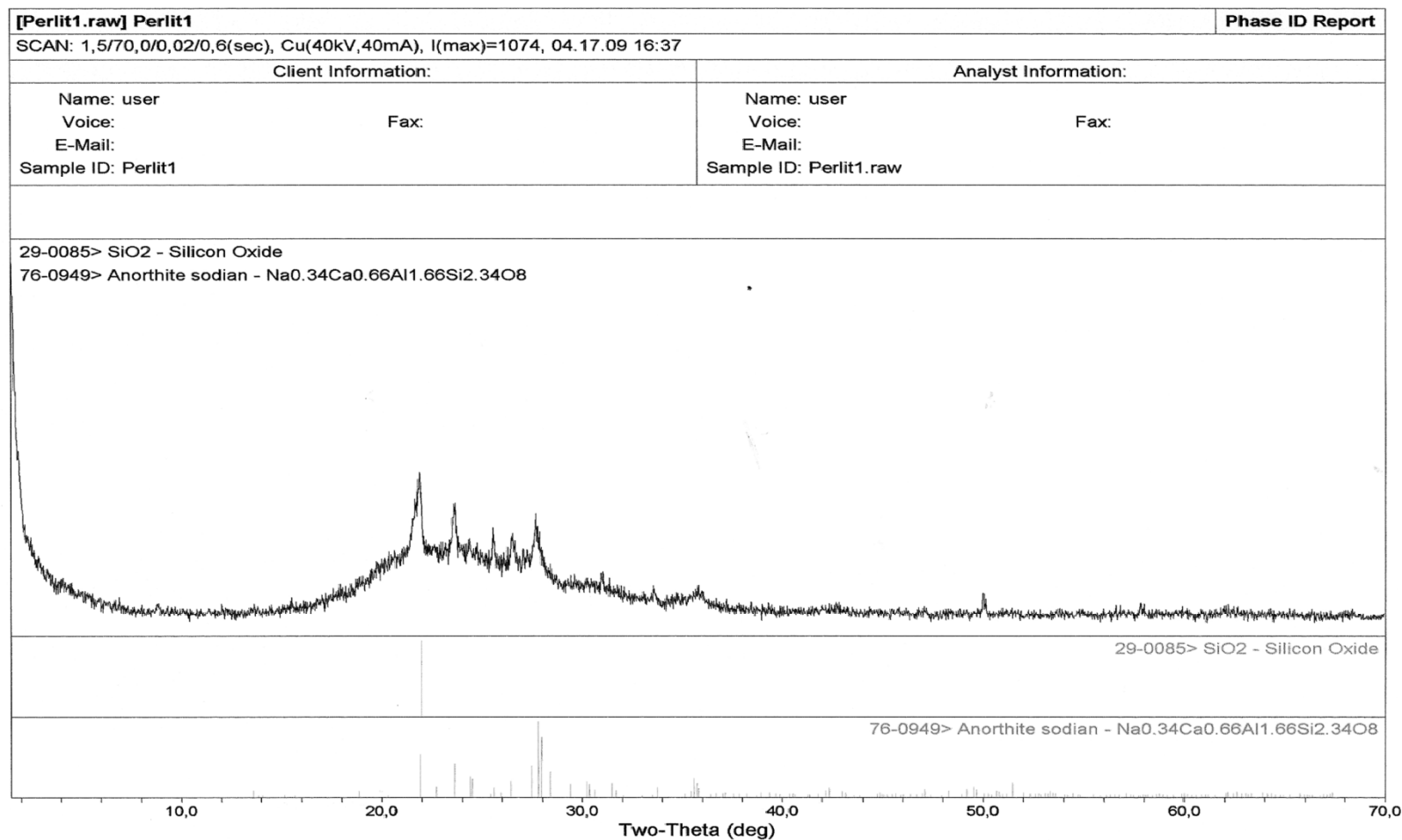


Table B.2. Continued.

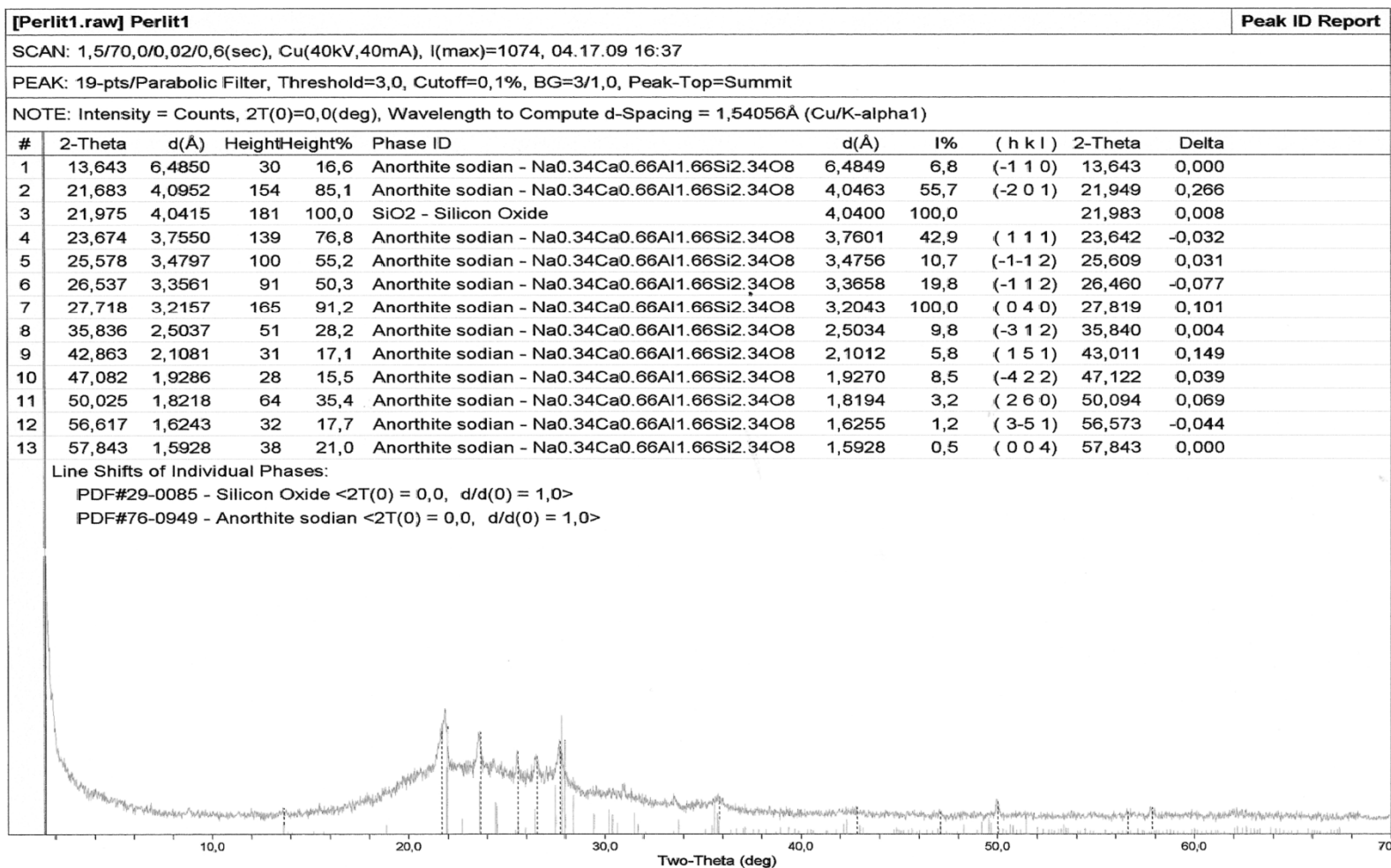


Table B.3. Interlayer spacings and peak intensities of virgin sepiolite.

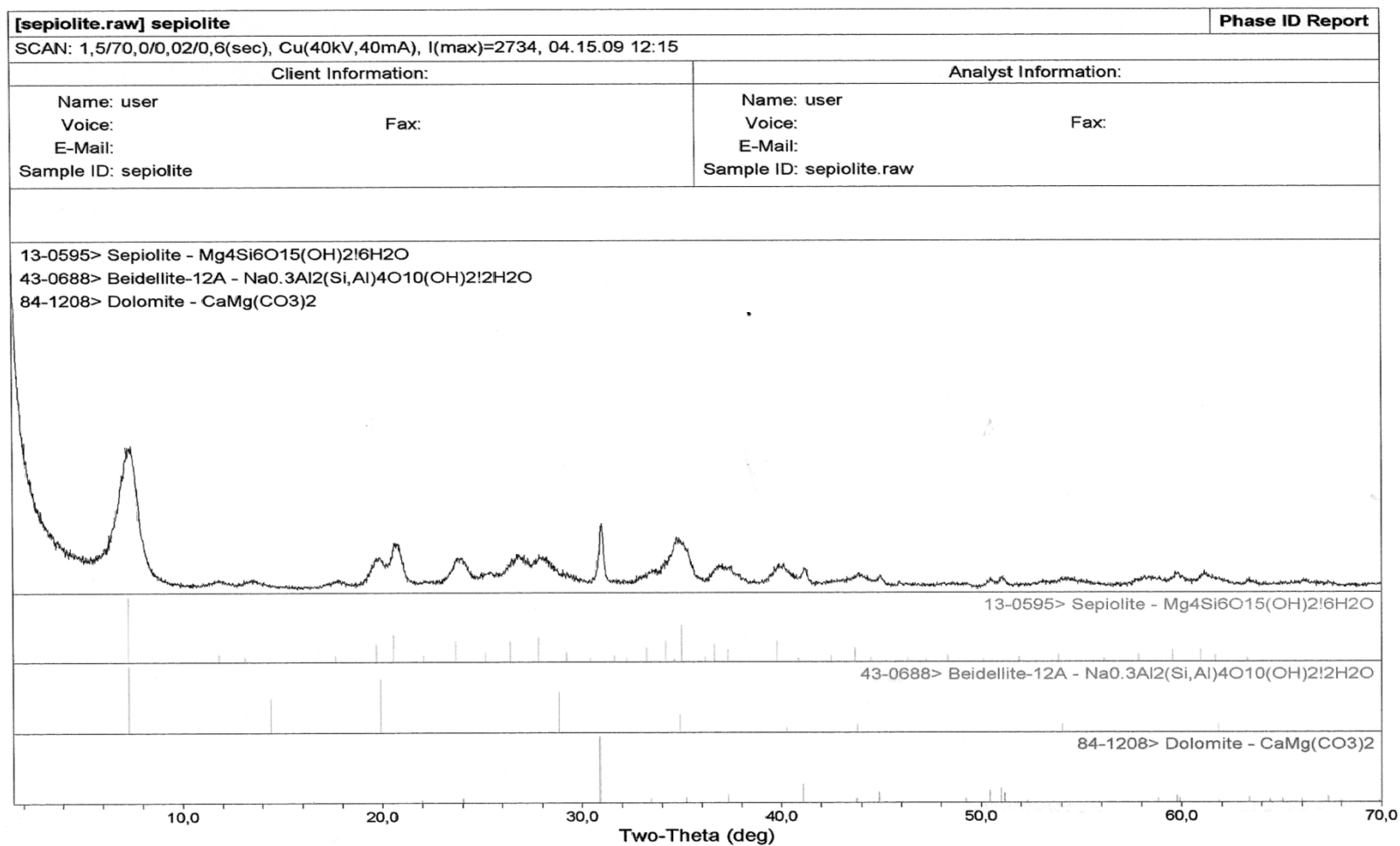


Table B.3. Continued.

[sepiolite.raw] sepiolite										Peak ID Report
SCAN: 1,5/70,0/0,02/0,6(sec), Cu(40kV,40mA), I(max)=2734, 04.15.09 12:15										
PEAK: 33-pts/Parabolic Filter, Threshold=3,0, Cutoff=0,1%, BG=3/1,0, Peak-Top=Summit										
NOTE: Intensity = Counts, 2T(0)=0,0(deg), Wavelength to Compute d-Spacing = 1,54056Å (Cu/K-alpha1)										
#	2-Theta	d(Å)	Height	Height%	Phase ID	d(Å)	I%	(h k l)	2-Theta	Delta
1	7,460	11,8411	980	100,0	Beidellite-12A - Na0.3Al2(Si,Al)4O10(OH)2!2...	12,0264	100,0	(0 0 1)	7,345	-0,115
2	11,941	7,4052	38	3,9	Sepiolite - Mg4Si6O15(OH)2!6H2O	7,4700	10,0	(1 3 0)	11,837	-0,104
3	13,243	6,6800	33	3,4	Sepiolite - Mg4Si6O15(OH)2!6H2O	6,7300	6,0	(0 4 0)	13,144	-0,099
4	17,935	4,9416	39	4,0	Sepiolite - Mg4Si6O15(OH)2!6H2O	5,0100	8,0	(1 5 0)	17,688	-0,247
5	19,880	4,4623	213	21,7	Beidellite-12A - Na0.3Al2(Si,Al)4O10(OH)2!2...	4,4462	80,0	(1 0 0)	19,953	0,073
6	20,740	4,2793	320	32,7	Sepiolite - Mg4Si6O15(OH)2!6H2O	4,3100	40,0	(1 3 1)	20,590	-0,150
7	23,960	3,7110	176	18,0	Dolomite - CaMg(CO3)2	3,6976	5,2	(0 1 2)	24,048	0,088
8	25,438	3,4985	36	3,7	Sepiolite - Mg4Si6O15(OH)2!6H2O	3,5300	12,0	(2 4 1)	25,208	-0,231
9	26,539	3,3559	102	10,4	Sepiolite - Mg4Si6O15(OH)2!6H2O	3,3700	30,0	(0 8 0)	26,426	-0,113
10	28,064	3,1769	99	10,1	Sepiolite - Mg4Si6O15(OH)2!6H2O	3,2000	35,0	(3 3 1)	27,857	-0,206
11	31,020	2,8806	478	48,8	Dolomite - CaMg(CO3)2	2,8899	100,0	(1 0 4)	30,917	-0,102
12	33,560	2,6681	109	11,1	Dolomite - CaMg(CO3)2	2,6745	4,5	(0 0 6)	33,478	-0,083
13	34,781	2,5772	297	30,3	Sepiolite - Mg4Si6O15(OH)2!6H2O	2,5860	2,0	(5 3 0)	34,659	-0,122
14	36,918	2,4328	112	11,4	Sepiolite - Mg4Si6O15(OH)2!6H2O	2,4490	25,0	(2 0 2)	36,665	-0,253
15	37,500	2,3964	106	10,8	Dolomite - CaMg(CO3)2	2,4055	10,4	(1 1 0)	37,352	-0,148
16	40,102	2,2467	127	13,0	Beidellite-12A - Na0.3Al2(Si,Al)4O10(OH)2!2...	2,2362	5,0	(2 0 0)	40,298	0,196
17	41,181	2,1903	101	10,3	Dolomite - CaMg(CO3)2	2,1939	26,2	(1 1 -3)	41,110	-0,071
18	43,936	2,0591	61	6,2	Beidellite-12A - Na0.3Al2(Si,Al)4O10(OH)2!2...	2,0635	10,0	(0 0 6)	43,838	-0,098
19	44,983	2,0136	58	5,9	Dolomite - CaMg(CO3)2	2,0164	13,7	(2 0 2)	44,917	-0,066
20	50,517	1,8052	71	7,2	Dolomite - CaMg(CO3)2	1,8073	15,6	(0 1 8)	50,453	-0,064
21	51,117	1,7854	74	7,6	Dolomite - CaMg(CO3)2	1,7830	11,4	(0 0 9)	51,191	0,074
22	54,257	1,6893	35	3,6	Beidellite-12A - Na0.3Al2(Si,Al)4O10(OH)2!2...	1,6946	10,0	(2 1 0)	54,072	-0,185
23	58,059	1,5874	44	4,5	Sepiolite - Mg4Si6O15(OH)2!6H2O	1,5920	10,0	(3 15 1)	57,874	-0,185
24	59,860	1,5438	74	7,6	Dolomite - CaMg(CO3)2	1,5453	7,9	(2 1 -2)	59,798	-0,062
25	61,181	1,5136	83	8,5	Sepiolite - Mg4Si6O15(OH)2!6H2O	1,5180	16,0	(0 17 1)	60,986	-0,195
26	63,439	1,4651	52	5,3	Dolomite - CaMg(CO3)2	1,4659	5,5	(1 2 -4)	63,400	-0,039
Line Shifts of Individual Phases:										
PDF#13-0595 - Sepiolite <2T(0) = 0,0, d/d(0) = 1,0>										

Table B.4. Interlayer spacings and peak intensities of spent sepiolite.

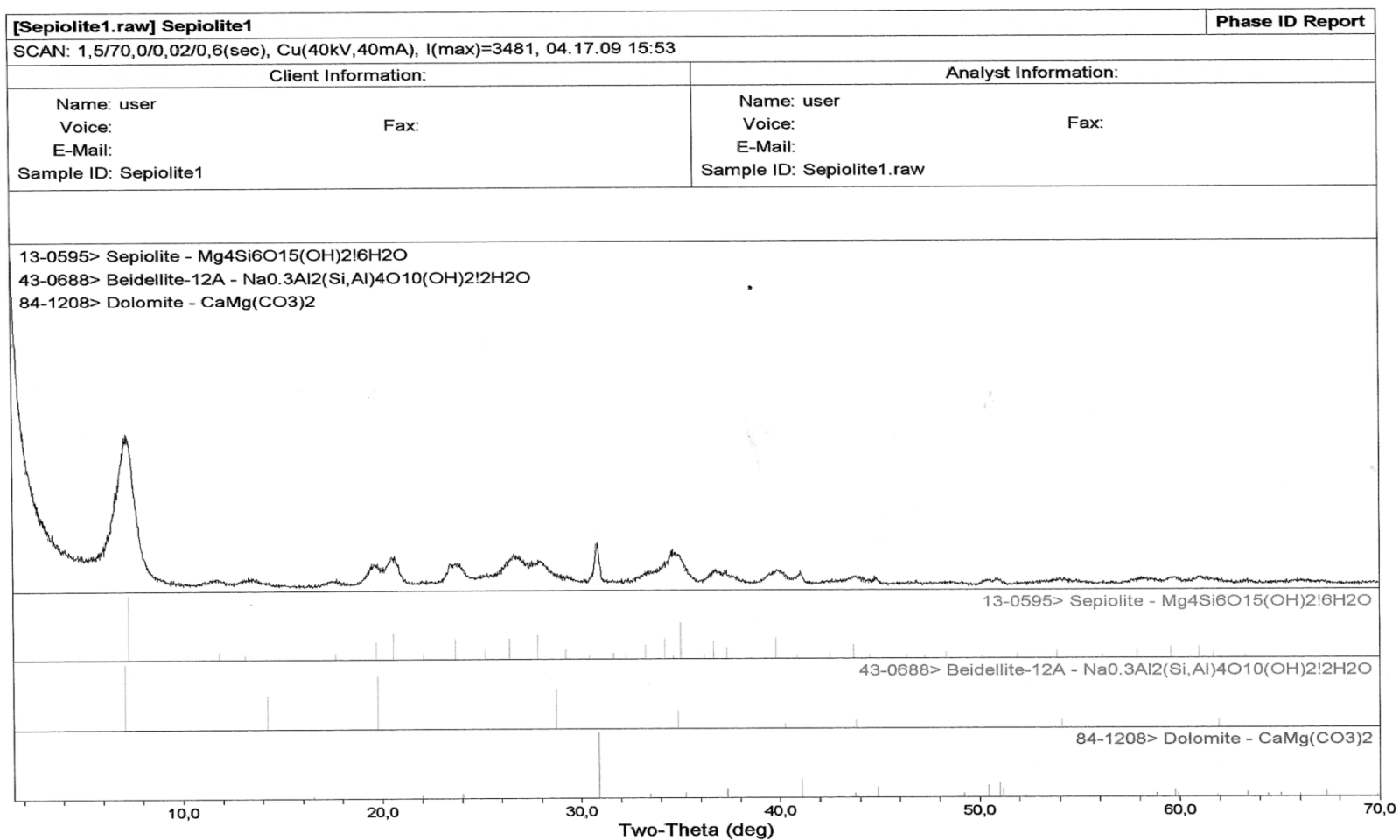


Table B.4. Continued.

[Sepiolite1.raw] Sepiolite1										Peak ID Report
SCAN: 1,5/70,0/0,02/0,6(sec), Cu(40kV,40mA), I(max)=3481, 04.17.09 15:53										
PEAK: 35-pts/Parabolic Filter, Threshold=3,0, Cutoff=0,1%, BG=3/1,0, Peak-Top=Summit										
NOTE: Intensity = Counts, 2T(0)=0,0(deg), Wavelength to Compute d-Spacing = 1,54056Å (Cu/K-alpha1)										
#	2-Theta	d(Å)	Height	Height%	Phase ID	d(Å)	I%	(h k l)	2-Theta	Delta
1	7,200	12,2674	1251	100,0	Beidellite-12A - Na0.3Al2(Si,Al)4O10(OH)2!2...	12,4000	100,0	(0 0 1)	7,123	-0,077
2	11,899	7,4315	43	3,4	Sepiolite - Mg4Si6O15(OH)2!6H2O	7,4700	10,0	(1 3 0)	11,837	-0,062
3	13,245	6,6789	41	3,3	Sepiolite - Mg4Si6O15(OH)2!6H2O	6,7300	6,0	(0 4 0)	13,144	-0,101
4	14,140	6,2583	5	0,4	Beidellite-12A - Na0.3Al2(Si,Al)4O10(OH)2!2...	6,2000	50,0	(0 0 2)	14,274	0,134
5	17,760	4,9899	55	4,4	Sepiolite - Mg4Si6O15(OH)2!6H2O	5,0100	8,0	(1 5 0)	17,688	-0,072
6	19,541	4,5391	216	17,3	Sepiolite - Mg4Si6O15(OH)2!6H2O	4,5000	25,0	(0 6 0)	19,712	0,172
7	19,800	4,4802	196	15,7	Beidellite-12A - Na0.3Al2(Si,Al)4O10(OH)2!2...	4,4800	80,0	(1 0 0)	19,801	0,001
8	20,678	4,2918	286	22,9	Sepiolite - Mg4Si6O15(OH)2!6H2O	4,3100	40,0	(1 3 1)	20,590	-0,088
9	22,118	4,0157	12	1,0	Sepiolite - Mg4Si6O15(OH)2!6H2O	4,0200	8,0	(3 3 0)	22,094	-0,024
10	23,679	3,7543	168	13,4	Sepiolite - Mg4Si6O15(OH)2!6H2O	3,7500	30,0	(2 6 0)	23,707	0,027
11	25,289	3,5188	16	1,3	Sepiolite - Mg4Si6O15(OH)2!6H2O	3,5300	12,0	(2 4 1)	25,208	-0,081
12	26,679	3,3385	166	13,3	Sepiolite - Mg4Si6O15(OH)2!6H2O	3,3700	30,0	(0 8 0)	26,426	-0,254
13	28,096	3,1734	92	7,4	Sepiolite - Mg4Si6O15(OH)2!6H2O	3,2000	35,0	(3 3 1)	27,857	-0,239
14	30,879	2,8933	405	32,4	Dolomite - CaMg(CO3)2	2,8899	100,0	(1 0 4)	30,917	0,038
15	34,639	2,5875	268	21,4	Sepiolite - Mg4Si6O15(OH)2!6H2O	2,5860	2,0	(5 3 0)	34,659	0,020
16	35,038	2,5589	266	21,3	Sepiolite - Mg4Si6O15(OH)2!6H2O	2,5600	55,0	(3 7 1)	35,022	-0,016
17	36,817	2,4392	116	9,3	Sepiolite - Mg4Si6O15(OH)2!6H2O	2,4490	25,0	(2 0 2)	36,665	-0,152
18	37,421	2,4012	55	4,4	Dolomite - CaMg(CO3)2	2,4055	10,4	(1 1 0)	37,352	-0,069
19	39,642	2,2716	91	7,3	Sepiolite - Mg4Si6O15(OH)2!6H2O	2,2630	30,0	(5 4 1)	39,800	0,158
20	40,060	2,2489	95	7,6	Beidellite-12A - Na0.3Al2(Si,Al)4O10(OH)2!2...	2,2380	5,0	(2 0 0)	40,264	0,204
21	41,062	2,1963	103	8,2	Dolomite - CaMg(CO3)2	2,1939	26,2	(1 1-3)	41,110	0,048
22	43,841	2,0633	52	4,2	Beidellite-12A - Na0.3Al2(Si,Al)4O10(OH)2!2...	2,0640	10,0	(0 0 6)	43,826	-0,015
23	44,856	2,0190	42	3,4	Dolomite - CaMg(CO3)2	2,0164	13,7	(2 0 2)	44,917	0,061
24	50,540	1,8044	53	4,2	Dolomite - CaMg(CO3)2	1,8073	15,6	(0 1 8)	50,453	-0,087
25	51,095	1,7861	49	3,9	Dolomite - CaMg(CO3)2	1,7885	19,6	(1 1-6)	51,022	-0,073
26	54,275	1,6887	42	3,4	Beidellite-12A - Na0.3Al2(Si,Al)4O10(OH)2!2...	1,6930	10,0	(2 1 0)	54,127	-0,147
27	58,081	1,5868	41	3,3	Sepiolite - Mg4Si6O15(OH)2!6H2O	1,5920	10,0	(3 15 1)	57,874	-0,208
28	59,761	1,5461	39	3,1	Dolomite - CaMg(CO3)2	1,5453	7,9	(2 1-2)	59,798	0,037
29	60,979	1,5181	46	3,7	Sepiolite - Mg4Si6O15(OH)2!6H2O	1,5180	16,0	(0 17 1)	60,986	0,007

Table B.5. Interlayer spacings and peak intensities of virgin bentonite.

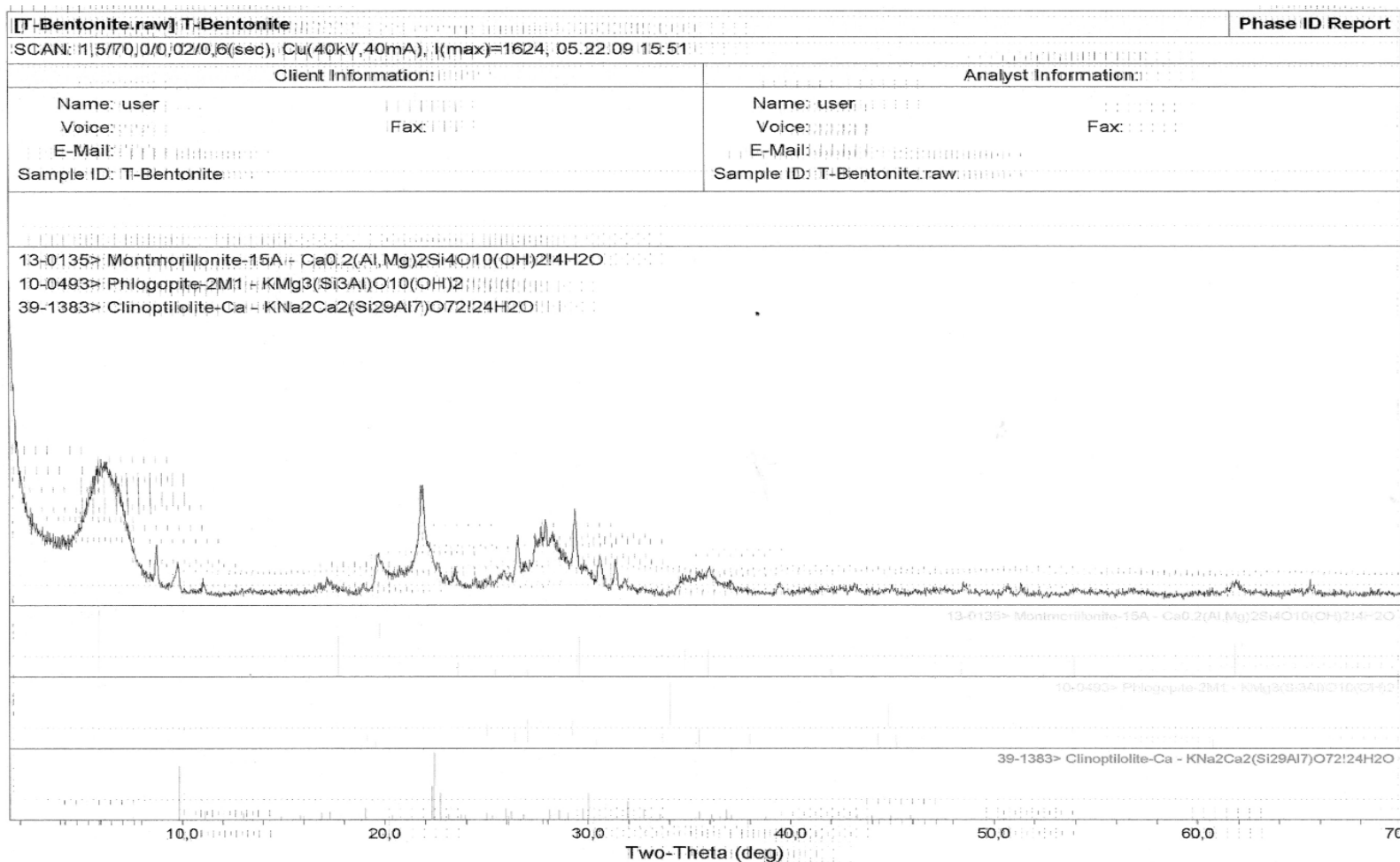


Table B.5. Continued.

[T-Bentonite.raw] T-Bentonite											Peak ID Report
SCAN: 1,5/70,0/0,02/0,6(sec), Cu(40kV,40mA), I(max)=1624, 05.22.09 15:51											
PEAK: 23-pts/Parabolic Filter, Threshold=3,0, Cutoff=0,1%, BG=3/1,0, Peak-Top=Summit											
NOTE: Intensity = Counts, 2T(0)=0,0(deg), Wavelength to Compute d-Spacing = 1,54056Å (Cu/K-alpha1)											
#	2-Theta	d(Å)	Height	Height%	Phase ID	d(Å)	I%	(h k l)	2-Theta	Delta	
1	6,180	14,2896	263	60,7	Montmorillonite-15A - Ca0,2(Al,Mg)2Si4O10(O...	14,9746	100,0	(0 0 1)	5,897	-0,283	
2	9,781	9,0356	118	27,3	Clinoptilolite-Ca - KNa2Ca2(Si29Al7)O72!24H2O	8,9500	79,4	(0 2 0)	9,875	0,094	
3	11,075	7,9826	41	9,5	Clinoptilolite-Ca - KNa2Ca2(Si29Al7)O72!24H2O	7,9300	10,3	(2 0 0)	11,148	0,074	
4	16,804	5,2716	39	9,0	Clinoptilolite-Ca - KNa2Ca2(Si29Al7)O72!24H2O	5,2400	7,9	(3 1-1)	16,906	0,102	
5	17,179	5,1574	63	14,5	Clinoptilolite-Ca - KNa2Ca2(Si29Al7)O72!24H2O	5,1200	9,5	(1 1 1)	17,305	0,127	
6	19,718	4,4986	179	41,3	Montmorillonite-15A - Ca0,2(Al,Mg)2Si4O10(O...	4,4977	80,0	(1 0 0)	19,722	0,004	
7	21,860	4,0624	433	100,0	Phlogopite-2M1 - KMg3(Si3Al)O10(OH)2	4,1023	6,0	(1 1 2)	21,645	-0,215	
8	22,318	3,9801	122	28,2	Clinoptilolite-Ca - KNa2Ca2(Si29Al7)O72!24H2O	3,9760	48,4	(1 3 1)	22,341	0,023	
9	23,480	3,7857	81	18,7	Montmorillonite-15A - Ca0,2(Al,Mg)2Si4O10(O...	3,7684	20,0	(0 0 4)	23,589	0,109	
10	25,210	3,5297	44	10,2	Clinoptilolite-Ca - KNa2Ca2(Si29Al7)O72!24H2O	3,5130	3,2	(1 1-2)	25,332	0,122	
11	25,844	3,4445	44	10,2	Clinoptilolite-Ca - KNa2Ca2(Si29Al7)O72!24H2O	3,4240	14,3	(2 2-2)	26,002	0,158	
12	26,560	3,3533	162	37,4	Phlogopite-2M1 - KMg3(Si3Al)O10(OH)2	3,3777	100,0	(0 0 6)	26,365	-0,195	
13	27,921	3,1928	208	48,0	Clinoptilolite-Ca - KNa2Ca2(Si29Al7)O72!24H2O	3,1700	12,7	(4 2-2)	28,126	0,205	
14	28,297	3,1512	145	33,5	Phlogopite-2M1 - KMg3(Si3Al)O10(OH)2	3,1697	10,0	(-1 1 5)	28,129	-0,169	
15	29,380	3,0375	277	64,0	Phlogopite-2M1 - KMg3(Si3Al)O10(OH)2	3,0527	40,0	(0 2 5)	29,230	-0,149	
16	30,603	2,9189	129	29,8	Phlogopite-2M1 - KMg3(Si3Al)O10(OH)2	2,9377	10,0	(1 1 5)	30,401	-0,201	
17	31,381	2,8482	136	31,4	Phlogopite-2M1 - KMg3(Si3Al)O10(OH)2	2,8289	20,0	(-1 1 6)	31,602	0,220	
18	31,857	2,8068	48	11,1	Clinoptilolite-Ca - KNa2Ca2(Si29Al7)O72!24H2O	2,7950	25,4	(5 3 0)	31,995	0,138	
19	34,669	2,5853	95	21,9	Montmorillonite-15A - Ca0,2(Al,Mg)2Si4O10(O...	2,5793	40,0	(1 1 0)	34,752	0,083	
20	35,481	2,5279	60	13,9	Clinoptilolite-Ca - KNa2Ca2(Si29Al7)O72!24H2O	2,5270	9,5	(6 2 0)	35,495	0,013	
21	36,019	2,4914	75	17,3	Clinoptilolite-Ca - KNa2Ca2(Si29Al7)O72!24H2O	2,4850	4,8	(3 5 1)	36,115	0,097	
22	39,458	2,2818	52	12,0	Phlogopite-2M1 - KMg3(Si3Al)O10(OH)2	2,2769	10,0	(-1 3 5)	39,547	0,090	
23	43,147	2,0949	37	8,5	Clinoptilolite-Ca - KNa2Ca2(Si29Al7)O72!24H2O	2,0890	4,8	(3 7-2)	43,275	0,128	
24	44,997	2,0130	41	9,5	Clinoptilolite-Ca - KNa2Ca2(Si29Al7)O72!24H2O	2,0160	3,2	(6 4-3)	44,926	-0,071	
25	47,591	1,9091	32	7,4	Phlogopite-2M1 - KMg3(Si3Al)O10(OH)2	1,9188	6,0	(1 3 7)	47,337	-0,254	
26	48,655	1,8698	46	10,6	Montmorillonite-15A - Ca0,2(Al,Mg)2Si4O10(O...	1,8796	10,0	(0 0 8)	48,385	-0,270	
27	54,022	1,6960	28	6,5	Montmorillonite-15A - Ca0,2(Al,Mg)2Si4O10(O...	1,6997	30,0	(2 1 0)	53,896	-0,126	
28	60,724	1,5239	30	6,9	Phlogopite-2M1 - KMg3(Si3Al)O10(OH)2	1,5238	10,0	(0 6 2)	60,728	0,003	
29	61,901	1,4977	62	14,3	Montmorillonite-15A - Ca0,2(Al,Mg)2Si4O10(O...	1,4998	50,0	(0 0 10)	61,807	-0,094	

Table B.6. Interlayer spacings and peak intensities of spent bentonite.

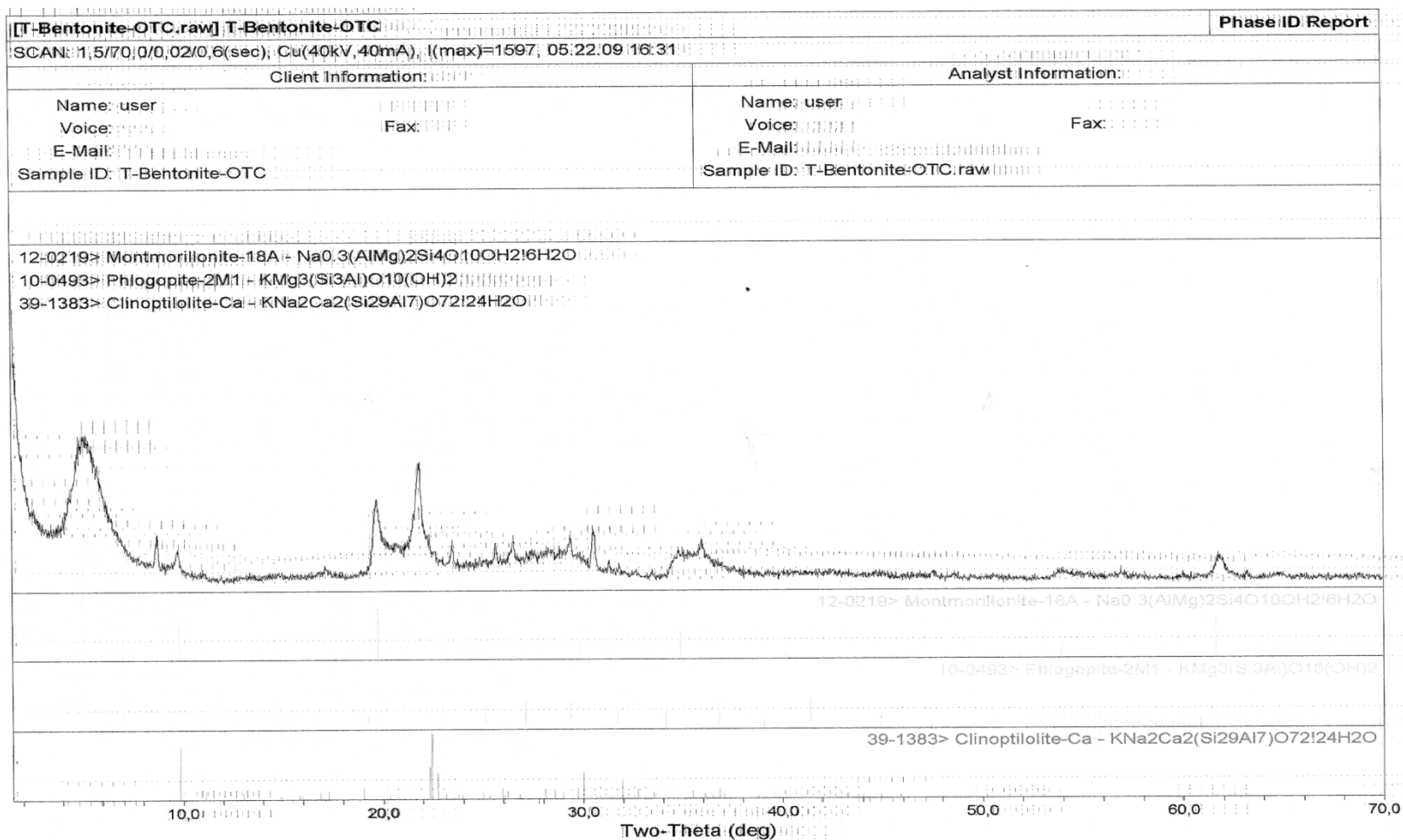


Table B.6. Continued.

[T-Bentonite-OTC.raw] T-Bentonite-OTC											Peak ID Report
SCAN: 1,5/70,0/0,02/0,6(sec), Cu(40kV,40mA), I(max)=1597, 05.22.09 16:31											
PEAK: 23-pts/Parabolic Filter, Threshold=3,0, Cutoff=0,1%, BG=3/1,0, Peak-Top=Summit											
NOTE: Intensity = Counts, 2 θ (0)=0,0(deg), Wavelength to Compute d-Spacing = 1,54056Å (Cu/K-alpha1)											
#	2-Theta	d(Å)	Height	Height%	Phase ID	d(Å)	I%	(h k l)	2-Theta	Delta	
1	5,118	17,2507	364	82,2	Montmorillonite-18A - Na0.3(AlMg)2Si4O10OH...	17,6000	100,0	(0 0 1)	5,017	-0,102	
2	8,761	10,0845	151	34,1	Phlogopite-2M1 - KMg3(Si3Al)O10(OH)2	10,1000	100,0	(0 0 2)	8,748	-0,014	
3	9,798	9,0198	104	23,5	Montmorillonite-18A - Na0.3(AlMg)2Si4O10OH...	9,0000	50,0	(0 0 2)	9,820	0,022	
4	17,236	5,1403	34	7,7	Clinoptilolite-Ca - KNa2Ca2(Si29Al7)O72!24H2O	5,1200	9,5	(1 1 1)	17,305	0,069	
5	19,739	4,4939	368	83,1	Montmorillonite-18A - Na0.3(AlMg)2Si4O10OH...	4,4900	80,0	(0 0 4)	19,756	0,017	
6	21,918	4,0518	443	100,0	Phlogopite-2M1 - KMg3(Si3Al)O10(OH)2	4,0790	6,0	(1 1 2)	21,770	-0,148	
7	22,381	3,9690	100	22,6	Clinoptilolite-Ca - KNa2Ca2(Si29Al7)O72!24H2O	3,9760	48,4	(1 3 1)	22,341	-0,040	
8	23,522	3,7790	120	27,1	Phlogopite-2M1 - KMg3(Si3Al)O10(OH)2	3,8140	20,0	(0 2 3)	23,303	-0,219	
9	25,777	3,4533	22	5,0	Clinoptilolite-Ca - KNa2Ca2(Si29Al7)O72!24H2O	3,4240	14,3	(2 2-2)	26,002	0,225	
10	26,595	3,3489	122	27,5	Phlogopite-2M1 - KMg3(Si3Al)O10(OH)2	3,3620	100,0	(0 0 6)	26,490	-0,105	
11	27,340	3,2594	20	4,5	Phlogopite-2M1 - KMg3(Si3Al)O10(OH)2	3,2830	40,0	(1 1 4)	27,139	-0,200	
12	28,234	3,1581	51	11,5	Phlogopite-2M1 - KMg3(Si3Al)O10(OH)2	3,1560	10,0	(-1 1 5)	28,254	0,019	
13	29,422	3,0333	119	26,9	Phlogopite-2M1 - KMg3(Si3Al)O10(OH)2	3,0400	40,0	(0 2 5)	29,355	-0,067	
14	30,580	2,9210	197	44,5	Phlogopite-2M1 - KMg3(Si3Al)O10(OH)2	2,9260	10,0	(1 1 5)	30,526	-0,053	
15	31,883	2,8045	46	10,4	Clinoptilolite-Ca - KNa2Ca2(Si29Al7)O72!24H2O	2,7950	25,4	(5 3 0)	31,995	0,112	
16	33,536	2,6700	33	7,4	Clinoptilolite-Ca - KNa2Ca2(Si29Al7)O72!24H2O	2,6670	6,3	(2 0 2)	33,575	0,038	
17	34,878	2,5702	126	28,4	Montmorillonite-18A - Na0.3(AlMg)2Si4O10OH...	2,5700	40,0	(1 1 1)	34,882	0,003	
18	35,423	2,5319	53	12,0	Clinoptilolite-Ca - KNa2Ca2(Si29Al7)O72!24H2O	2,5270	9,5	(6 2 0)	35,495	0,072	
19	36,000	2,4927	100	22,6	Clinoptilolite-Ca - KNa2Ca2(Si29Al7)O72!24H2O	2,4850	4,8	(3 5 1)	36,115	0,115	
20	47,595	1,9090	32	7,2	Phlogopite-2M1 - KMg3(Si3Al)O10(OH)2	1,9140	6,0	(1 3 7)	47,462	-0,133	
21	54,058	1,6950	48	10,8	Montmorillonite-18A - Na0.3(AlMg)2Si4O10OH...	1,6990	20,0	(2 1 0)	53,921	0,138	
22	61,898	1,4978	107	24,2	Montmorillonite-18A - Na0.3(AlMg)2Si4O10OH...	1,5040	60,0	(3 0 0)	61,615	-0,283	
Line Shifts of Individual Phases:											
PDF#12-0219 - Montmorillonite-18A <2 θ (0) = 0,0; d/d(0) = 1,0>											
PDF#10-0493 - Phlogopite-2M1 <2 θ (0) = 0,0; d/d(0) = 1,0>											
PDF#39-1383 - Clinoptilolite-Ca <2 θ (0) = 0,0; d/d(0) = 1,0>											

Table B.7. Interlayer spacings and peak intensities of ozonated bentonite.

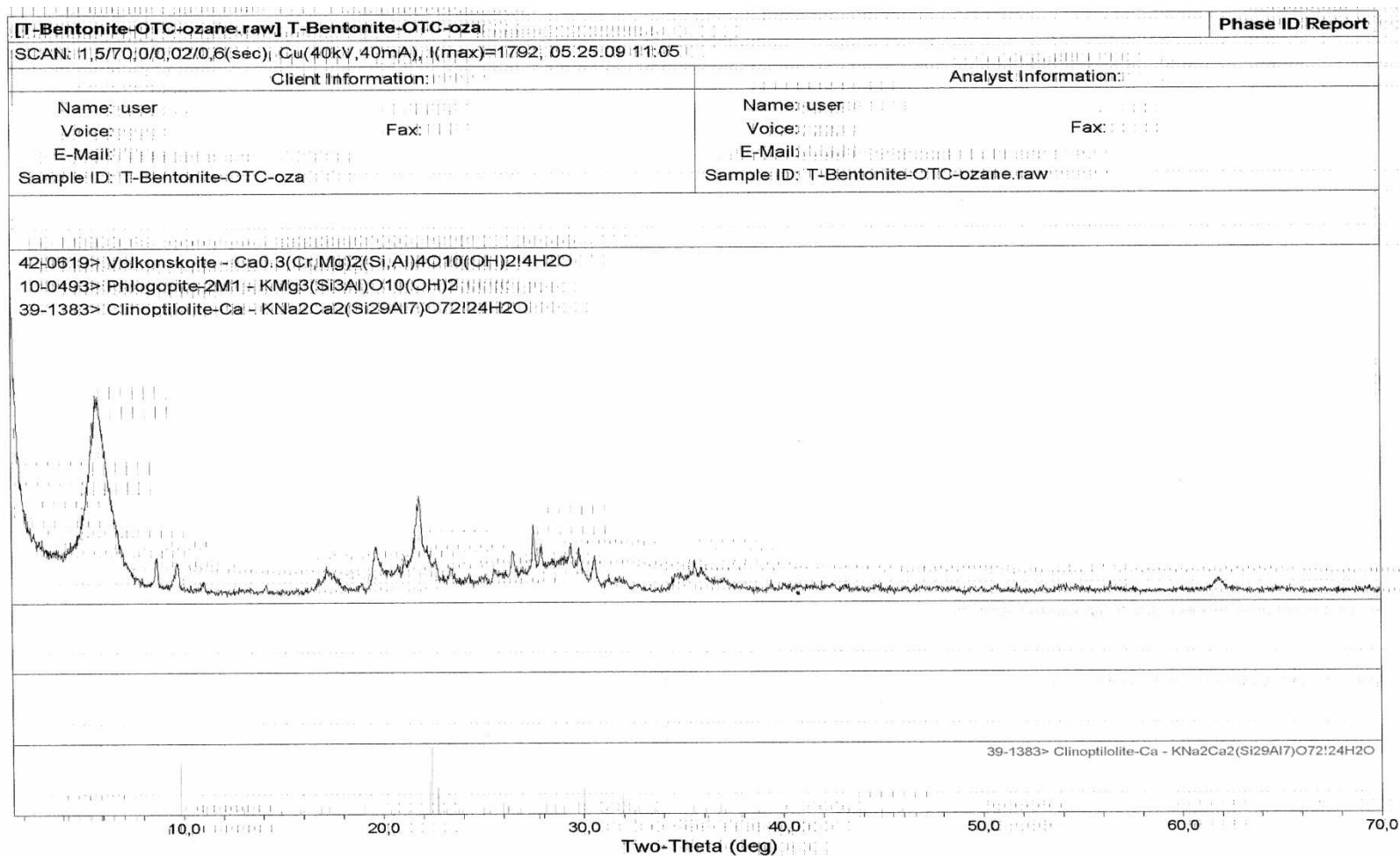


Table B.7. Continued.

[T-Bentonite-OTC-ozane.raw] T-Bentonite-OTC-oz											Peak ID Report
SCAN: 1,5/70,0/0,02/0,6(sec), Cu(40kV,40mA), I(max)=1792, 05.25.09 11:05											
PEAK: 23-pts/Parabolic Filter, Threshold=3,0, Cutoff=0,1%, BG=3/1,0, Peak-Top=Summit											
NOTE: Intensity = Counts, 2T(0)=0,0(deg), Wavelength to Compute d-Spacing = 1,54056Å (Cu/K-alpha1)											
#	2-Theta	d(Å)	Height	Height%	Phase ID	d(Å)	I%	(h k l)	2-Theta	Delta	
1	5,820	15,1720	752	100,0	Volkonskoite - Ca0.3(Cr,Mg)2(Si,Al)4O10(OH)...	15,0000	100,0	(0 0 1)	5,887	0,067	
2	8,759	10,0868	145	19,3	Phlogopite-2M1 - KMg3(Si3Al)O10(OH)2	10,1000	100,0	(0 0 2)	8,748	-0,011	
3	9,760	9,0544	135	18,0	Clinoptilolite-Ca - KNa2Ca2(Si29Al7)O72!24H2O	8,9500	79,4	(0 2 0)	9,875	0,114	
4	11,101	7,9634	53	7,0	Clinoptilolite-Ca - KNa2Ca2(Si29Al7)O72!24H2O	7,9300	10,3	(2 0 0)	11,148	0,047	
5	17,238	5,1398	117	15,6	Clinoptilolite-Ca - KNa2Ca2(Si29Al7)O72!24H2O	5,1200	9,5	(1 1 1)	17,305	0,067	
6	18,985	4,6708	37	4,9	Clinoptilolite-Ca - KNa2Ca2(Si29Al7)O72!24H2O	4,6500	15,1	(1 3-1)	19,070	0,086	
7	19,680	4,5072	230	30,6	Phlogopite-2M1 - KMg3(Si3Al)O10(OH)2	4,5150	8,0	(0 2 1)	19,646	-0,034	
8	20,337	4,3631	43	5,7	Clinoptilolite-Ca - KNa2Ca2(Si29Al7)O72!24H2O	4,3500	4,0	(4 0-1)	20,399	0,062	
9	21,861	4,0622	411	54,7	Phlogopite-2M1 - KMg3(Si3Al)O10(OH)2	4,0790	6,0	(1 1 2)	21,770	-0,091	
10	22,280	3,9869	142	18,9	Clinoptilolite-Ca - KNa2Ca2(Si29Al7)O72!24H2O	3,9760	48,4	(1 3 1)	22,341	0,062	
11	23,429	3,7938	65	8,6	Phlogopite-2M1 - KMg3(Si3Al)O10(OH)2	3,8140	20,0	(0 2 3)	23,303	-0,126	
12	25,608	3,4758	47	6,3	Clinoptilolite-Ca - KNa2Ca2(Si29Al7)O72!24H2O	3,5130	3,2	(1 1-2)	25,332	-0,276	
13	26,542	3,3556	126	16,8	Phlogopite-2M1 - KMg3(Si3Al)O10(OH)2	3,3620	100,0	(0 0 6)	26,490	-0,052	
14	27,360	3,2570	12	1,6	Phlogopite-2M1 - KMg3(Si3Al)O10(OH)2	3,2830	40,0	(1 1 4)	27,139	-0,221	
15	27,955	3,1890	123	16,4	Clinoptilolite-Ca - KNa2Ca2(Si29Al7)O72!24H2O	3,1700	12,7	(4 2-2)	28,126	0,171	
16	29,124	3,0636	55	7,3	Clinoptilolite-Ca - KNa2Ca2(Si29Al7)O72!24H2O	3,0740	7,1	(1 3-2)	29,024	-0,101	
17	29,456	3,0299	156	20,7	Phlogopite-2M1 - KMg3(Si3Al)O10(OH)2	3,0400	40,0	(0 2 5)	29,355	-0,100	
18	29,857	2,9901	112	14,9	Clinoptilolite-Ca - KNa2Ca2(Si29Al7)O72!24H2O	2,9980	14,3	(3 5-1)	29,776	-0,080	
19	30,639	2,9155	140	18,6	Phlogopite-2M1 - KMg3(Si3Al)O10(OH)2	2,9260	10,0	(1 1 5)	30,526	-0,112	
20	31,875	2,8052	55	7,3	Phlogopite-2M1 - KMg3(Si3Al)O10(OH)2	2,8180	20,0	(-1 1 6)	31,727	-0,148	
21	31,957	2,7982	42	5,6	Clinoptilolite-Ca - KNa2Ca2(Si29Al7)O72!24H2O	2,7950	25,4	(5 3 0)	31,995	0,037	
22	34,919	2,5673	96	12,8	Volkonskoite - Ca0.3(Cr,Mg)2(Si,Al)4O10(OH)...	2,5600	35,0	(1 1 0)	35,022	0,103	
23	35,617	2,5186	102	13,6	Phlogopite-2M1 - KMg3(Si3Al)O10(OH)2	2,5220	30,0	(0 0 8)	35,567	-0,050	
24	35,994	2,4931	65	8,6	Clinoptilolite-Ca - KNa2Ca2(Si29Al7)O72!24H2O	2,4850	4,8	(3 5 1)	36,115	0,121	
25	39,435	2,2831	52	6,9	Phlogopite-2M1 - KMg3(Si3Al)O10(OH)2	2,2700	10,0	(-1 3 5)	39,672	0,237	
26	44,815	2,0207	29	3,9	Phlogopite-2M1 - KMg3(Si3Al)O10(OH)2	2,0170	65,0	(0 0 10)	44,902	0,087	
27	54,263	1,6891	33	4,4	Volkonskoite - Ca0.3(Cr,Mg)2(Si,Al)4O10(OH)...	1,6900	8,0	(2 1 0)	54,231	-0,032	
28	61,997	1,4956	50	6,6	Volkonskoite - Ca0.3(Cr,Mg)2(Si,Al)4O10(OH)...	1,5000	35,0	(3 0 0)	61,797	-0,200	

APPENDIX C

Surface Area Data of Adsorbents

Table C.1. Surface area data of virgin perlite.


Quantachrome NovaWin2 - Data Acquisition and Reduction for NOVA instruments ©1994-2007, Quantachrome Instruments version 9.0				 <small>Optimizing particle performance</small>	
Analysis		Report			
Operator: serife	Date: 2009/03/20	Operator:	Date: 3/25/2009		
Sample ID: perlite	Filename:	C:\QCdata\Physisorb\perlite20mart.qps			
Sample Desc:	Comment:				
Sample weight: 0.3554 g	Sample Volume: 0.3554 cc	Sample Density: 1 g/cc			
Outgas Time: 2.5 hrs	Outgas Temp: 200.0 C				
Analysis gas: Nitrogen	Bath Temp: 77.3 K				
Press. Tolerance: 0.100/0.100 (ads/des)	Equil time: 60/60 sec (ads/des)	Equil timeout: 240/240 sec (ads/des)			
Analysis Time: 257.5 min	End of run: 2009/03/20 16:07:25	Instrument: Nova Station A			
Cell ID: 1					
Area-Volume Summary					
Data Reduction Parameters Data					
Adsorbate	Nitrogen	Temperature	77.350K	Liquid Density: 0.808 g/cc	
	Molec. Wt.: 28.013 g	Cross Section:	16.200 Å²		
Surface Area Data					
MultiPoint BET.....					1.178e+01 m²/g
Langmuir surface area.....					2.017e+01 m²/g
t-method external surface area.....					1.178e+01 m²/g
DR method micropore area.....					1.279e+01 m²/g
NLDFT cumulative surface area.....					4.747e+00 m²/g
Pore Volume Data					
DR method micropore volume.....					4.545e-03 cc/g
HK method cumulative pore volume.....					3.029e-03 cc/g
SF method cumulative pore volume.....					3.155e-03 cc/g
NLDFT method cumulative pore volume.....					5.002e-03 cc/g
Pore Size Data					
DR method micropore Half pore width.....					2.048e+01 Å
DA method pore Radius (Mode).....					1.120e+01 Å
HK method pore Radius (Mode).....					1.838e+00 Å
SF method pore Radius (Mode).....					2.261e+00 Å
NLDFT pore Radius (Mode).....					1.210e+01 Å

Table C.2. Surface area data of virgin sepiolite.

Quantachrome NovaWin2 - Data Acquisition and Reduction for NOVA instruments ©1994-2007, Quantachrome Instruments version 9.0				Quantachrome INSTRUMENTS <i>Optimizing particle performance</i>	
Analysis		Report			
Operator: serife	Date: 2009/03/20	Operator:	Date: 3/25/2009		
Sample ID: sepiolite20mar	Filename:	C:\QCdata\Physisorb\sepiolite.qps			
Sample Desc:	Comment:				
Sample weight: 0.2595 g	Sample Volume: 0.2595 cc	Sample Density: 1 g/cc			
Outgas Time: 2.5 hrs	OutgasTemp: 200.0 C				
Analysis gas: Nitrogen	Bath Temp: 77.3 K				
Press. Tolerance: 0.100/0.100 (ads/des)	Equil time: 60/60 sec (ads/des)	Equil timeout: 240/240 sec (ads/des)			
Analysis Time: 260.2 min	End of run: 2009/03/20 16:10:09	Instrument: Nova Station B			
Cell ID: 66					
Area-Volume Summary					
Data Reduction Parameters Data					
Adsorbate	Nitrogen	Temperature	77.350K		
	Molec. Wt.: 28.013 g	Cross Section:	16.200 Å ²	Liquid Density: 0.808 g/cc	
Surface Area Data					
MultiPoint BET.....					3.320e+02 m ² /g
Langmuir surface area.....					4.786e+02 m ² /g
t-method external surface area.....					2.662e+02 m ² /g
t-method micropore surface area.....					6.581e+01 m ² /g
DR method micropore area.....					4.420e+02 m ² /g
NLDFT cumulative surface area.....					2.590e+02 m ² /g
Pore Volume Data					
t-method micropore volume.....					3.207e-02 cc/g
DR method micropore volume.....					1.571e-01 cc/g
HK method cumulative pore volume.....					1.391e-01 cc/g
SF method cumulative pore volume.....					1.416e-01 cc/g
NLDFT method cumulative pore volume.....					1.524e-01 cc/g
Pore Size Data					
DR method micropore Half pore width.....					1.265e+01 Å
DA method pore Radius (Mode).....					8.000e+00 Å
HK method pore Radius (Mode).....					1.838e+00 Å
SF method pore Radius (Mode).....					2.261e+00 Å
NLDFT pore Radius (Mode).....					6.159e+00 Å

Table C.3. Surface area data of virgin bentonite.

Analysis Report

Operator: serife Date: 2009/05/25 Operator: Date: 5/27/2009
Sample ID: Bentonite Filename: C:\QC\data\Physisorb\Bentonite.qp
Sample Desc: Comment:
Sample weight: 0.0744 g Sample Volume: 0.0744 cc Sample Density: 1 g/cc
Outgas Time: 2.5 hrs OutgasTemp: 200.0 C
Analysis gas: Nitrogen Bath Temp: 77.3 K
Press. Tolerance: 0.100/0.100 (ads/des)
Equil time: 60/60 sec (ads/des)
Equil timeout: 240/240 sec (ads/des)
Analysis Time: 180.1 min End of run: 2009/05/25 14:22:28
Instrument: Nova Station A
Cell ID: 67
Adsorbate Nitrogen Temperature 77.350K
Molec. Wt.: 28.013 g Cross Section: 16.200 Å² Liquid Density: 0.808 g/cc

Surface Area Data

MultiPoint BET	1.364e+02 m ² /g
Langmuir surface area	2.041e+02 m ² /g
t-method external surface area	1.364e+02 m ² /g
DR method micropore area	1.747e+02 m ² /g
NLDFT cumulative surface area	8.933e+01 m ² /g

Pore Volume Data

DR method micropore volume	6.207e-02 cc/g
HK method cumulative pore volume	5.181e-02 cc/g
SF method cumulative pore volume	5.326e-02 cc/g
NLDFT method cumulative pore volume	6.381e-02 cc/g

Pore Size Data

DR method micropore Half pore width	1.519e+01 Å
DA method pore Radius (Mode)	9.100e+00 Å
HK method pore Radius (Mode)	1.838e+00 Å
SF method pore Radius (Mode)	2.261e+00 Å
NLDFT pore Radius (Mode)	1.324e+01 Å